Stony Brook University

Electrospun Nanofibrous Membrane: Studies on Processing Parameters, Pore Sizes and Applications

A Dissertation Presented

By

Yang Liu

to

The Graduate School

In Partial Fulfillment of the

Requirements

for the Degree of

Doctor of Philosophy

in

Chemistry

Stony Brook University

August 2012

Stony Brook University

The Graduate School

Yang Liu

We, the dissertation committee for the above candidate for the
Doctor of Philosophy degree, hereby recommend
acceptance of this dissertation.

Benjamin Chu – Dissertation Advisor
Distinguished Professor of the Stony Brook University

Benjamin S. Hsiao – Dissertation Advisor
Professor of the Chemistry Department

Stephen A. Koch – Chairperson of Defense
Professor of the Chemistry Department

Lisa Miller – Third Member
Adjunct Associate Professor of the Chemistry Department

Gary P. Halada – Outside Member
Associate Professor of the Materials Science & Engineering Department

This dissertation is accepted by the Graduate School

Charles Taber
Interim Dean of the Graduate School

Abstract of the Dissertation

Electrospun Nanofibrous Membrane: Studies on Processing Parameters, Pore Sizes and Applications

By

Yang Liu

Doctor of Philosophy

in

Chemistry

Stony Brook University

2012

Nanofibrous membranes generated by the electrospinning technique possess several unique structural properties, such as high surface and bulk porosity, high surface-to-volume ratio and interconnected pores, and have attracted considerable attention in the past two decades. For many of the membrane applications, such as tissue engineering and water filtration, the pore size and its distribution are important parameters. A better understanding of the relationships between the pore size, membrane thickness, fiber diameter and porosity is crucial for tailoring such membranes for specific applications. Capillary flow porometry was used to study the pore size, and quantitative relationships between the mean flow pore size and other structure properties can be obtained.

The design and characterization of nanofibrous membranes with specific properties, as well as the exploration of their potential applications represent another part of the dissertation. In the nanofibrous membrane application to microfiltration, electrospun membranes with different pore sizes were evaluated for their performance in removing water-borne bacteria by using spherical particles with different sizes as the simulants. Another issue deals with the bonding between the nanofibrous membrane and its non-woven substrate which often requires further strengthening for many practical applications in the ultrafiltration and nanofiltration range. A simple hot-pressing method combined with an interfacial treatment has been tried to improve the bonding between the support and the electrospun layer. The further modified structure could provide better mechanical support when used as the scaffold of the UF/NF membranes to withstand backflushing.

The electrospun nanofibrous membrane also demonstrated its application to the lithium-ion battery. By depositing the electrospun polyethersulfone membrane onto the chemically treated commercial polyethylene microporous separator, the thermal property and the safety margin of such a separator could be greatly improved, without sacrificing other properties of the separator.

A simple method of preparing the efficient and cost-effective electrospun nanofibrous microfiltration membranes with hazard chromium (VI) removal ability was presented. A functional material with a high positive charge density was grafted onto the nanofibers. The resulting membrane demonstrated both superior Cr(VI) adsorption capacity to the commercial activated carbons and reusability after proper treatment.

Table of Contents

List of Figures

List of Tables

Acknowledgements

First of all, I owe an immeasurable amount of gratitude to my advisors Professor Benjamin Chu and Professor Benjamin S. Hsiao, for their continuous support, invaluable advice and encouragement to my Ph.D research. Thanks for their suggestions, revision and all help with this dissertation. I also have a great appreciation for their tolerance, patience, criticism and corrections every time I made mistakes during my graduate studies. In addition to research, thanks for providing me the opportunities of mentoring high school students and working on projects with industrial companies; these experience will be invaluable to me as I begin my professional career. I am also immensely grateful to my committee members, Professor Stephen A. Koch and Professor Lisa Miller for their insightful comments, suggestions and encouragements. I would also like to thank Professor Gary P. Halada for serving on my committee as an outside member.

I gratefully acknowledge the support given by faculty, staff and graduate students in finishing this dissertation. In particular, I would like to thank Dr. Jim Quinn and Cheng Pan from the Materials Science and Engineering Department for their tremendous help with SEM, AFM and water contact angle tests. I am grateful to Professor Martin A. A. Schoonen from the Department of Geosciences for his kind teaching with the BET surface area measurement. I also thank Dr. Andy H. Tsou from ExxonMobil Research and Engineering Company for the separator property tests. Specially, I would like to thank Dr. Dufei Fang for building up the electrospinning set-up.

Special thanks to Michael Hawes and Sylvie Chavanne from Liquidity Corporation. They have taught me much knowledge about working in industry during the collaboration.

I would like to thank all members in the Chu & Hsiao's Group. I have particularly benefited from discussions with Drs. Christian Burger, Hongyang Ma, Dufei Fang. Many thanks to Ran, Xiaowei, Xiao, Zhe, Mason, Justin for helping with each other and sharing a wonderful time together.

I am grateful to all my friends in the past five years, for their help and motivation. Finally, I would like to express my special appreciation to my parents for their understanding, endless love and support.

Chapter I Introduction to Electrospinning and Electrospun Nanofibrous Membranes

1.1 Electrospinning

Electrospinning is a process that produces nanofibers with diameters in the range from sub-micrometers to micrometers. The term "electrospinning" was frequently used with "electrostatic spinning". The earliest study that was related to the electrospinning technique could be dated back to 1745, when Bose generated aerosols by applying high electric potentials to drops of liquids [1]. In 1902, the first electrospraying devices spraying liquids though the application of electrical charges were patented [2,3]. The first patent on electrospinning came out in 1934, whose inventor was Anton Formhals [4]. The electrospinning technology went through a mild development in the 1960s and 1970s. In 1966, Simons patented an electrical spinning setup for the production of ultrathin non-woven fabrics [5]. In spite of the long history of the technique, the term "electrospinning" was not used until around 1994 [6]. With the electrospun fibers commercialized in air filtration and the surging research interest in nanotechnology in the early 1990s, electrospinning has gained more attention in recent years. The number of scientific publications related to electrospinning has increased dramatically since1994 (Figure 1.1).

Materials made of fibers with diameters in the submicron size range possess many advantages over microfibrous materials. For example, the surface area of a fibrous

material is theoretically reversely proportional to its fiber diameter, and a nanofibrous material could have 10^3 or more times higher surface area than a microfibrous one. The mechanical properties, such as tensile strength and stiffness, can also be superior. For instance, Kwon et al. reported with a membrane thickness of 140 μm and a membrane porosity of ~70%, the electrospun poly(L-lactide-co-ε-caprolactone) (PLCL) membrane with an average fiber diameter of ~ 320 nm showed approximately three times higher Young's Modules than the membrane with an average fiber diameter of ~7 μm [7]. Besides, the reduction of the fiber dimension has brought about many new nanotechnology-associated properties, such as the surface with the lotus effect (self-cleaning effect) [8], and applications, such as tissue engineering [9]. Besides electrospinning, a number of techniques have been used for the production of nanofibers or the ultrathin fibers, including melt-blown, multicomponent processes, template synthesis [10], etc. While the first two mays have higher production rate than electrospinning, electrospinning has its advantages, such as flexibility in controlling the fiber diameter, which make this technique very promising in nanofibers production [11].

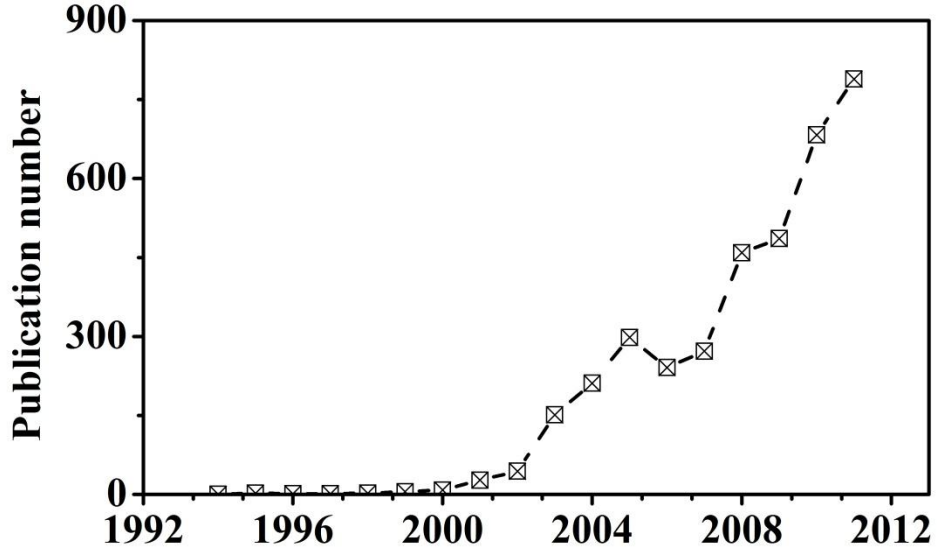

Figure 1.1 Number of scientific publications titled with the key words “electrospinning” and “electrospun” from 1994 to 2011 (Source: Thomson Reuters Web of Knowledge)

A general electrospinning set-up is composed of the polymer solution held in a syringe or other container, a capillary tube, a nozzle with an inner diameter in the millimeter or sub-millimeter size range, a high voltage power supply and a collector. A schematic diagram is shown in Figure 1.2. The high voltage is applied in a way that one electrode is connected to the nozzle and the other to the collector. The alignment of the electrodes can be vertically from top to bottom, from bottom to top, or in a horizontal manner. The distance between the nozzle to the counter electrode is several or tens of centimeters in laboratory systems, and the electric field is applied in the range of 100 - 500 kV m^{-1}. When the polymer solution is pumped to the nozzle, it forms a nearly spherical drop spontaneously due to its surface tension. With the applied electric field, charges are introduced into the polymer solution. The repulsive force within the polymer solution and the attractive force towards the counter electrode causes a cone-shaped (known as Taylor cone [12]) deformation of the drop in the direction of the collector. As the repulsive force is further increased to overcome the surface tension of the polymer solution, a charged jet is ejected from the tip of the Taylor cone. It undergoes an instable process and is stretched long and thin by the electrical force and gravity during travelling to the collector. With the solvents being evaporated on the way to the collector, solid fibers with diameters ranging from several nanometers to a few microns are formed [13]. Besides polymer solutions, polymers molten in high temperature can also be electrospun, but a vacuum condition has to be applied [14]. Up to now, over 100 polymer, such as polyarylonitrile (PAN) [15,16], polyethylene oxide (PEO) [17-19], polyethersulfone (PES) [20-23], polylactide (PLA) [24-26], cellulose acetate (CA) [27-29] and many

inorganic materials, such as TiO_2 [30,31], ZnO [32,33], CuO [34,35] have been electrospun or incorporated into nanofibers.

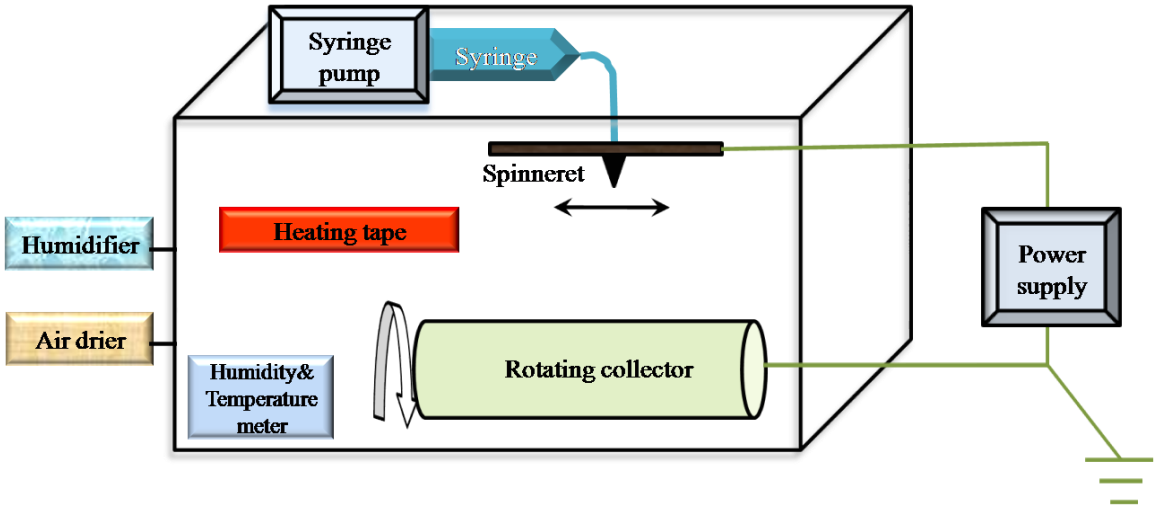

Figure 1.2 Schematic diagram of the electrospinning set-up with humidity and temperature controls

In some cases, shapes other than fibers, such as spindles and beads, can be formed during electrospinning. While they are desirable in a few applications, such as improvements on the adhesion between nanofibrous materials to other substrates, in most cases, they are unfavorable for the reasons that they significantly reduce the surface porosity and the porosity of the bulk membrane. The formation of these shapes is mostly attributed to the insufficient elongation of the fibers or insufficient evaporation of the solvents, due to a low charge density, a low solution viscosity or a high surface tension as indicated by Reneker et al [36,37]. The electrospinning process is very complex. Many parameters can affect the fiber diameter and the morphology, either directly or indirectly. These parameters include properties of the polymer solution, such as the solution viscosity, surface tension, solution conductivity, choice of solvent(s), and processing conditions, such as voltage, flow rate, distance between the tip and the collector [38]. Ambient parameters, like humidity, temperature, pressure, type of atmosphere are also considered to have an influence on the fiber formation [37,39,40]. Numerous studies have addressed the processing/property relationships in electrospun polymer fibers [41-44]. In general, fibers become uniform at a higher polymer solution concentration, and thinner fibers are formed at a lower polymer solution concentration, but a minimum concentration has to be reached for the electrospinning process to occur. The flow rate has a positive correlation with the fiber diameter, with a higher flow rate producing thicker fibers. For the other parameters, it is not quite simple to get straight forward conclusions of their effects on the fiber formation. Some researchers have also applied mathematical approaches to study the processing parameters and their effects on the fiber architecture. For example, Fridrikh and co-workers presented an analytical model

showing that the terminal diameter of the whipping jet was controlled by the flow rate, electric current, and the surface tension of the fluid [45]. However, this model was based on the assumption that the fluid was Newtonian and elastic effects were neglected. Moreover, the ambient parameters like the temperature and humidity that had been proven to have an influence in the fibers [46,47] were not taken into account, so this model could provide only a limited guide to actual operations. It is clear that, for electrospinning processes, the structure and morphology of the fibers are determined by a synergetic effect of solution parameters and electrostatic forces as well as other parameters such as ambient temperature and humidity.

The integrated structure formed by the electrospun nanofibers, usually named electrospun nanofibrous membrane, possesses a surface area ranging from 500 – 10 m^2/g for fiber diameters of 10 – 500 nm [48-50]. It has a very high surface porosity and bulk porosity of ~80% [51], light weight and good tensile strength. A unique characteristic of this membrane is that the pores are caused by the entanglement of nanofibers and are fully interconnected, and it is not likely to have "dead-end" pores in the structure. The pore size is highly correlated with the fiber diameter, and could be in the range of tens of nanometers to several microns. The membrane could also be modified with different functionalities. These structural features, plus the functionality from the polymer or by chemical modifications, have gained the electrospun nanofibrous membrane many advanced applications, such as air filtration [48,52], tissue engineering [53-59], catalyst carrier [60,61], fuel cells [62-64], and so on. This dissertation is mainly focusing on the applications in water purification and the lithium-ion battery separator. Some reported work about these two applications is briefly introduced as follows.

1.2 Applications of electrospun nanofibrous membranes

1.2.1 Water purification

In addition to air filtration, liquid filtration, especially water purification, has become one of the promising applications of electrospun nanofibrous membranes. Membrane filtration technology, due to its cost-effectiveness, energy-efficiency and environmentally friendly operation, has increased dramatically over the past 30 years and become one of the most important water purification methods [65,66]. Different from air filtration, the principle of liquid filtration is mostly based on size rejection, with other mechanisms, such as the Donnan effect, being involved in nanofiltration and reverse osmosis. Filtration membranes, depending on the driven pressure, the pore size and the particle size they can reject, are classified into microfiltration (MF), ultrafiltration (UF), nanofiltration (NF) and reverse osmosis (RO) membranes. Conventional porous polymeric membranes are generally prepared by the phase inversion method [67-72], and suffer from several major limitations: (1) relatively low surface porosity (2) fairly broad pore-size distribution and (3) "dead-end" pores [73-75]. As a result, one deficiency of these membranes is the low flux rate due to the low porosity [76]. The electrospun nanofibrous membrane, due to its advantage of high porosity, should be very suitable in water filtration. MF is an important technology for a wide range of applications, including pretreatment of waste water, clarification of beer and wine, especially in the removal of bacteria, algae or protozoan from surface water or contaminated water [77]. As most of the water borne microorganisms, such as Salmonella Bacteria, Escherichia coli and Vibrio cholerae, have sizes $\geq$ 0.3 microns [78], it is then within reason to expect that we should be able to sterilize contaminated water by filtration using MF membranes

with proper pore size design. In the MF level, the electrospun membrane itself has been demonstrated to be efficient to reject micro particles and bacteria. For example, Gopal and coworkers used electrospun PES membrane as the prefilter of a ultra- or nano-filtration process, and it demonstrated over 90% rejection ratio to the 1, 5, 10 μm polystyrene particles [79]. Wang et al. have developed an electrospun PAN microfiltration membrane with an average pore size of ~ 0.22 μm. The membrane showed two to three times higher flux than that of the commercial Millipore membrane with a comparable pore size, and maintained a very high rejection ratio of bacteria (LRV = 6) [80]. Liu et al. used a water soluble polymer PVA as the membrane material. The electrospun membrane after crosslinking showed perfect stability in water. The membrane possesses an average pore size of ~ 0.22 μm and a maximum pore size of ~ 0.47 μm at a membrane thickness of ~ 40 μm. Due to the hydrophilic nature of PVA, the membrane possessed a three to four times higher flux than the commercial Millipore GSWP 0.22 μm membrane, and a rejection ratio of ~ 99% to spherical particles with an average diameter of 0.189 ± 0.011 μm (unpublished data). In the UF level, Yoon et al. proposed a novel concept of high flux media, which consisted of a three-tier composite structure: (1) a conventional non-woven microfibrous support (melt blown PET mat), (2) an electrospun nanofibrous substrate mid-layer, and (3) a hydrophilic chitosan coating layer. Based on the idea, the Chu/Hsiao group at Stony Brook University developed a series of thin-film composite (TFC) membranes using different materials such as PVA and cellulose nanofibers as the selective layer. All these UF membrane demonstrated higher water flux and better rejection performance than the commercial UF membranes based on the phase inversion method [51,73,81-83]. By performing interfacial

polymerization (IP) of piperazine (PIP) using ionic liquids (IL) on the electrospun PES nanofibrous scaffold, a TFC membrane for nanofiltration was also prepared. The results showed 2 times higher permeation flux compared to that of the commercial NF membrane NF-90 with comparable salt rejection ratio, and comparable permeation flux and salt rejection performance as those of NF-270 [84].

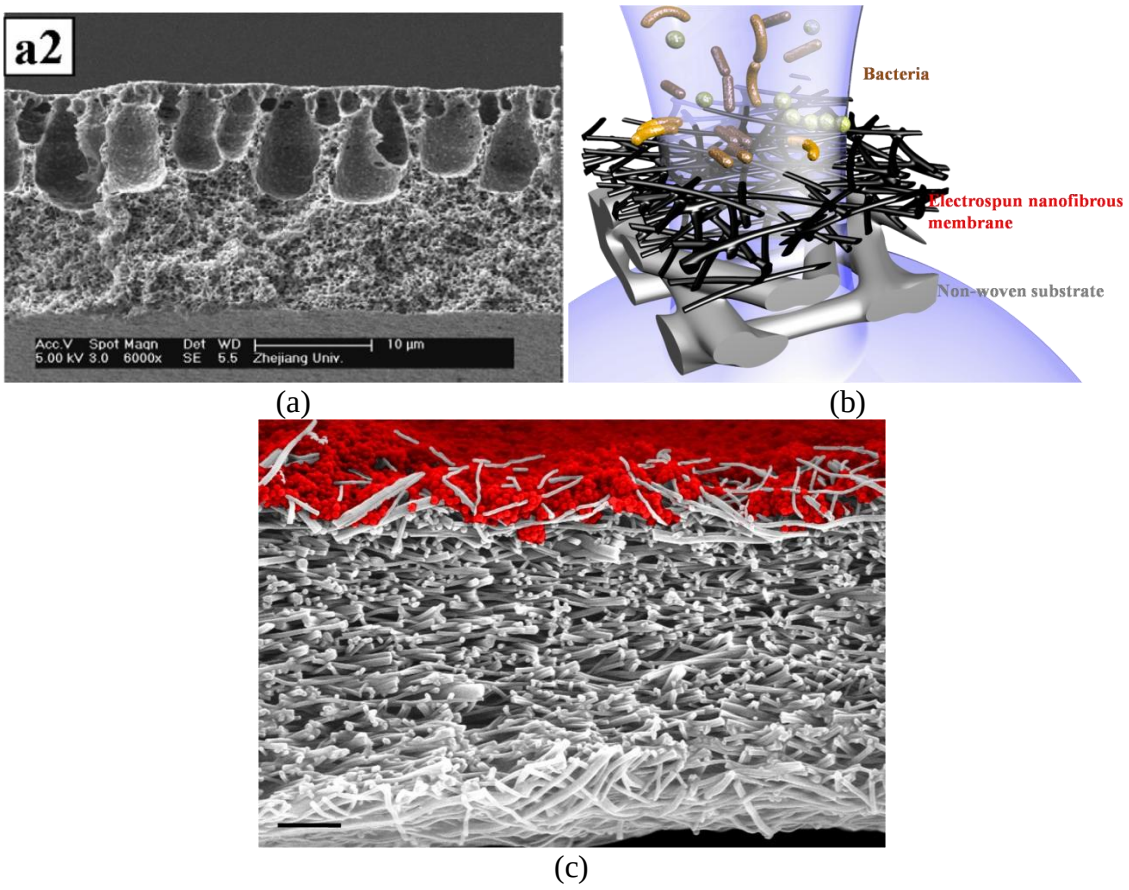

Figure 1.3 (a) Cross-section SEM image of a microporous membrane prepared by phase inversion method [85]; (b) Schematic diagram of novel electrospun nanofibrous microfiltration membrane [86]; (c) Cross-section SEM image of an electrospun PVA membrane showing successful rejection 0.2 µm spherical particles (red spheres), unpublished data

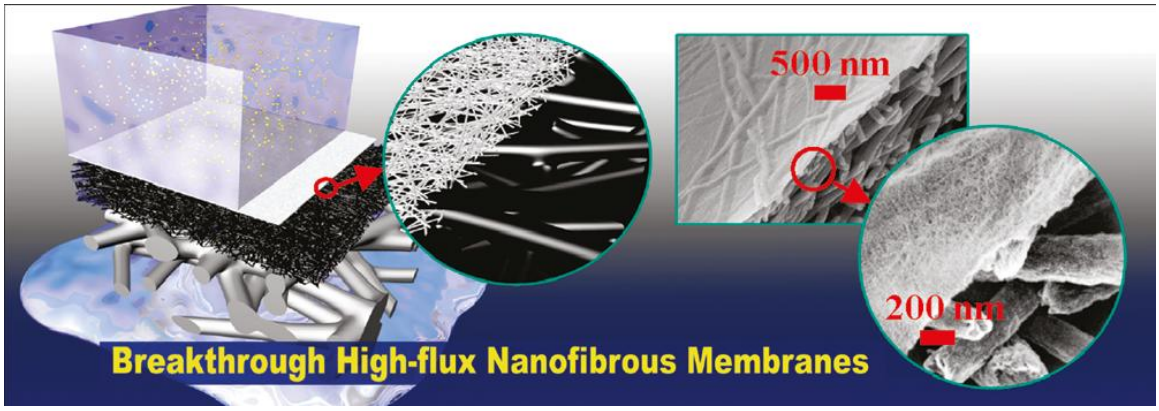

Figure 1.4 The novel three-tier structure of UF/NF membrane achieving high flux and low fouling developed by the Chu/Hsiao's Group, with ultrafine polysaccharide nanofibers with 5-10 nm diameters used as the barrier layer [87]

1.2.2 Lithium-ion battery

Similar to the PEM in lithium-ion batteries, the porous separator is placed between the electrodes to stop the short circuit, but allow the transport of ions. The porous feature and small pore sizes of electrospun nanofibrous membranes make them possible candidates of the battery separators. Cho et al. prepared microporous PAN nonwoven separators using electrospun nanofibers with the diameter between 380 to 250 nm. The pore size was comparable to the conventional membrane separators, but the e-spun membrane showed higher porosity, lower gurley value, better wettability and less shrinkage at the high testing temperature (150 ℃) than the conventional polyolefin separators. Cells with PAN membrane also demonstrated better performance in cycle lives, rate capabilities than conventional ones [88]. Choi et al. prepared electrospun PVDF membrane with a fiber diameter of ~ 250 nm and mean pore size of ~ 0.65 μm. The polymer electrolyte consisting of PVDF membrane and LiPF6-Ethylene carbonate (EC)/Dimethyl carbonate (DMC) showed higher ion conductivity and electrochemical stability, lower interfacial resistance and sufficient mechanical strength compared to that with the conventional membrane [89]. Choi et al. treated the electrospun PVDF nanofibers with ethylene plasma to introduce PE chains onto the membrane surface, to further functionalize the e-spun membrane with the shutdown feature. The SEM images showed at 110 ℃, PE on the PVDF mat was melted and shut the pores of the mat [90]. However, the PE was not uniformly deposited on the membrane surface and some areas were not treated at all, which leaves the plasma method highly doubtable in achieving the purpose.

1.3 Overview of the dissertation

Chapter II Studies of Electrospinning and Pore Size Relationship for Nanofibrous Membranes

In many applications of electrospun nanofibrous membranes (ENM), such as filtration, tissue engineering and batteries, pore size is an important parameter. ENM is known for high porosity and small pore size in the range of hundreds of nanometers to microns. A quantitative understanding of the pore size with its other structural properties such as membrane thickness, fiber diameter and porosity is useful for designing suitable membranes for specific applications.

In this chapter, capillary flow porometry has been used to characterize the maximum pore size, mean flow pore size and pore size distribution of electrospun membranes. Polyacrylonitrile (PAN) was used as the membrane material. One target was to control the morphology of the membrane, i.e., to produce consistent and bead-free nanofibers, which could be achieved with the assistance of very little amount of a high molecular weight PAN. Uniform nanofibers with average diameters ranging from 104 nm to 655 nm were obtained from polymer solutions having different polymer concentrations. By investigating the correlation of the mean flow pore size with other membrane structural parameters, several findings were revealed in Section 2.3.2. First, the mean flow pore size of the electrospun membrane decreased with the increase of membrane thickness, until reached a plateau value at a certain thickness. Second, for the membranes with a porosity of ~ 80% and a thickness of 100 μm where the mean flow pore size became insensitive to membrane thickness, the mean flow pore size was found to be proportional to the average fiber diameter. Third, the porosity of the membrane could be reduced from its initial

value of ~ 80% to a relatively low value of ~ 30% by compressing the membrane with a compress machine. The mean flow pore size was also reduced with the porosity in an almost inversely proportional relationship with one minus the porosity.

We have also paid special attention to the water filtration application of electrospun nanofibrous membranes, especially for water-borne bacteria removal. Since most of the water-borne bacteria have the smallest dimension of ~ 0.5 μm, with a few of them having the smallest dimension of ~ 0.2 μm [78], spherical polymeric beads with a nominal diameter of 1.0 μm, 0.5 μm and 0.2 μm were used as the simulants of bacteria to test the membrane's rejection performance at different membrane thickness, fiber diameter as well as porosity.

Chapter III Improving Interfacial Bonding Strength between Electrospun Membrane and Substrate by using Hot Pressing Method

The three-tier TFC membranes using the electrospun membrane as the mid-layer scaffold have demonstrated superior performances to the conventional UF and NF membranes. However, one problem is the relatively weak bonding strength between the bottom non-woven substrate and the middle electrospun membrane layer. As the bonding between the two layers is primarily resulted from the deposition of the electrospun nanofibers on the non-woven (PET) substrate, it is often weaker than that resulted from the phase inversion method. In UF or NF operations, in order to maintain high filtration efficiency and to be able to reuse the membrane, back flushing is often used to remove the fouling layer on the membrane surface. The weaker bonding strength between the supporting substrate and the electrospun membrane may not be able to withstand the high reverse applied pressure in the back flushing process.

In this chapter the bonding strength between the bottom PET substrate and the middle layer electrospun PAN membrane was investigated, and a method has been proposed to improve the bonding, hopefully without reducing the corresponding flux. The peel strength test showed that the original bonding strength was indeed very weak. An interfacial treatment and a hot-pressing method were utilized to improve the bonding between the two layers. Both higher pressure and temperature were shown to be able to improve the bonding. Results indicated that with no interfacial treatment, solely applying the hot-pressing method only improved the bonding strength by 2 ~ 3 folds in the lower value range. With both methods applied, the bonding strength was enhanced by over 40 folds, and achieved a level higher than that of the commercial Koch UF membrane produced by the phase inversion method. The membrane morphology at different hot-pressing conditions was characterized with scanning electron microscopy (SEM). After-compress membrane properties associated with filtration, such as membrane porosity, maximum pore size, mean pore size and pure water flux were investigated and fully discussed in Section 3.3.2. The thin-film composite UF membranes using the cellulose nanofiber as the barrier layer and the different PAN-PET membrane as the scaffolds were prepared. The ultrafiltration performance was also evaluated in Section 3.3.3.

Chapter IV Improvements of Meltdown Temperature of Polyethylene Lithium-Ion Battery Separator using Electrospun Polyethersulfone Membrane

The application of electrospun nanofibrous membrane as the lithium ion battery (LIB) separator was explored in this chapter. Traditional LIB separators were generally fabricated from microporous polyolefins, such as polyethylene (PE) or polypropylene (PP). The separator is immersed in the ionically conductive electrolyte between the anode

and cathode. It separates the two electrodes from directly contacting each other, but allows the ion transport through the pores. Polyolefins were often selected as separator materials because of the shutdown feature of the porous membrane, due to its low melting point. Shutdown is an important safety feature in the lithium ion batteries, referring to the pores being closed as a result of membrane melting at temperatures higher than the melting point of the separator material. This feature can prevent severe damage to the battery or battery explosion at high temperatures. Thus, a lower shutdown temperature (SDT) is preferred. Meanwhile, the separator is also required to have a high meltdown temperature (MDT) to hold its mechanical integrity at high temperatures. A MDT is favorable for a separator. For the commercially available PE separator, the SDT and MDT are very close, which provides a very narrow safety margin. In another aspect, electrospun nanofibrous membrane itself has been proved to be a good candidate for the LIB separators. Its unique features, such as high porosity and small pore size, have gained better performances when compared with conventional PE films. However one drawback is that it does not provide the shutdown feature. By using it solely as the separator could lead to safety issues.

In this chapter, a composite separator composed of a commercial microporous PE separator and two layers of electrospun PES nanofibrous membranes were prepared. It possesses the low shutdown characteristic of the PE film and the high meltdown feature of PES membrane. Also due to the high porosity of the electrospun PES membrane, it is not likely to reduce the performance of the base PE film. To prepare such a composite membrane, bonding strength between the PE film to the electrospun membrane is critical. Due to the low surface energy and very hydrophobic nature of the PE film, its adhesion to

other materials is often relatively weak. In this work, the PE film was first modified with chromic acid before the electrospun PES membrane was deposited onto it and the corresponding property changes were characterized. Results indicated longer acid treating time resulted in a better bonding between the PE film and the electrospun membrane. The bonding strength was also improved in another way, i.e., by changing the morphology of the electrospun PES membrane. A higher electrospinning flow rate was demonstrated to result in more dripping in the final structure, which led to more contact areas and therefore better bonding between the two layers. Lastly, the separator performance of the composite membrane was evaluated, and compared to those of the base PE film and a commercial Celgard separator with a PP/PE/PP three layer structure.

Chapter V Removal of Cr (VI) from Aqueous Solution using Polyvinylamine Grafted Electrospun Polyacrylonitrile Nanofirous Membrane

Chromium (VI) contamination in drinking water is a great threat to human health and has already become an environmental problem, not only in developing countries but also in the U.S. The Environmental Working Group (EWP) tested the drinking water in 35 U.S. cities. The report, released on Dec 20, 2010, showed that the carcinogenic Cr (VI) was found in drinking water of 31 cities. Many methods have been published for Cr (VI) removal, including chemical precipitation, electrolysis, nanofiltration and so on [91-98]. Adsorption is considered to be an efficient and economical one when compared with other methods. The electrospun nanofibrous membrane, due to its higher surface area and surface to volume ratio than many other structure forms, such as film, is especially desirable for metal adsorption.

As Cr(VI) exists in aqueous solution in the forms of anions, preparing an electrospun membrane with positive surface charge becomes the target of this study. While it is possible to directly electrospin polycationic polymers into nanofibers, a simple method is to electrospin a base polymer, followed by functionalizing it with positive charges. PAN was selected as the base material as its –CN group was easy to be modified. After it was electrospun into nanofibers with an average diameter of ~200 nm, it was pretreated with sulfuric acid and then grafted with polyvinylamine (PVAm), a linear hydrocarbon chain with primary amine groups on alternating carbon atoms. The treatment of sulfuric acid was aimed to introduce –COOH groups on the fiber surface, which was believed to facilitate binding of the functional polymer onto the nanofibers. The membrane properties for the original membrane, the hydrolyzed membrane, and the functionalized membrane were fully investigated. These properties include membrane morphology, fiber diameter, membrane porosity, maximum and mean pore sizes, pure water flux, BET surface area and mechanical strength are presented in section 5.3.1.

The Cr (VI) adsorption using the functionalized membrane was tested at different pH values in the range of 1.0 ~ 13.0. Experimental data showed that the adsorption was highly pH dependent. To illustrate the results, a mathematical calculation with the equilibrium chemistry was performed, which showed a good agreement with the experimental data, and both indicated the optimal pH range for Cr (VI) was between 3.0 ~ 5.0. Adsorption was also performed at different initial Cr (VI) concentrations at pH = 3.0. Isotherm data showed that the adsorption process followed the Langmuir model well, and a saturated adsorption capacity of 57.1 mg Cr (VI) per gram of the membrane was obtained. This result was comparable to some commercial activated carbon. If

considering the adsorption capacity per gram of the functional material, or per surface area, the PVAm grafted electrospun membrane showed much superior performance to activated carbons and chitosan because of the higher density of functional groups of PVAm. The membrane was also demonstrated to be able to remove Cr (VI) efficiently in a dynamic flow condition. The adsorption capacity, however, was decreased with higher flow rate as a result of shorter contact time between the chromium ions and the active sites of the membrane. Lastly, the attracted metal ions could be released from the membrane in 0.1 M NaOH solution, resulting in a regenerated membrane.

References

1. Greiner, A., and Wendorff, J. H. (2007) *Angew Chem Int Edit* **46**, 5670-5703
2. Morton, W. J. (1902) *US Patent 705,691*
3. Cooley, J. F. (1902) *US Patent 692,631*
4. Formhals, A. (1934) *US Patent 1,975,504*
5. Simons, H. (1966) *US Patent 3,280,229*
6. Huang, Z. M., Zhang, Y. Z., Kotaki, M., and Ramakrishna, S. (2003) *Compos Sci Technol* **63**, 2223-2253
7. Kwon, I. K., Kidoaki, S., and Matsuda, T. (2005) *Biomaterials* **26**, 3929-3939
8. Barthlott, W., and Neinhuis, C. (1997) *Planta* **202**, 1-8
9. Katti, D. S., Robinson, K. W., Ko, F. K., and Laurencin, C. T. (2004) *J Biomed Mater Res B* **70B**, 286-296
10. Martin, C. R. (1996) *Chem Mater* **8**, 1739-1746
11. Fang, J., Niu, H. T., Lin, T., and Wang, X. G. (2008) *Chinese Sci Bull* **53**, 2265-2286
12. Taylor, G. (1964) *Proc R Soc Lon Ser-A* **280**, 383-397
13. Haghi, A. K., and Zaikov, G. E. (2011) *Electrospinning of nanofibers from introduction to application*, Nova Science Publishers, Hauppauge, N.Y.
14. Larrondo, L., and Manley, R. S. J. (1981) *J Polym Sci Pol Phys* **19**, 933-940
15. Gu, S. Y., Ren, J., and Vancso, G. J. (2005) *Eur Polym J* **41**, 2559-2568
16. He, J. H., Wan, Y. Q., and Yu, J. Y. (2008) *Fiber Polym* **9**, 140-142
17. Nagamine, S., Tanaka, Y., and Ohshima, M. (2009) *Chem Lett* **38**, 258-259

18. Ajao, J. A., Abiona, A. A., Chigome, S., Fasasi, A. Y., Osinkolu, G. A., and Maaza, M. (2010) *J Mater Sci* **45**, 2324-2329

19. Uyar, T., Hacaloglu, J., and Besenbacher, F. (2011) *J Nanosci Nanotechno* **11**, 3949-3958

20. Homaeigohar, S. S., Buhr, K., and Ebert, K. (2010) *J Membrane Sci* **365**, 68-77

21. Tang, Z. H., Qiu, C. Q., McCutcheon, J. R., Yoon, K., Ma, H. Y., Fang, D. F., Lee, E., Kopp, C., Hsiao, B. S., and Chu, B. (2009) *J Polym Sci Pol Phys* **47**, 2288-2300

22. Ma, Z. W., Lan, Z. W., Matsuura, T., and Ramakrishna, S. (2009) *J Chromatogr B* **877**, 3686-3694

23. Yoon, K., Hsiao, B. S., and Chu, B. (2009) *Polymer* **50**, 2893-2899

24. Toncheva, A., Spasova, M., Paneva, D., Manolova, N., and Rashkov, I. (2011) *J Bioact Compat Pol* **26**, 161-172

25. Wang, S. D., Zhang, Y. Z., Wang, H. W., Yin, G. B., and Dong, Z. H. (2009) *Biomacromolecules* **10**, 2240-2244

26. You, Y., Min, B. M., Lee, S. J., Lee, T. S., and Park, W. H. (2005) *J Appl Polym Sci* **95**, 193-200

27. Celebioglu, A., and Uyar, T. (2011) *Mater Lett* **65**, 2291-2294

28. Tungprapa, S., Puangparn, T., Weerasombut, M., Jangchud, I., Fakum, P., Semongkhol, S., Meechaisue, C., and Supaphol, P. (2007) *Cellulose* **14**, 563-575

29. Ding, B., Li, C. R., Hotta, Y., Kim, J. H., Kuwaki, O., and Shiratori, S. (2006) *Nanotechnology* **17**, 4332-4339

30. Im, J. S., Il Kim, M., and Lee, Y. S. (2008) *Mater Lett* **62**, 3652-3655

31. Formo, E., Lee, E., Campbell, D., and Xia, Y. N. (2008) *Nano Lett* **8**, 668-672

32. Kim, Y., Lee, D. Y., Lee, M. H., Cho, N. I., Song, Y. S., and Lee, S. J. (2008) *J Korean Phys Soc* **53**, 421-425

33. Wu, S. J., Tai, Q. D., and Yan, F. (2010) *J Phys Chem C* **114**, 6197-6200

34. Vijayakumar, G. N. S., Devashankar, S., Rathnakumari, M., and Sureshkumar, P. (2010) *J Alloy Compd* **507**, 225-229

35. He, X. L., Zhao, Y., Li, J. P., Gao, X. G., and Jia, J. A. (2011) *Sensor Lett* **9**, 294-298

36. Lin, T., Wang, H. X., Wang, H. M., and Wang, X. G. (2004) *Nanotechnology* **15**, 1375-1381

37. Fong, H., Chun, I., and Reneker, D. H. (1999) *Polymer* **40**, 4585-4592

38. Seeram Ramakrishna, K. F., Wee-Eong Teo, Teik-Cheng Lim, Zuwei Ma. (2005) *An introduction to Electrospinning and Nanofibers*,

39. Doshi, J., and Reneker, D. H. (1995) *Journal of Electrostatics* **35**, 151-160

40. Baumgart.Pk. (1971) *Journal of Colloid and Interface Science* **36**, 71-79

41. Thompson, C. J., Chase, G. G., Yarin, A. L., and Reneker, D. H. (2007) *Polymer* **48**, 6913-6922

42. Tripatanasuwan, S., Zhong, Z. X., and Reneker, D. H. (2007) *Polymer* **48**, 5742-5746

43. Supaphol, P., Mit-uppatham, C., and Nithitanakul, M. (2005) *Macromol Mater Eng* **290**, 933-942

44. Deitzel, J. M., Kleinmeyer, J., Harris, D., and Tan, N. C. B. (2001) *Polymer* **42**, 261-272

45. Fridrikh, S. V., Yu, J. H., Brenner, M. P., and Rutledge, G. C. (2003) *Physical Review Letters* **90**, 144502

46. Megelski, S., Stephens, J. S., Chase, D. B., and Rabolt, J. F. (2002) *Macromolecules* **35**, 8456-8466

47. Bognitzki, M., Czado, W., Frese, T., Schaper, A., Hellwig, M., Steinhart, M., Greiner, A., and Wendorff, J. H. (2001) *Advanced Materials* **13**, 70-72

48. Gibson, P., Schreuder-Gibson, H., and Rivin, D. (2001) *Colloid Surface A* **187**, 469-481

49. Tomadakis, M. M., and Sotirchos, S. V. (1991) *Aiche J* **37**, 1175-1186

50. Tomadakis, M. M., and Sotirchos, S. V. (1991) *Aiche J* **37**, 74-86

51. Yoon, K., Kim, K., Wang, X. F., Fang, D. F., Hsiao, B. S., and Chu, B. (2006) *Polymer* **47**, 2434-2441

52. Grafe, T. H., and Graham, K. M. (May, 2003) *Nonwovens in Filtration - Fifth International Conference*

53. Li, W. J., Tuli, R., Huang, X. X., Laquerriere, P., and Tuan, R. S. (2005) *Biomaterials* **26**, 5158-5166

54. Zong, X. H., Bien, H., Chung, C. Y., Yin, L. H., Fang, D. F., Hsiao, B. S., Chu, B., and Entcheva, E. (2005) *Biomaterials* **26**, 5330-5338

55. Carampin, P., Conconi, M. T., Lora, S., Menti, A. M., Baiguera, S., Bellini, S., Grandi, C., and Parnigotto, P. P. (2007) *J Biomed Mater Res A* **80A**, 661-668

56. Wang, H. Y., Feng, Y. K., Zhao, H. Y., Xiao, R. F., Lu, J., Zhang, L., and Guo, J. T. (2012) *Macromol Res* **20**, 347-350

57. Alhosseini, S. N., Moztarzadeh, F., Mozafari, M., Asgari, S., Dodel, M., Samadikuchaksaraei, A., Kargozar, S., and Jalali, N. (2012) *Int J Nanomed* **7**, 25-34

58. Liu, H. F., Li, X. M., Zhou, G., Fan, H. B., and Fan, Y. B. (2011) *Biomaterials* **32**, 3784-3793

59. Lee, C. H., Shin, H. J., Cho, I. H., Kang, Y. M., Kim, I. A., Park, K. D., and Shin, J. W. (2005) *Biomaterials* **26**, 1261-1270

60. Stasiak, M., Studer, A., Greiner, A., and Wendorff, J. H. (2007) *Chem-Eur J* **13**, 6150-6156

61. Lindner, J. P., Roben, C., Studer, A., Stasiak, M., Ronge, R., Greiner, A., and Wendorff, H. J. (2009) *Angew Chem Int Edit* **48**, 8874-8877

62. Ramakrishna, S., Fujihara, K., Teo, W. E., Yong, T., Ma, Z. W., and Ramaseshan, R. (2006) *Mater Today* **9**, 40-50

63. Choi, J., Lee, K. M., Wycisk, R., Pintauro, P. N., and Mather, P. T. (2008) *Macromolecules* **41**, 4569-4572

64. Tamura, T., and Kawakami, H. (2010) *Nano Lett* **10**, 1324-1328

65. Pathak, A. N. (1997) *J Sci Ind Res India* **56**, 335-345

66. Li, Z. J., Zhou, S. Q., and Qiu, J. H. (2007) *Environ Eng Sci* **24**, 1245-1256

67. Mchugh, A. J., and Miller, D. C. (1995) *J Membrane Sci* **105**, 121-136

68. Zhang, S. H., Jian, X. G., and Dai, Y. (2005) *J Membrane Sci* **246**, 121-126

69. Lin, D. J., Chang, C. L., Chen, T. C., and Cheng, L. P. (2002) *Desalination* **145**, 25-29

70. Kim, I. C., Yoon, H. G., and Lee, K. H. (2002) *J Appl Polym Sci* **84**, 1300-1307

71. KastelanKunst, L., Dananic, V., Kunst, B., and Kosutic, K. (1996) *J Membrane Sci* **109**, 223-230

72. Boussu, K., Vandecasteele, C., and Van der Bruggen, B. (2006) *Polymer* **47**, 3464-3476

73. Wang, X. F., Fang, D. F., Yoon, K., Hsiao, B. S., and Chu, B. (2006) *J Membrane Sci* **278**, 261-268

74. Akthakul, A., McDonald, W. F., and Mayes, A. M. (2002) *J Membrane Sci* **208**, 147-155

75. Nakao, S. (1994) *J Membrane Sci* **96**, 131-165

76. Marshall, A. D., Munro, P. A., and Tragardh, G. (1993) *Desalination* **91**, 65-108

77. Farahbakhsh, K., Svrcek, C., Guest, R. K., and Smith, D. W. (2004) *Journal of Environmental Engineering and Science* **3**, 237-253

78. Wang, Y. Y., Hammes, F., Duggelin, M., and Egli, T. (2008) *Environmental Science & Technology* **42**, 6749-6754

79. Gopal, R., Kaur, S., Ma, Z. W., Chan, C., Ramakrishna, S., and Matsuura, T. (2006) *J Membrane Sci* **281**, 581-586

80. Wang, R., Liu, Y., Li, B., Hsiao, B. S., and Chu, B. (2012) *J Membrane Sci* **392**, 167-174

81. Ma, H. Y., Yoon, K., Rong, L. X., Shokralla, M., Kopot, A., Wang, X., Fang, D. F., Hsiao, B. S., and Chu, B. (2010) *Ind Eng Chem Res* **49**, 11978-11984

82. Wang, X. F., Chen, X. M., Yoon, K., Fang, D. F., Hsiao, B. S., and Chu, B. (2005) *Environ Sci Technol* **39**, 7684-7691

83. Tang, Z. H., Wei, J., Yung, L., Ji, B. W., Ma, H. Y., Qiu, C. Q., Yoon, K., Wan, F., Fang, D. F., Hsiao, B. S., and Chu, B. (2009) *J Membrane Sci* **328**, 1-5

84. Yung, L., Ma, H. Y., Wang, X., Yoon, K., Wang, R., Hsiao, B. S., and Chu, B. (2010) *J Membrane Sci* **365**, 52-58

85. Zhao, Y. H., Qian, Y. L., Zhu, B. K., and Xu, Y. Y. (2008) *J Membrane Sci* **310**, 567-576

86. http://www.chem.sunysb.edu/WaterFilter/Figures/.

87. Ma, H. Y., Burger, C., Hsiao, B. S., and Chu, B. (2011) *Biomacromolecules* **12**, 970-976

88. Cho, T. H., Tanaka, M., Onishi, H., Kondo, Y., Nakamura, T., Yamazaki, H., Tanase, S., and Sakai, T. (2008) *J Power Sources* **181**, 155-160

89. Choi, S. W., Jo, S. M., Lee, W. S., and Kim, Y. R. (2003) *Advanced Materials* **15**, 2027-2032

90. Choi, S. S., Lee, Y. S., Joo, C. W., Lee, S. G., Park, J. K., and Han, K. S. (2004) *Electrochim Acta* **50**, 339-343

91. Sapari, N., Idris, A., and AbHamid, N. H. (1996) *Desalination* **106**, 419-422

92. Kongsricharoern, N., and Polprasert, C. (1995) *Water Sci Technol* **31**, 109-117

93. Nenov, V., Zouboulis, A. I., Dimitrova, N., and Dobrevsky, I. (1994) *Environ Pollut* **83**, 283-289

94. Janssen, L. J. J., and Koene, L. (2002) *Chem Eng J* **85**, 137-146

95. Muthukrishnan, M., and Guha, B. K. (2008) *Desalination* **219**, 171-178

96. Hafiane, A., Lemordant, D., and Dhahbi, M. (2000) *Desalination* **130**, 305-312

97. Abu Qdais, H., and Moussa, H. (2004) *Desalination* **164**, 105-110

98. Gupta, S. K., and Chen, K. Y. (1978) *J Water Pollut Con F* **50**, 493-506

Chapter II Studies of Electrospinning and Pore Size Relationship for Nanofibrous Membranes

The pore size and pore structure of an electrospun membrane are important features in many of the membrane applications, such as water filtration and tissue engineering. In this work, the pore size of the electrospun polyacrylonitrile (PAN) membrane was fully investigated by capillary flow porometry. The relationships of mean flow pore size of the membrane with its membrane thickness, fiber diameter and membrane porosity were quantitatively characterized. Results showed that the mean pore size initially decreased as the membrane got thicker and reached to a plateau value at a certain membrane thickness, being 100 μm and beyond in our studies. The mean flow pore size was found to follow a proportional relationship with the fiber diameter, and a factor of two was found in the studied PAN system. Changing the porosity by compressing the membrane also showed a substantial effect on the pore size. Typically, the mean flow pore size was almost proportional to the final compressed thickness and inversely proportional to one minus the porosity. The relationships of the mean flow pore size with the membrane thickness, fiber diameter and membrane porosity were not likely to be material dependent, and it is therefore possible to tailor the pore size for different membrane applications by tuning these variables. Particle challenge tests using spherical beads of different sizes were used to evaluate the microfiltration performance of electrospun membranes with different pore

sizes. Results also revealed that compression of electrospun membrane in the through-membrane direction could increase its particle retention ability.

2.1 Introduction

Electrospun membranes, due to their unique structural properties, have been used in many applications including filtration [1-6], biomedical scaffolds [7-11], catalysis [12] and sensors [13] as discussed in section 1.1. The pores (or the void space) of electrospun membranes are caused by the entanglement of nanofibers and are fully interconnected. The open porous structure plays an essential role in these applications, and therefore understanding the structure property of the membranes and controlling the pore size become crucial. For example, smaller pores are favorable in the microfiltration application while larger pores are required for ingrowth of cells to the nanofibrous network in tissue engineering [14]. A number of studies have been carried out to evaluate the physical properties of electrospun nanofibrous membrane. For example, Kim and coworkers varied the pore size of electrospun nylon-6 nanofibrous membrane in the range of 0.17 to 2.7 μm by changing the fiber diameter [15]. Li and co-workers found that the electrospun membranes with a fiber diameter of 2.58 μm exhibited the mean pore sizes of 3.25 ~ 4.38 μm depending on the mass of the membrane, while membranes with a fiber diameter of 281 nm possessed the mean pore sizes of 0.66~0.79 μm as the membrane mass was varied [16]. Ma et al. reported the mean pore size of the electrospun nanofibrous membrane was 3 ± 1 times of the mean fiber diameter. However, some pore sizes were determined from the SEM analysis, which left the measurement method quite challenging [17]. Eichohorn and Sampson applied a theoretical model to study the

relationships of pore size with fiber density, fiber width and porosity [18]. Nonetheless, there is still lack of systematic experimental studies in addressing the numerical relationships of pore size with its affecting factors such as the fiber diameter and porosity.

Pore size and its distribution in a microporous membrane can be determined using methods such as mercury intrusion porosimetry, liquid extrusion porosimetry [19], electron microscopy, adsorption-base methods and capillary flow porometry [16,19,20]. The pore size measured with different methods may vary within a certain extent, due to different pore definition and measurement principles. Among these methods, capillary flow porometry is a simple, non-toxic and non-destructive technique, and is most suitable for the measurement of the through pores of a solid-liquid separation membrane [21]. In a capillary flow porometry measurement, a wetting liquid with known surface tension is used to wet the membrane and filled in all the pores. When the air pressure is applied and a minimum pressure is reached, the maximum pore is "open", and an initial air flow through the membrane is monitored with a flow meter. With increasing air pressure, more pores are open until the membrane reaches a "dry" state, and a complete "wet" air flow curve with the applied pressure is obtained. A "dry" air flow curve is also obtained by collecting the air flow through a dry membrane over the same pressure range. Based on the two curves and the Young-Laplace equation [22], the pore size and its distribution can be calculated by the differentiation method.

Studies have revealed that fiber diameter plays an important role in affecting the pore size, and hence fine control of the fiber diameter and morphology must be done before any further investigations. In this study, a PAN with a lower molecular weight (LMw PAN) was used as the main electrospinning material. Different amounts of PAN with a

higher molecular weight (HMw PAN) were added to adjust the properties of electrospinning solution. Due to the higher polymer chain entanglement of HMw PAN, solution electrospinability could be enhanced and the formation of beadless nanofibers were more favored at the low solution concentration. In another aspect, the diameter of nanofibers electrospun from a single polymer solution might be limited to a certain range, and adding a polymer with a higher molecular weight could broaden the range of the fiber diameter as produced. The electrospun fiber diameter was carefully controlled by tuning electrospinning conditions such as the flow rate and applied voltage. The maximum pore size, mean flow pore size as well as pore size distribution of membranes were measured using the capillary flow porometry, and their relationships with the membrane thickness, fiber diameter and porosity were fully discussed. In our research group, we are especially interested in the application of electrospun membrane as a microfiltration filter. The retention abilities of the membranes to spherical particles with different sizes in simulating water-borne bacteria were also investigated.

2.2 Experimental

2.2.1 Materials

Poly (acrylonitrile) (PAN) samples with a weight-average molecular weight (M_w) of 150,000 g/mol and 700,000 g/mol were purchased from Scientific Polymer Products. Dimethylformamide (DMF, 99.9%) was purchased from Sigma-Aldrich Co and used as the solvent. The non-woven polyethylene terephthalate (PET) with an average fiber diameter of around 10 μm was purchased from Sanko Ltd, Japan, and was used as the substrate. Polycarboxylate microspheres with a nominal diameter of 1.0 μm (average

diameter 1.03 ± 0.01 μm), 0.5 μm (average diameter 0.489 ± 0.013 μm), and 0.2 μm (average diameter 0.189 ± 0.011 μm), respectively, were purchased from Polysciences Inc. and used in the rejection test.

2.2.2 Preparation and characterization of PAN solutions

PAN powders were dissolved in DMF at 60 ℃ and were stirred for 1 day to ensure homogeneity. Solutions with different ratios of two PAN and total PAN concentrations were prepared to investigate the solution property effects on the fiber diameter. The viscosity of polymer solutions was measured with an Annto-Paar Physica MCR 301 rheometer at 25 ℃.

2.2.3 Electrospinning of PAN nanofibrous membrane

PAN solutions were electrospun into nanofibers using the lab-built electrospinning device shown in Figure 1.2. The polymer solution was fed to the spinneret (diameter 1 mm) tip through a 20 mL BD Luer-Lok ™ syringe (Catalog number 309661, BD, USA). The feeding flow rate was controlled by a programmable syringe pump (Model M061-FD08, Superior Electric Company, USA). The power supply from the Glassman High Voltage, Inc. was used to supply the applied voltage of 0-40 kV. The process was operated in a closed chamber, with the temperature and the humidity monitored using a temperature and a humidity sensor manufactured by Fisher Scientific (Catalog number: 11-661-19). The relative humidity was controlled at 55 % ± 5 % and the temperature was controlled at 24 ℃ ± 1 ℃ during the electrospinning process, by using an air drier, a humidifier and a heating tape purchased from McMaster, all placed on the back wall of the chamber. A grounded metal drum with a rotating speed of 300 rpm was used as the collector and was placed 7.5 cm below the tip of the spinneret. A stepping motor was

used to control the oscillatory translational motion perpendicular to the drum rotation direction. Travel distance of the spinneret was set to be 10 cm in the experiment to ensure the production of uniform electrospun membrane with sufficient membrane area. The thickness of membranes was controlled by the target volume of polymer solution.

2.2.4 Determination of electrospun nanofiber diameters

The morphology of electrospun PAN membrane was characterized with a LEO 1550 (LEO, USA) scanning electron microscope (SEM) after gold coating. Cross-section SEM images were obtained after fracturing of samples in liquid nitrogen. The fiber diameter was measured from the SEM images using the LeicaIMGRead software (http://dell.chem.sunysb.edu). The fiber diameter was reported as mean ± standard deviation.

2.2.5 Characterizations of electrospun membrane

The thickness of the electrospun membrane was measured by using a micrometer. The porosity of the membrane was calculated by

$$\text{porosity} = (1 - \rho / \rho_0) \times 100 \qquad (2\text{-}1)$$

where ρ is the apparent density of the membrane, calculated as the membrane weight divided by the volume of the membrane, and ρ_0 is the density of the bulk polymer (1.184 g/cm^3 provided by the supplier). To investigate the porosity effect on the pore size of the membrane, a hydraulic press machine (Catalog number 4386) from Carver, Inc. U.S.A was used to compress the membrane to different thicknesses.

The mean pore size, the maximum pore size, and the pore size distribution of the electrospun PAN membranes were determined by using a capillary flow porometer (Model # CFP-1500A, Porous Materials Inc., USA). A wetting fluid Galwick^{TM} (Porous

Materials Inc., USA) with a surface tension of 15.9 dynes/cm was used to wet the membrane and to fill the pores spontaneously. Under differential pressures of compressed air, the wetting liquid was gradually removed and the pores were successively opened. The air flow rates through the dry and wet membrane were recorded at different pressures. The pore size distribution, the maximum pore size and the mean pore size of the membrane were automatically calculated with the software (Capwin version 6.71.51) from Porous Materials Inc. (Ithaca, NY), based on the Young-Laplace equation [22],

$$D = \frac{4r}{\Delta P}\cos\theta \qquad (2\text{-}2)$$

where D is the maximum diameter of the pore, ΔP is the differential pressure, γ is the surface tension of the wetting reagent, and θ is the wetting angle. In the above equation, the pores are assumed to be cylindrical and straight. For pore shapes other than cylinder (e.g. non-woven media), a shape factor of 0.715 was multiplied on the right side of the above equation in the PMI report program, following American Society for Testing and Materials (ASTM) Designation F 316 [21,23]. The mean flow pore size is such that 50 % of the flow is through pores larger than it and 50 % of the flow is through pores smaller than it.

2.2.6 Particle rejection test

The particle rejection test was carried out in a lab built dead-end filtration system. A dead-end filtration cell with an effective area of 3.9 cm^2 (Catalogue Number: XX3002500, Millipore, USA) was used to hold the membrane. Polycarboxylate micro-particles with different nominal diameters (0.2 μm, 0.5 μm, 1.0 μm) was diluted in water, each to 200 ppm to serve as the feed solution. The total feed volume was 10 mL for each test and the applied pressure was kept at 5 psi. A total Organic Carbon (TOC) Analyzer

(Shimadzu Corporation, Japan) was used to measure the particle concentrations in the feed solution and the permeate solution through the membrane. The rejection ratio was calculated using the equation below,

$$\text{Rejection } (\%) = (1 - C_{\text{permeate}} / C_{\text{feed}}) \times 100 \qquad (2\text{-}3)$$

where $C_{permeate}$ and C_{feed} are the polycarboxylate concentration in the permeate and the feed solution, respectively.

2.3 Results and discussion

2.3.1 Control of nanofiber morphology and diameter

In order to systematically study the pore size of electrospun membrane, the morphology of the membrane has to be well tuned to achieve bead-less structure. The controls of fiber morphology and fiber diameter by adjusting electrospinning parameters including the applied voltage, flow rate as well as solution property were discussed as follows.

2.3.1.1 Electric filed effect

The solution combination of 0.5 wt% HMw PAN and 7.5 wt% LMw PAN (labeled as 0.5 H + 7.5 L for convenience of discussion) was used as the electrospinning solution to investigate the electric field effect on the fiber diameter. The applied flow rate was 35 μL/min.

Figure 2.1 shows the SEM images of electrospun nanofibers at different applied voltages. The structure of relatively uniform fiber diameters with no beads was achieved, indicating that the jet was very stable in the experimental voltage range. The average diameter of the nanofibers were 682 ± 62 nm, 562 ± 89 nm, 528 ± 30 nm in accordance

with the applied voltage of 19 kV, 22 kV, 25 kV, respectively at the spinneret tip-to-collector distance of 7.5 cm, showing a decreasing tendency of the fiber diameter with increasing voltage. In the electrospinning process, a higher voltage contributed to greater columbic forces in the jet, which resulted in higher stretching force on the jet stream and led to thinner nanofibers [24]. However, another effect of voltage on the fiber diameter was that, with the higher voltage, the jet stream flight time from the spinneret to the collector was reduced, and the jet stretching time was shortened, which could lead to an adverse effect in reducing the fiber diameter. But from the experimental results it was seen this adverse effect of increasing voltage in the fiber was not in the dominating role.

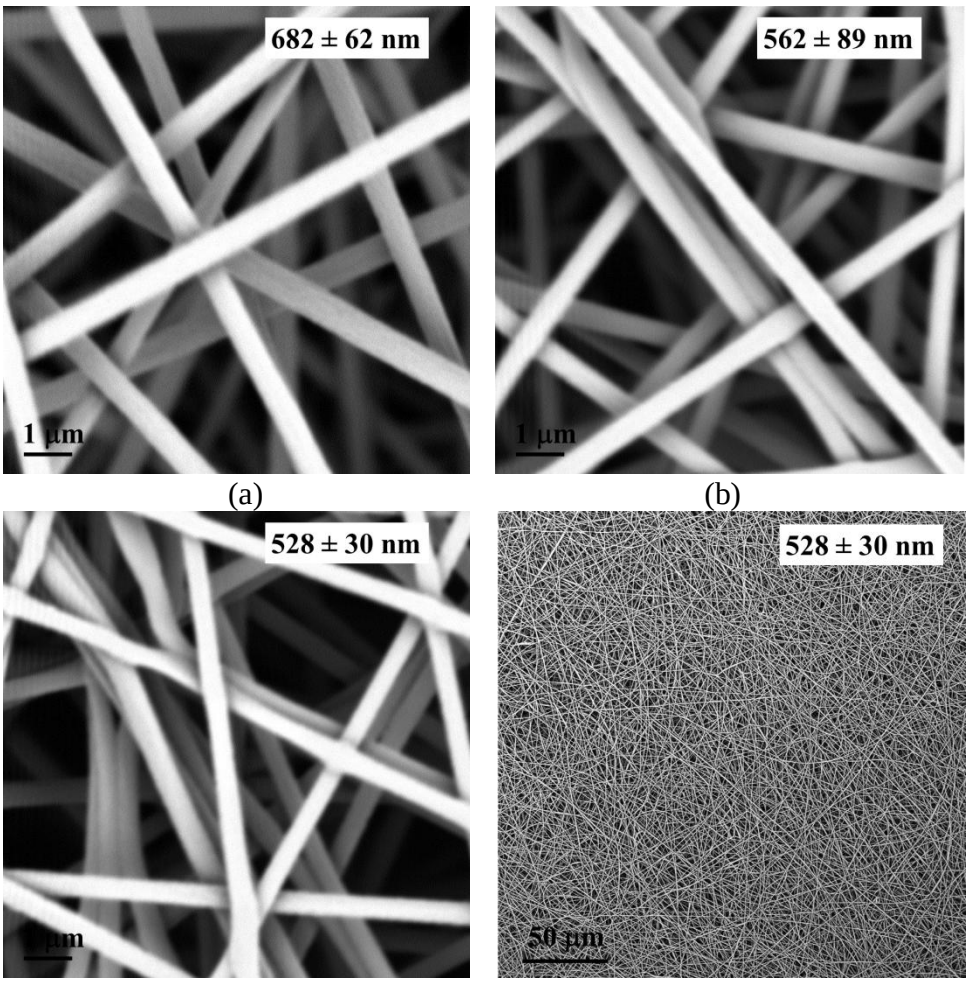

Figure 2.1 SEM images of PAN nanofibers electrospun at (a) 19 kV; (b) 22 kV; (c) 25 kV (d) membrane (c) at the magnification of 500 ×(scale bar: 1 μm; electrospinning solution: 0.5 H + 7.5 L; flow rate: 35 μL/min; spinneret tip-to-collector distance: 7.5 cm, humidity: 55% ±5%, temperature: 24 ℃ ±1 ℃)

2.3.1.2 Flow rate effect

Flow rate determines the amount of the solution available for the electrospinning process. As shown in Figure 2.2, the average fiber diameter increases with a corresponding increase in the flow rate. The average fiber diameter electrospun at flow rates of 25 μl/min, 35 μl/min, 45 μl/min and 55 μl/min ranged from 497 ± 55 nm, 528 ± 30 nm, 581 ± 61 nm, and 612 ± 55 nm, respectively. The increase could partially be due to a greater volume of the solution that was drawn away from the needle tip at the higher flow rates [7]. Another observation was that uniform nanofibers were produced and no beads were formed even at a high flow rate of 55 μl/min. Although the flow rate doubled from 25 μl/min to 55 μl/min, the fiber diameter increased only from an average of 497 nm to 612 nm, or by 23%, indicating that flow rate could provide a limited range for adjusting the range of the nanofiber diameter. On the other hand, a higher flow rate may induce solution dripping from the spinnerets, especially at high solution viscosity. A lower flow rate of 25 μl/min was used for subsequent experiments.

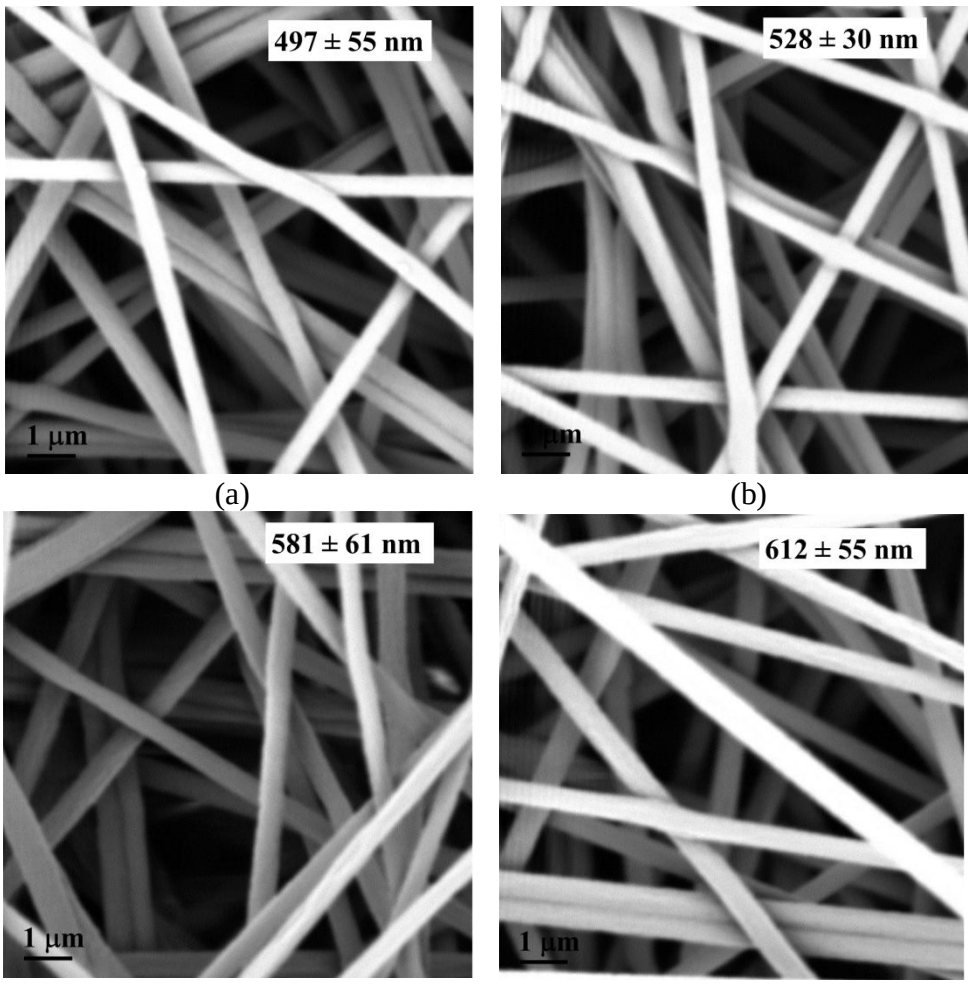

Figure 2.2 SEM images of electrospun PAN nanofibers from solution consisting of 0.5 H + 7.5 L and a flow rate of (a) 25 μl/min; (b) 35 μl/min; (c) 45 μl/min; (d) 55 μl/min (scale bar: 1 μm; applied voltage: 25 kV, spinneret tip-to-collector distance: 7.5 cm, humidity: 55% ±5%, temperature: 24 ℃ ±1 ℃)

2.3.1.3 Solution property effect

One of the conditions necessary for electrospinning to occur and fibers to form is that the solution must be at concentrations above the overlap concentration. During the jet stretching process, it is primarily the entanglement of the macromolecular chains that prevents the electrically driven jet from breaking up and thereby maintaining a continuous jet stream [25]. Many studies have reported that a minimum concentration of polymer solution is required for smooth fiber formation [26-29]. Our previous studies showed that for the LMw PAN (Mw = 150,000 g/mol, radius of gyration = 21 nm [30], overlap concentration = 0.71 wt%), the bead-dominated structures were formed when the polymer solution concentration was below 4 wt% [31], and the dripping was still considerable at 6 wt%. By blending a small amount of HMw PAN into the LMw PAN solution, an obvious effect on improving the ability for the polymer solution to undergo better electrospinning could be achieved. By blending 0.1 wt% HMw PAN and maintaining the total concentration at 6 wt%, the appearance of beads was greatly reduced as shown, while the fiber diameter was barely changed, as shown in Figure 2.3.

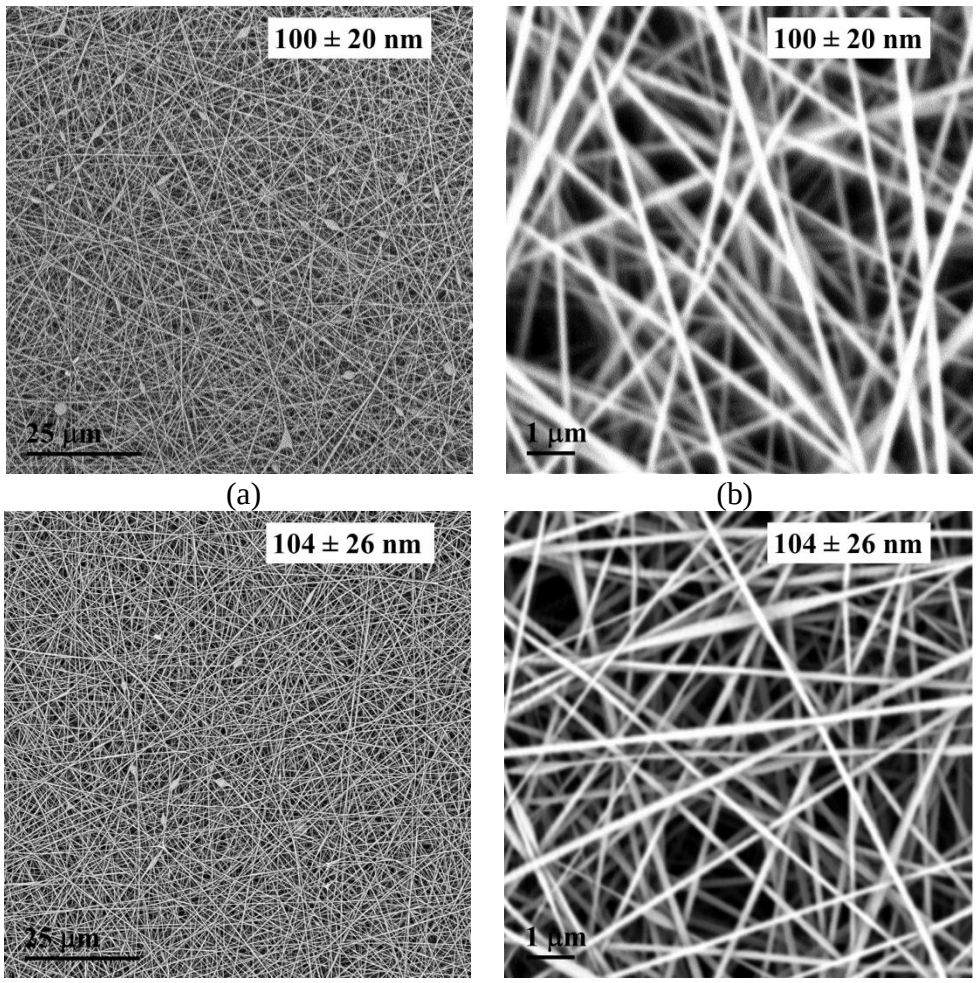

Figure 2.3 SEM images of membranes electrospun from (a) 6 wt% LMw PAN solution at the magnification of 2,000 ×; (b) 6 wt% LMw PAN solution at the magnification of 20,000 ×; (c) 0.1 H + 5.9 L PAN solution at the magnification of 2,000 ×; (d) 0.1 H + 5.9 L PAN solution at the magnification of 20,000 × (applied voltage: 25 kV, spinneret tip-to-collector distance: 7.5 cm, humidity: 55 % ±5 %, temperature: 24 ℃ ±1 ℃)

Solution viscosities of different combinations of two PANs and the resulting fiber diameters are listed in Table 2.1. Uniform nanofibers with diameters ranging from 104 nm to 655 nm were prepared. It can be seen that when the concentration of HMw PAN was constant at 0.1 wt%, the solution viscosity increased with the concentration of LMw PAN, and there was a sharp increase in the solution viscosity at the LMw PAN concentration from 10 wt% to 11 wt%. The average fiber diameter increased from 104 nm to 430 nm when the LMw concentration was increased from 5.9 wt% to 11 wt%. When fixing the total concentration of PAN at 8 wt% and tuning the ratios of HMw PAN to LMw PAN (0.1:7.9, 0.3:7.7, 0.5:7.5, 0.7:7.3), it was found that by increasing the ratio of HMw to LMw PAN, the solution viscosity was increased from 507 cp to 614 cp, 706 cp and 871 cp, due to an increase in the effective overlap concentration which could be translated into higher polymer chain entanglement. The extent of the jet being stretched during traveling down to the collector therefore became less. Accordingly, the average fiber diameter was increased from 160 nm to 264 nm, 497 nm and 655 nm, respectively. The observation that the fiber diameter became large with an increase of solution viscosity was in consistence with the results obtained by many other researchers [15,32-34] .

It should also be noted that when both the total polymer concentration and the HMw-to-LMw PAN ratio was varied, viscosity was not the only determining parameter in the fiber diameter. By comparing the solution at 0.1 H + 11.0 L with that at 0.7 H + 7.3 L, the former solution had a higher viscosity of 2.77×10^3 cP and the latter one had 871 cP, the fiber diameter, however, was only 430 nm, not much thinner than the 655 nm of the latter system. A similar result was seen for the solutions of 0.3 H +7.7 L and 0.5 H + 5.5

L. While the viscosities of two solutions were much different, being 614 cP and 306 cP, respectively, the fiber diameter were almost the same to be around 260 nm.

Table 2.1 Solution viscosity and electrospun nanofiber diameter at different total PAN concentrations and HMw PAN-to-LMw PAN ratios

Electrospinning solution HMw + LMw PAN concentration (%)	Viscosity (cp)	Mean fiber diameter (nm)
0.1 + 5.9	152	104 ± 26
0.1 + 7.9	507	160 ± 26
0.1 + 10	1161	355 ± 54
0.1 + 11	2767	430 ± 71
0.3 + 7.7	614	264 ± 40
0.5 + 5.5	306	256 ± 38
0.5 + 7.5	706	497 ± 55
0.5 + 10	1677	553 ± 64
0.7 + 7.3	871	655 ± 195

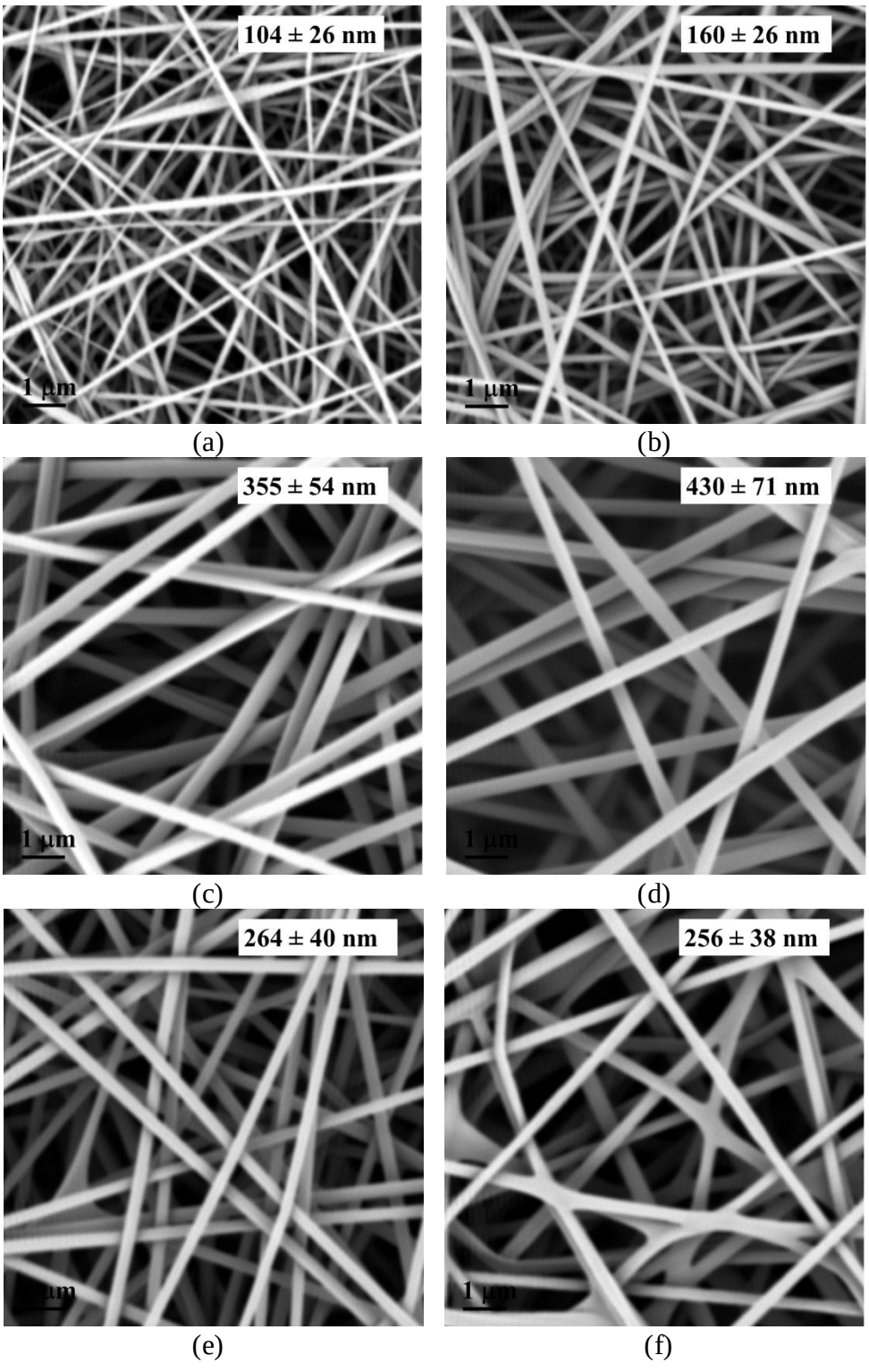
104 ± 26 nm
1 μm
160 ± 26 nm
1 μm
355 ± 54 nm
1 μm
430 ± 71 nm
1 μm
264 ± 40 nm
256 ± 38 nm
1 μm

(a) (b)

(c) (d)

(e) (f)

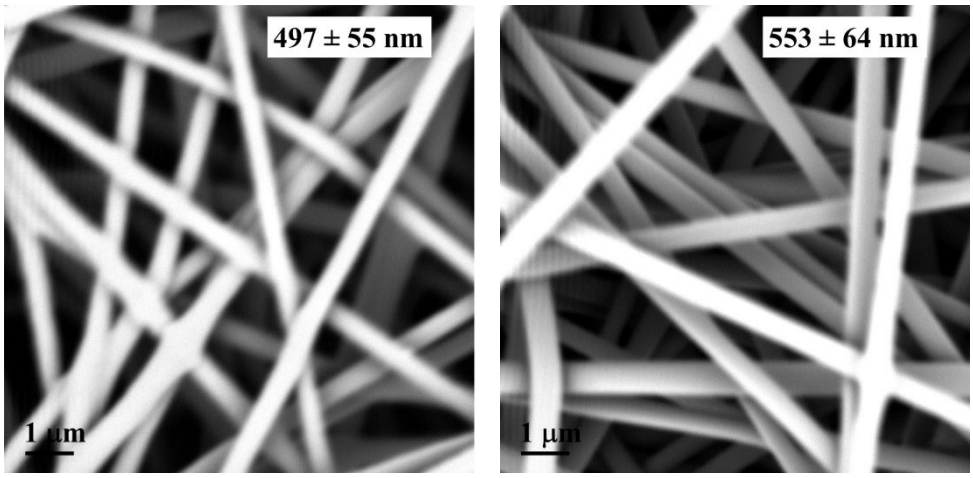

(g) (h)

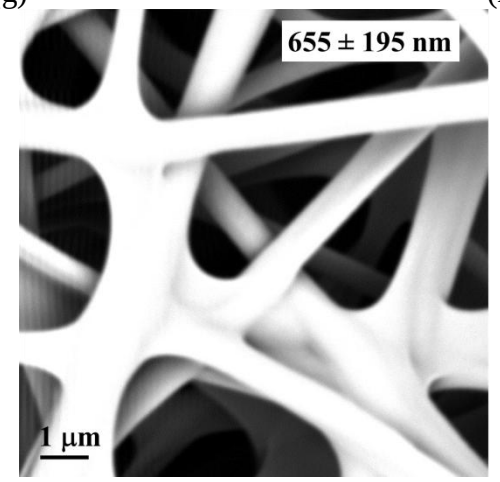

(i)

Figure 2.4 SEM images of PAN membranes electrospun from solution (a) 0.1 H + 5.9 L; (b) 0.1 H + 7.9 L; (c) 0.1 H + 10.0 L; (d) 0.1 H + 11.0 L; (e) 0.3 H + 7.7 L; (f) 0.5 H + 5.5 L; (g) 0.5 H + 7.5 L (h) 0.5 H + 10.0 L; (i) 0.7 H + 7.3 L at a flow rate of 25 μl/min (scale bar: 1 μm; applied voltage: 25 kV, spinneret tip-to-collector distance: 7.5 cm, humidity: 55% ±5%, temperature: 24 ℃ ±1 ℃)

2.3.2 Studies of pore size and particle rejection ability of electrospun nanofibrous membrane

Pore size properties of electrospun membranes, such as maximum pore size, mean pore size and pore size distribution, are essential information to many of the membrane applications, such as tissue engineering, air filtration and liquid filtration. The effects of some structural properties on pore size were thoroughly studied. The capillary flow porometry was used to quantitatively characterize the maximum flow pore size, mean flow pore size and the pore size distribution. The membranes with different pore sizes were also tested for their capability to reject spherical particles with different sizes.

2.3.2.1 Membrane thickness effect on pore size

The effect of membrane thickness was investigated with the membranes electrospun from two solutions 0.3 H +7.7 L and 0.1 H +7.9 L at a flow rate of 25 μl/min, an applied voltage of 25 kV and a spinneret tip-to-collector distance of 7.5 cm. The thickness of membranes was measured by using a micrometer. Membranes with average thicknesses of 20 μm, 40 μm, 60 μm, 80 μm, 100 μm, 200 μm, 300 μm were prepared, with the relative standard error being within 5 %. The porosity of each membrane was measured to be within 80.0 % ±2.0 %.

Figure 2.5 shows the typical dry curve and wet curve obtained from the capillary flow porometry, with the sample being the electrospun PAN membrane from a solution of 0.3 H + 7.7 L with an average thickness of 100 μm. Figure 2.6 shows the pore size distribution of the membrane calculated from the data in Figure 2.5. The maximum pore size was in correspondence to the initial bubble point, i.e., when the initial flow was detected. It was calculated based on Young-Laplace equation using the bubble point

pressure, and was 0.87 μm. The mean flow pore size was 0.61 μm calculated from the pressure at the intersecting point of the half dry curve and the wet curve.

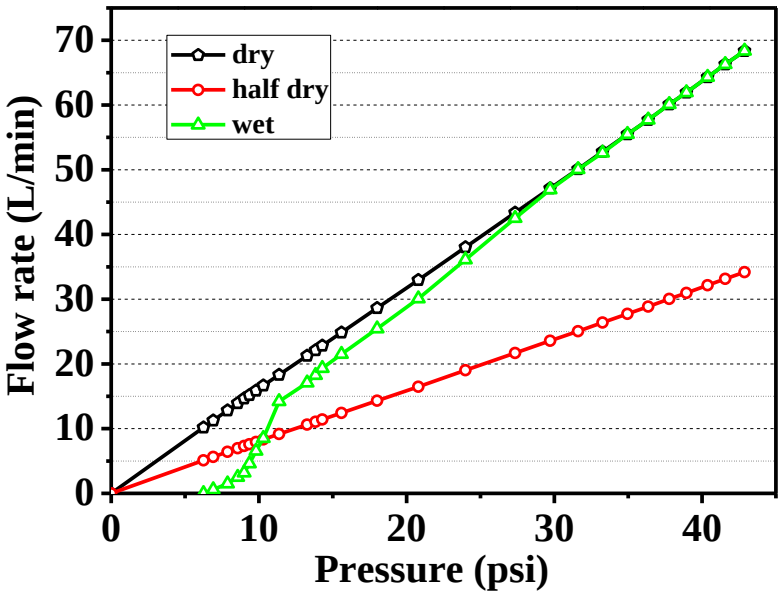

Figure 2.5 Wet and dry curves of electrospun PAN membrane obtained from the capillary flow porometry (electrospinning solution: 0.3 H + 7.7 L, membrane thickness: ~ 100 μm, fiber diameter: 264 ±40 nm, membrane porosity: 81.8 % ±0.8 %)

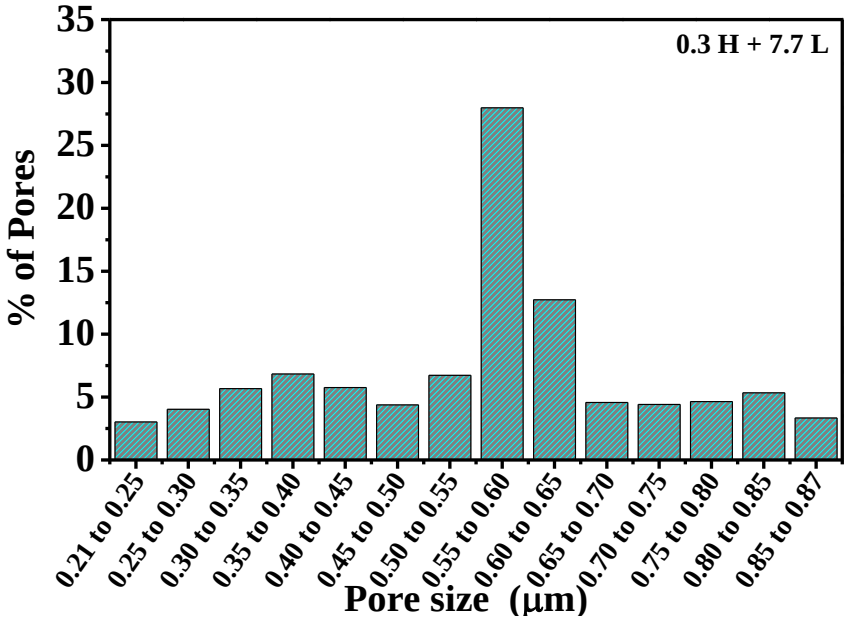

Figure 2.6 Pore size distribution of electrospun PAN membrane obtained from the capillary flow porometry (electrospinning solution: 0.3 H + 7.7 L, membrane thickness: ~ 100 μm, fiber diameter: 264 ±40 nm, membrane porosity 81.8 % ±0.8%)

Table 2.3 summarizes the maximum pore size and the mean pore size at different membrane thicknesses. Results showed that for the membranes electrospun from both solutions, by increasing the membrane thickness from 20 μm to 80 μm, the maximum pore size and mean pore size for the membrane gradually decreased. This could be explained as follows. Thicker membranes were produced by depositing more fibers on the substrate. As the pores of the electrospun membrane were caused by the entanglement of fibers, with other variables (such as fiber diameter and fiber length) being fixed, more fibers crossing a certain volume should result in smaller pores. It should also be noted that as the electrospun membranes became thicker, e.g., 100 μm and beyond, the mean pore size of the electrospun membranes showed very little or no change (Figure 2.7). This observation should suggest that for the electrospun PAN membranes, the membrane thickness did not play an important role in reducing the pore size when it had reached ~100 μm and beyond, in agreement with results from the literature [16].

Along with the maximum and mean flow pore size changes, the pore size distribution also have shifted to a smaller pore size range with the thickness increasing in the range below 100 μm. This could be seen when comparing the pore size distribution of the membrane electrospun from the solution 0.3 H + 7.7 L at a thickness of 20 μm (Figure 2.8) to that of the membrane electrospun from the same solution at a thickness of 100 μm(Figure 2.6).

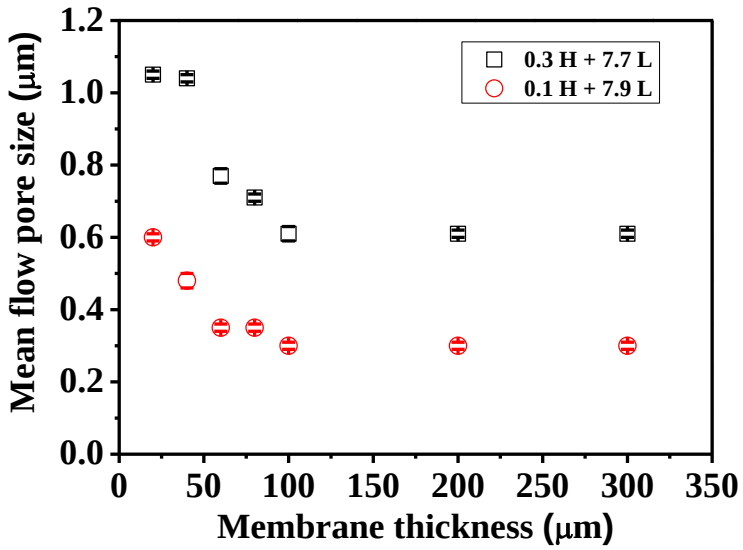

Figure 2.7 Change of mean flow pore size of electrospun membranes as a function of membrane thickness (-□- membrane electrospun from the polymer solution 0.3 H+ 7.7 L with an average fiber diameter of 264 ± 40 nm and a membrane porosity of ~ 80 %; and -○- membrane electrospun from the polymer solution 0.1 H + 7.9 L with an average fiber diameter of 160 ± 26 nm and a membrane porosity of ~ 80 %)

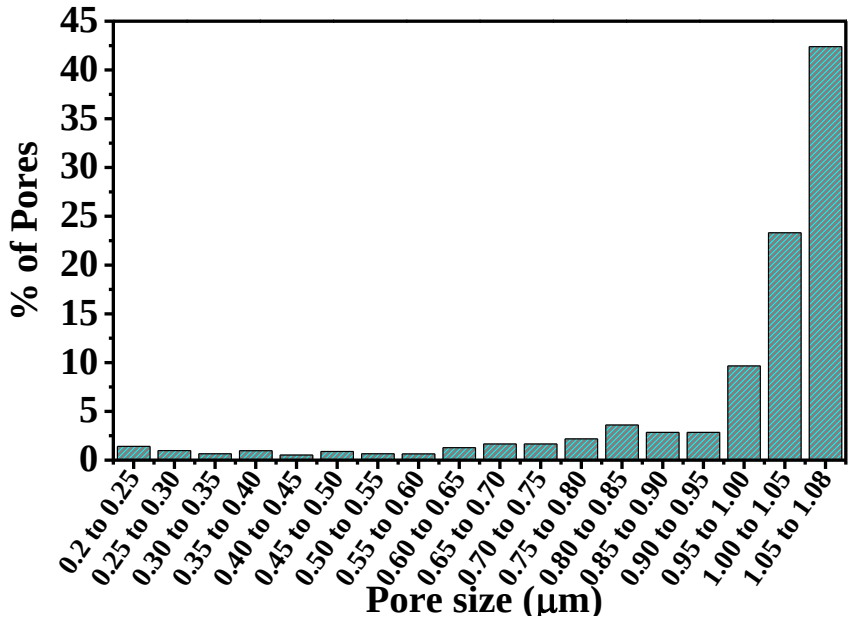

Figure 2.8 Pore size distribution of electrospun PAN membrane obtained from the capillary flow porometry (electrospinning solution: 0.3 H+7.7 L, membrane thickness: ~ 20 μm, fiber diameter: 264 ± 40 nm, membrane porosity 81.0 ± 0.7%)

The effect of the membrane thickness on the pore size was also confirmed by the particle rejection test. By considering the membranes electrospun form 0.3 H + 7.7 L as an example, we can see from Table 2.2 that at a membrane thickness of 20 μm and 40 μm, the membrane rejection ratios for the 0.5 μm particle suspension were almost identically low at 27 %. By increasing the membrane thickness, the rejection ratio was increased to about 50 % at a thickness of 60 μm and close to around 58 % at a thickness of 80 μm and beyond. The same trend has also been observed in the rejection tests for the 1.0 μm particle suspension. But for the 0.2 μm particle suspension, the membranes showed mere rejection ratios despite of the membrane thickness, as almost all the pore were greater than 0.2 μm even at a membrane thickness of ~ 100 μm from the pore size distribution measurement (Figure 2.6). For the membranes electrospun from the 0.1 H + 7.9 L solution, as the pore sizes were measured to be smaller than those of membranes from the 0.3 H + 7.7 L solution, the rejection ratio to the corresponding particle suspensions were shown to be higher. It was also notable that all membranes produced from the 0.1 H + 7.9 L solution demonstrated a rejection ratio of greater than 95 % to the 0.5 μm particle suspension, which indicated they could be used as the microfiltration filter to effectively remove *E. coli* or other bacteria with the size of 0.5 μm or greater from aqueous solution [31].

Table 2.2 Pore size properties of electrospun membranes at different thickness and their performance in the particle rejection test

Electro-spinning solution	Membrane thickness (μm)	Maximum pore size[1] (μm)	Mean flow pore size[2] (μm)	Rejection ratio (%) to particle suspension with nominal size of		
				1.0 μm[a]	0.5 μm[b]	0.2 μm[c]
0.3 H+7.7 L	20	1.08 ±0.01	1.05 ±0.01	82.6 ±1.1	27.3 ±1.3	< 1
	40	1.05 ±0.02	1.04 ±0.01	82.5 ±0.8	27.8 ±1.1	
	60	0.90 ±0.01	0.77 ±0.02	83.5 ±1.2	50.7 ±0.8	
	80	0.90 ±0.01	0.71 ±0.01	85.0 ±0.8	56.7 ±1.2	
	100	0.87 ±0.01	0.61 ±0.02	87.0 ±0.7	58.1 ±0.9	
	200	0.87 ±0.01	0.61 ±0.01	86.5 ±1.9	58.6 ±1.8	
	300	0.87 ±0.01	0.61 ±0.01	87.5 ±0.5	58.0 ±1.5	
0.1H+7.9 L	20	0.73 ±0.02	0.60 ±0.01	> 98	> 95	< 4
	40	0.72 ±0.01	0.48 ±0.02			
	60	0.71 ±0.01	0.35 ±0.01			
	80	0.72 ±0.01	0.35 ±0.01			
	100	0.71 ±0.01	0.30 ±0.01			
	200	0.71 ±0.01	0.30 ±0.01			
	300	0.71 ±0.01	0.30 ±0.01			

[1] Maximum pore size was calculated based on the initial bubble point pressure
[2] Mean flow pore size was calculated based on the pressure at the intersecting point of the half dry curve and the wet curve
[a] Mean particle size: 1.03 ±0.01 μm, obtained from the supplier
[b] Mean particle size: 0.489 ±0.013 μm, obtained from the supplier
[c] Mean particle size: 0189 ±0.011 μm, obtained from the supplier

2.3.2.2 Fiber diameter effect on pore size

To address the effect of the fiber diameter on the pore size, the electrospun membranes with fiber diameters ranging from 104 nm to 655 nm were prepared at a thickness of 100 μm, where the pore size became relatively insensitive to the thickness.

Table 2.3 summarizes the results on membrane porosity and mean flow pore size of membranes with different fiber diameters. The pore size distributions of corresponding membranes were plotted in Figure 2.9. It should be noted that the porosity of all membranes was all in the range of 80 ~ 82 %, which was the typical porosity of electrospun nanofibrous membranes using the current set up. At constant porosity, the pore size distribution shifted rightwards and the mean flow pore size showed a steady increase with increasing fiber diameter. The change in the mean flow pore size with the fiber diameter is shown in Figure 2.10. A good linear relationship with $R^2 = 0.98$ was obtained, and the mean flow pore size was found to be almost twice of the fiber diameter. For example, the membrane electrospun from solution 0.1 H + 5.9 L had an average fiber diameter of 104 ± 26 nm, and the mean flow pore size was 0.22 ± 0.02 μm, about 2.1 times of the fiber diameter. The solution 0.7 H + 7.3 L produced a membrane with an average fiber diameter of 655 ± 195 nm and a mean flow pore size of 1.30 ± 0.03 μm, corresponding to twice the mean-flow pore-size-to-fiber-diameter ratio.

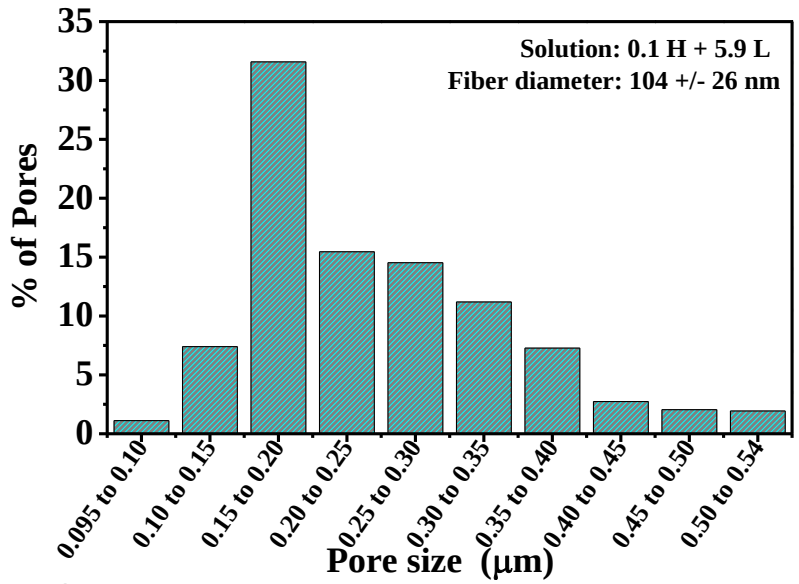
Solution: 0.1 H + 5.9 L
Fiber diameter: 104 +/- 26 nm
% of Pores
0
5
10
15
20
25
30
35
0.095 to 0.10
0.10 to 0.15
0.15 to 0.20
0.20 to 0.25
0.25 to 0.30
0.30 to 0.35
0.35 to 0.40
0.40 to 0.45
0.45 to 0.50
0.50 to 0.54
Pore size (μm)

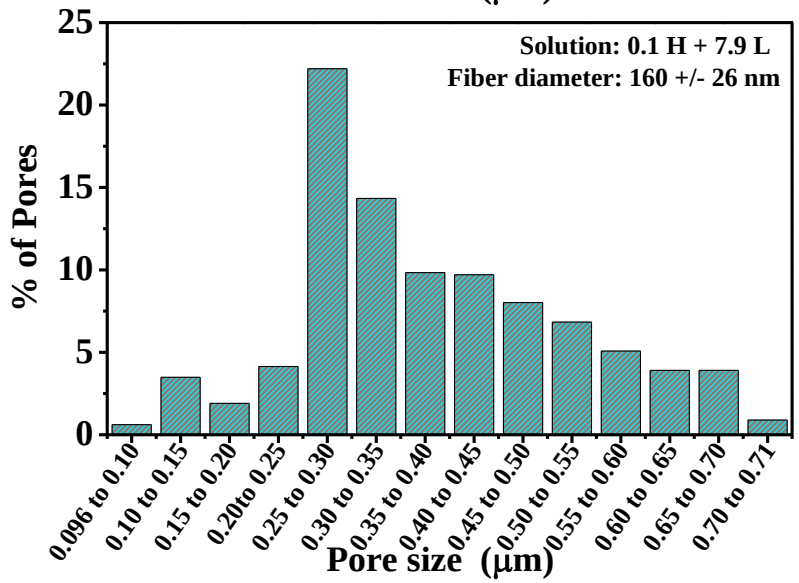
Solution: 0.1 H + 7.9 L
Fiber diameter: 160 +/- 26 nm
% of Pores
0
5
10
15
20
25
0.096 to 0.10
0.10 to 0.15
0.15 to 0.20
0.20to 0.25
0.25 to 0.30
0.30 to 0.35
0.35 to 0.40
0.40 to 0.45
0.45 to 0.50
0.50 to 0.55
0.55 to 0.60
0.60 to 0.65
0.65 to 0.70
0.70 to 0.71
Pore size (μm)

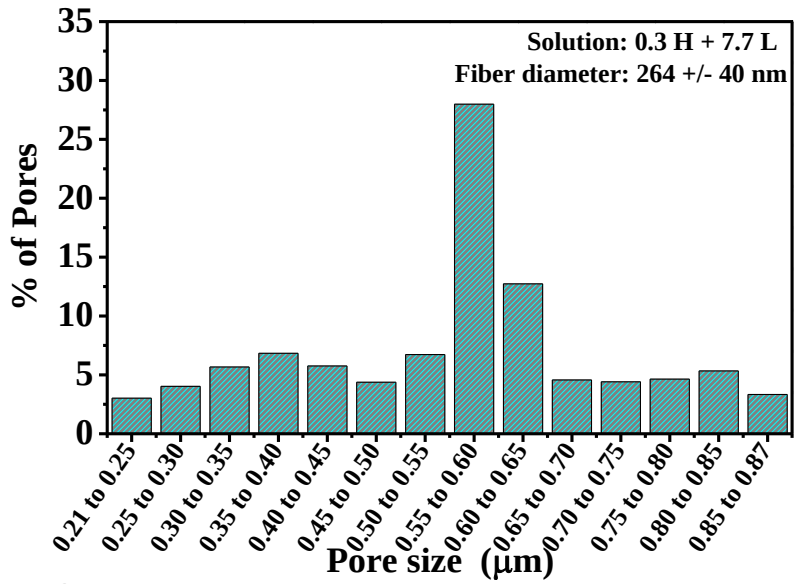
Solution: 0.3 H + 7.7 L
Fiber diameter: 264 +/- 40 nm
% of Pores
0
5
10
15
20
25
30
35
0.21 to 0.25
0.25 to 0.30
0.30 to 0.35
0.35 to 0.40
0.40 to 0.45
0.45 to 0.50
0.50 to 0.55
0.55 to 0.60
0.60 to 0.65
0.65 to 0.70
0.70 to 0.75
0.75 to 0.80
0.80 to 0.85
0.85 to 0.87
Pore size (μm)

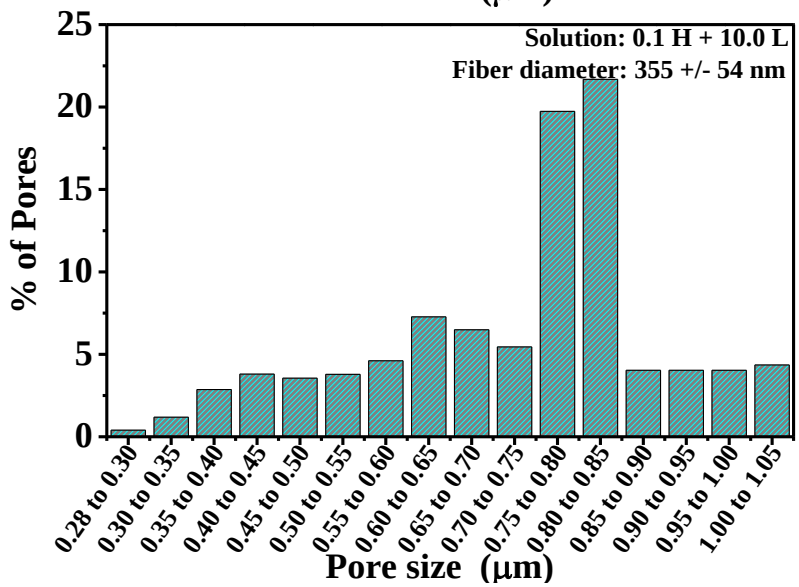
Solution: 0.1 H + 10.0 L
Fiber diameter: 355 +/- 54 nm
% of Pores
0
5
10
15
20
25
0.28 to 0.30
0.30 to 0.35
0.35 to 0.40
0.40 to 0.45
0.45 to 0.50
0.50 to 0.55
0.55 to 0.60
0.60 to 0.65
0.65 to 0.70
0.70 to 0.75
0.75 to 0.80
0.80 to 0.85
0.85 to 0.90
0.90 to 0.95
0.95 to 1.00
1.00 to 1.05
Pore size (μm)

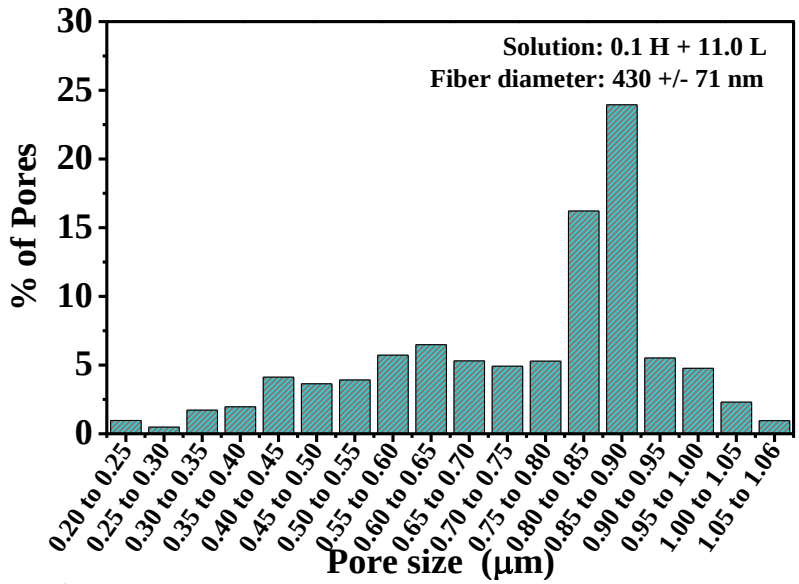
Solution: 0.1 H + 11.0 L
Fiber diameter: 430 +/- 71 nm
% of Pores
Pore size (μm)
0
5
10
15
20
25
30
0.20 to 0.25
0.25 to 0.30
0.30 to 0.35
0.35 to 0.40
0.40 to 0.45
0.45 to 0.50
0.50 to 0.55
0.55 to 0.60
0.60 to 0.65
0.65 to 0.70
0.70 to 0.75
0.75 to 0.80
0.80 to 0.85
0.85 to 0.90
0.90 to 0.95
0.95 to 1.00
1.00 to 1.05
1.05 to 1.06

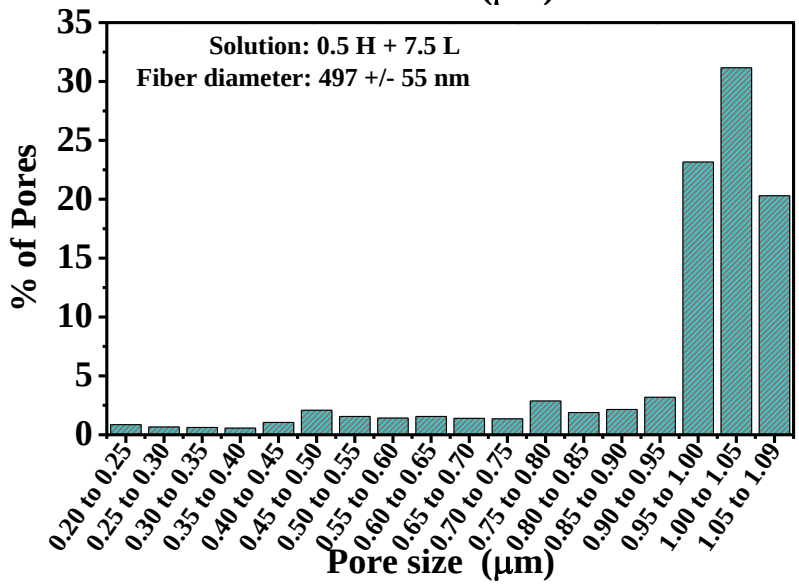
Solution: 0.5 H + 7.5 L
Fiber diameter: 497 +/- 55 nm
% of Pores
Pore size (μm)
0
5
10
15
20
25
30
35
0.20 to 0.25
0.25 to 0.30
0.30 to 0.35
0.35 to 0.40
0.40 to 0.45
0.45 to 0.50
0.50 to 0.55
0.55 to 0.60
0.60 to 0.65
0.65 to 0.70
0.70 to 0.75
0.75 to 0.80
0.80 to 0.85
0.85 to 0.90
0.90 to 0.95
0.95 to 1.00
1.00 to 1.05
1.05 to 1.09

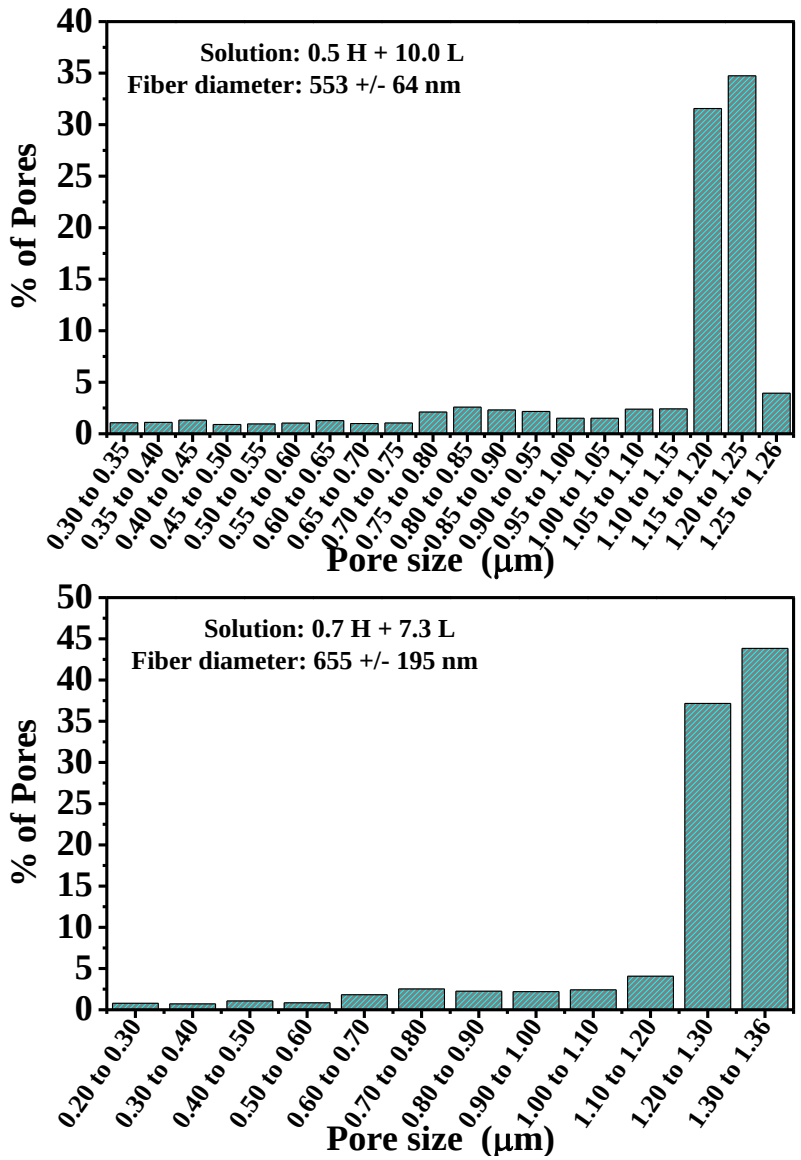

Figure 2.9 Pore size distributions of electrospun PAN membranes from different PAN solutions. All membranes have a thickness of ~100 μm and a porosity of ~ 80 %

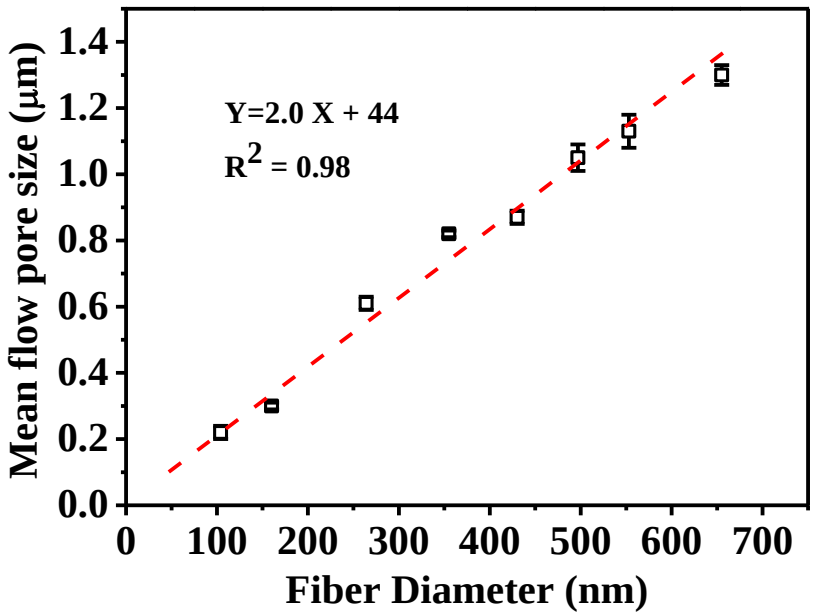

Figure 2.10 Relationship of mean flow pore size of electrospun membrane and average fiber diameter at constant membrane thickness and porosity (Membrane thickness: ~ 100 μm, porosity ~ 80 %)

The linear relationship finding above from the porometry was also in agreement with results from other studies using SEM measurements or 2D simulation [17,18]. Li et al. proposed that when linking both fiber mass and fiber diameter, fiber length could be used as a single reference parameter in evaluation of pore sizes. In our studies, for the membranes with different fiber diameters, the membrane weight, membrane thickness and area were statistically identical in the experiments, and therefore so was the porosity. Assuming the fibers were cylindrical in shape, let m be the membrane weight, ρ_0 be the density of PAN, V be the total volume of the nanofibers, D be the average fiber diameter, L be the total fiber length in the membrane, and P be the mean flow pore size. The relationship of total fiber length with the fiber diameter can be derived as follows,

$$V = \frac{m}{\rho_0} = \pi\left(\frac{D}{2}\right)^2 L \tag{2-4}$$

$$L = \frac{4m}{\rho_0 \pi D^2} \tag{2-5}$$

Since m is the same for all membrane, the above equation indicates the total fiber length L is inversely proportional to the square of fiber diameter D. While in a confined space, membranes with smaller fibers have longer fiber length, which increases the probability of bisecting pores and generate smaller pore sizes. More specifically under the above conditions (membranes with identical weight, thickness and porosity) in our studies, and the mean flow pore size is proportional to the fiber diameter, it could be inferred that the mean flow pore size has the following relationship with the fiber length

$$P \sim D \sim \frac{1}{\sqrt{L}} \tag{2-6}$$

The results of the particles challenge test using the 0.5 μm spherical bead suspension are listed in the last column in Table 2.3. It was noted that for the membrane electrospun from the solution 0.1 H + 5.9 L, the maximum pore size was 0.54 μm, and very few pores (~ 2%) were greater than 0.5 μm (Figure 2.9), and therefore a high rejection ratio of greater than 98 % was achieved. As the fiber diameter increased to 264 ± 40 nm for the membrane from the solution 0.3 H + 7.7 L, the overall membrane pore sizes became larger, and the rejection ratios dropped to 58.1%, which indicated it would not be a suitable filter to be used for removal of bacteria such as *E. coli.* For the membranes with a fiber diameter greater than 355 ± 54 nm, very few pores were populated below 0.5 μm as seen in the pore size distribution measurement, and therefore the rejection ratios to the 0.5 μm particles were very low (< 1%).

It should be noted that in the particle rejection process of a microfiltration membrane, besides size exclusion, many other mechanisms can result in or affect the rejection, such as rejections due to inner membrane fouling or cake layer formation on the surface. In the latter case, the fouling speed should also be affected by factors such as membrane pore size, concentration of particle suspension and applied pressure on the membrane. Therefore, the rejection ratio of a membrane may vary under different experimental conditions.

Table 2.3 Porosity and mean flow pore size of electrospun membranes at different fiber diameters and their corresponding rejection ratio to the 0.5 μm particle suspension

Electrospinning solution	Fiber diameter (nm)	Porosity (%)	Mean flow pore size (μm)	Rejection rate to 0.5 um particle suspension (%)
0.1 L+5.9 H	104 ±26	81.7 ±0.8	0.22 ±0.02	> 98
0.1 L+ 7.9 H	160 ±26	82.2 ±0.8	0.30 ±0.01	96.7 ±1.3
0.3 L+ 7.7 H	264 ±40	81.8 ±0.8	0.61 ±0.02	58.1 ±0.9
0.1 L+ 10 H	355 ±54	80.1 ±0.8	0.82 ±0.01	2.9 ±0.7
0.1 L+ 11 H	430 ±71	80.7 ±0.9	0.87 ±0.02	< 1
0.5 L+ 7.5 H	497 ±55	81.8 ±1.0	1.05 ±0.04	
0.5 L+ 10 H	553 ±64	80.8 ±0.6	1.13 ±0.05	
0.7 L+ 7.3 H	655 ±195	79.7 ±1.1	1.30 ±0.03	

2.3.2.3 Porosity effect on pore size

The studies above were all carried out on the electrospun membrane with a porosity of about 80 %, being a typical value of the porosity for the naturally electrospun membranes. However, in some of the membrane applications, the membrane could undergo compression due to high applied pressure (such as in the application as a substrate used in the reverse osmosis membrane), or other membrane post-treatment involving substantial compression. It is therefore worth investigating the pore size change resulting from a reduction in the third dimension, responsible to the membrane thickness.

Figure 2.11(a) shows the cross-sectional SEM images of the as-spun membrane from the PAN solution 0.3 H + 7.7 L with a membrane thickness of 200 μm, and (b) ~ (e) show the membrane after being compressed at different pressures, with the resulting porosities ranging from 75.8 % to 31.3 %. For membranes with a porosity of greater than 70 %, non-uniform and large void space was observed in the cross-membrane direction. The dimension of the void space became visibly decreased when the membrane was compressed to a porosity of ~ 55 % (Figure 2.11(c)). When the membrane was compressed to the porosity of ~ 40 % or less, the nanofibers became greatly twisted or even fused together (Figure 2.11(e)), and almost filled up the void space in the third dimension of the membrane.

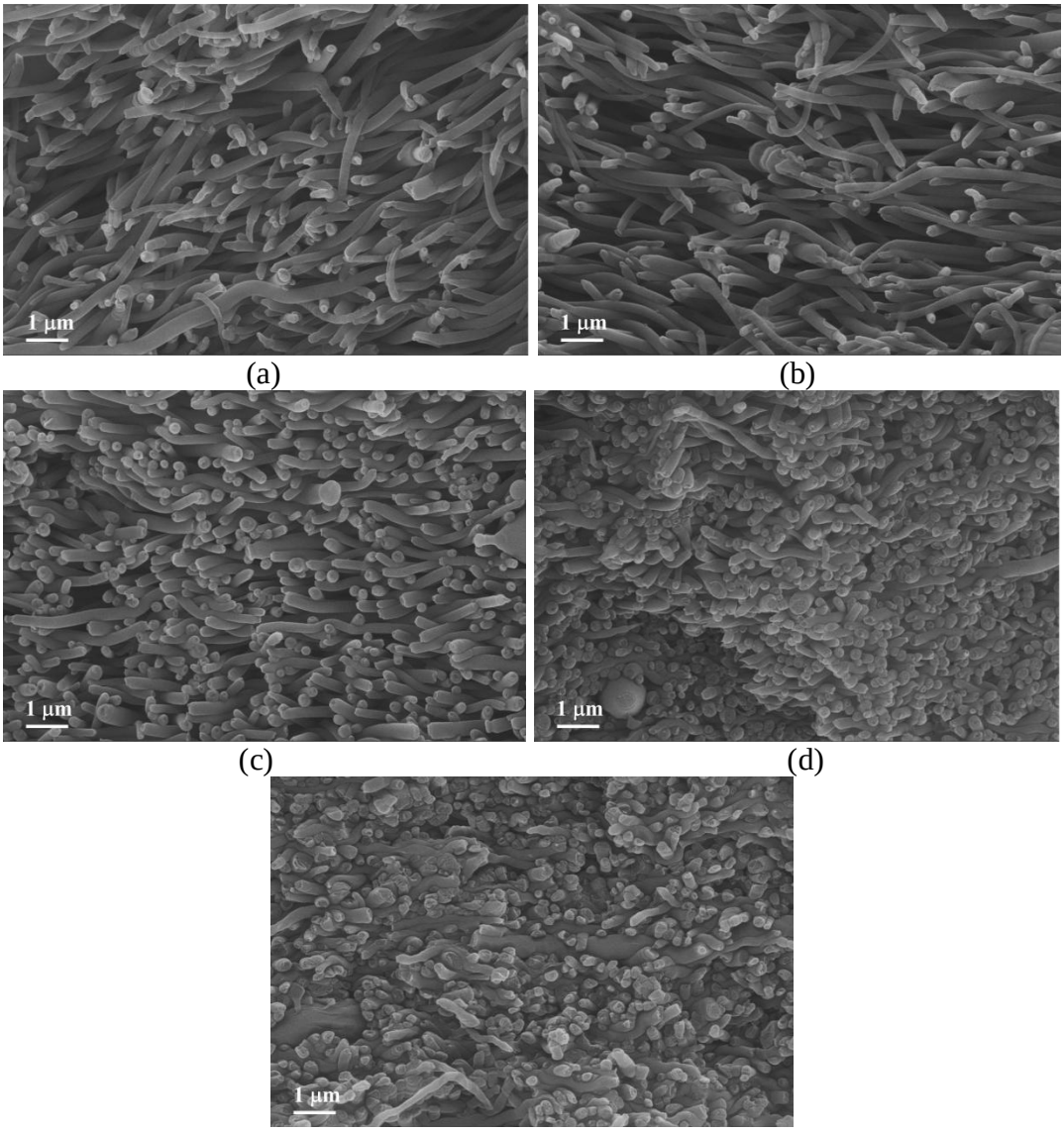

Figure 2.11 SEM images of the cross-section of membranes electrospun from the solution 0.3 H + 7.7 L with a porosity of (a) 81.9 % ± 0.8 %; (b) 75.8 % ± 0.8 %; (c) 54.4 % ± 2.2 %; (d) 39.3 % ± 2.9 %; (e) 31.3 % ± 2.7 %

The mean pore size and mean flow pore size, as well as the particle rejection ratio of the membranes at different porosities are shown in Table 2.4. As the membrane was compressed and the porosity was reduced, the maximum and mean pore size both showed an obvious decrease. For example, for the membranes prepared from the solution 0.3 H + 7.7 L, the mean flow pore size was reduced from 0.61 $\pm$ 0.02 μm to 0.30 $\pm$ 0.01 μm and 0.15 $\pm$ 0.01 μm, respectively, when the porosity was reduced from 81.8 % $\pm$ 0.8 % to 54.5 % $\pm$ 2.2 % and 31.3 % $\pm$ 2.7 %. For membranes electrospun from the solution 0.1 H + 7.9 L, the same trend on the pore size was also observed in relation with the porosity. The mean flow pore size was decreased from 0.30 $\pm$ 0.01 μm to 0.1 μm as the porosity of the membrane was lowered down from the original porosity of 82.2 % $\pm$ 0.8 % to 56.6 % $\pm$ 2.1 %.

Table 2.4 Maximum pore size, mean flow pore size and particle challenge test results at different membrane porosities

Electro-spinning solution	Membrane porosity (%)	Maximum pore size (μm)	Mean pore size (μm)	Rejection rate (%) to particle suspension with nominal size of		
				1.0 μm	0.5 μm	0.2 μm
0.3 H+7.7 L	81.8 ±0.8	0.87 ±0.01	0.61 ±0.02	> 98	58.1 ±0.9	< 3
	75.8 ±0.8	0.76 ±0.02	0.43 ±0.02		62.4 ±0.6	
	54.5 ±2.2	0.52 ±0.01	0.30 ±0.01		75.9 ±0.8	
	39. 3 ±2.9	0.38 ±0.02	0.17 ±0.01		85.1 ±0.7	
	31.3 ±2.7	0.33 ±0.02	0.15 ±0.01		87.4 ±1.2	
0.1 H+7.9 L	82.2 ±0.8	0.71 ±0.01	0.30 ±0.01	> 98		3.6 ±0.3
	76.3 ±0.8	0.68 ±0.01	0.29 ±0.02			14.8 ±0.9
	67.7 ±1.1	0.35 ±0.01	0.15 ±0.01			65.1 ±1.2
	60.5 ±1.7	0.19	0.11			90.7 ±0.8
	56.6 ±2.1	0.17	0.10			92.9 ±1.7

Figure 2.12 shows the numerical relationship of mean flow pore size with porosity at a fixed membrane weight or original membrane thickness. A careful analysis of the data revealed that both sets of data could be well fitted by using curves that the mean flow pore size was inversely proportional to one minus the membrane porosity, i.e.,

$$P \sim \frac{1}{1 - porosity} \tag{2-7}$$

Recalling that the porosity was defined and calculated as,

$$porosity = (1 - \frac{\rho}{\rho_0}) \times 100 = (1 - \frac{m/V}{\rho_0}) \times 100 = (1 - \frac{m/(T \cdot A)}{\rho_0}) \times 100 \tag{2-8}$$

with m denoting the weight of the membrane, A being the membrane area and T being membrane thickness. By replacing equation (8) into equation (7), it was found that at a constant weight of the membrane and fiber diameter, the mean flow pore size was directly proportional to the membrane thickness after compression, i.e.,

$$P \sim T \tag{2-9}$$

in the experimental membrane porosity range of 30 % ~ 80 % of this study.

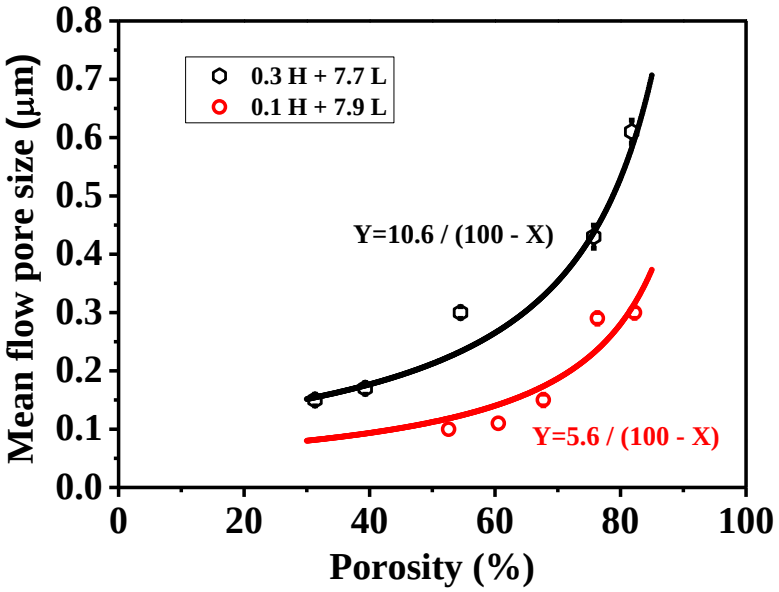

Figure 2.12 Relationship of mean flow pore size of electrospun membranes with membrane porosity (All membranes have an original thickness of ~ 200 μm)

The particle rejection tests were also carried out on the membranes after compression. The effect of reducing the third dimension on enhancing the particle rejection ability was obvious. For the membrane produced from solution 0.3 H + 7.7 L, the rejection ratio to the 0.5 μm particle suspension increased from 58.1 % ± 0.9 % to 87.4 % ± 1.2 % when the membrane porosity was decreased from 81.8 % ± 0.8 % to 31.3 % ± 2.7 %. This finding could partially be explained because the particles had less possibility to move sideways in the void space of the membrane as the dimension of void space had been greatly reduced in the third dimension, and therefore the chance of particles going through the membrane was reduced, resulting in a higher rejection ratio. It was also notable that although the mean flow pore size was measured to be below 0.2 μm at the porosity of 39.3 % ± 2.9 %, the membrane still showed a mere rejection to the particle of 0.2 μm. This may be explained as follows. During the membrane compression, although the fibers were packed more tightly in the cross-membrane direction and the void space was greatly reduced, the fiber orientation in the other two directions remained almost the same (Figure 2.13). Although the pore size in the in-plane direction might be reduced by more fibers crossing due to twisted and penetrating nanofibers into neighboring layers, the 0.2 μm particles could still go into the pores and through the membrane.

For the membranes electrospun from the solution 0.1 H + 7.9 L, a dramatic increase in the rejection ratio to the 0.2 μm particle suspension was observed as the membrane was compressed. At the membrane porosity of 82.2 % ± 0.8 %, the membrane showed very little rejection to the particles (with a rejection ratio of 3.6 % ± 0.3 %). As the membrane porosity was reduced to 76.3 % ± 0.8 % and 67.7 % ± 1.1 %, the rejection ratio was increased to 14.8 % ± 0.9 % and 65.1 % ± 1.2 %, respectively. A further

compression of the membrane to even denser states with the porosity of 60.5 % ± 1.7 % or lower increased the 0.2 μm particle rejection ratio of the membrane to above 90%. These membranes could be potentially effective in purifying water containing bacteria with a diameter above 0.2 μm such as H. pseudoflava and B. diminuta [35].

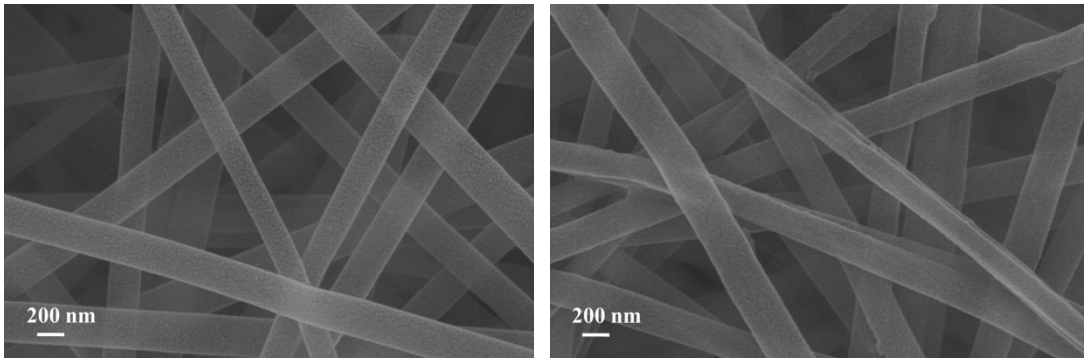

(a) (b)

Figure 2.13 SEM images of electrospun membrane from solution 0.3 H + 7.7 H (a) surface of original membrane with the porosity of 81.8 % ± 0.8 %; (b) surface of compressed membrane with the porosity of 54.5 % ± 2.2 %

2.4 Conclusions

Pore size and its distribution are the important properties of electrospun nanofibrous membranes for applications to water filtration, tissue engineering, fuel cells, batteries and so on. Therefore a proper understanding of the pore size is essential for better membrane applications. In this study, the morphology and diameter of electrospun nanofibers were controlled with due care before investigating its effect on the membrane pore size. Results indicated that increasing the polymer solution flow rate during the electrospinning process increased the fiber diameter, while a higher applied voltage produced thinner diameter fibers due to greater stretching force on the jet stream. To prepare bead-free membranes over a relatively broader fiber diameter range, a PAN solution with a higher molecular weight (700K) was used to blend with one with a lower molecular weight (150K) at different ratio and total polymer solution concentration. Uniform nanofibrous membranes with an average fiber diameter ranging from 104 nm to 655 nm were produced.

In studying the pore size of the electrospun membrane, several parameters, such as membrane thickness, mean fiber diameter and porosity were investigated. Capillary flow porometry was used to quantitatively characterize the pore size and its distribution. Results indicated that for the membrane with a certain average fiber diameter, the mean flow pore size initially decreased with an increase of membrane thickness and then converged to a steady value as the thickness was further increased. The thickness effect on the pore size almost disappeared when the membrane reached a thickness of about 100 μm. The fiber diameter was shown to be a dominant parameter that could determine the mean flow pore size of the membrane. A proportional relationship showing the mean

flow pore size was almost twice of the average fiber diameter was found based on the capillary flow porometry result in our PAN system. In terms of membrane porosity, it was quite intuitive that the pore size became smaller when the porosity was reduced because of the compressed void space in the third dimension. The data further revealed that the mean flow pore size was inversely proportional to one minus the membrane porosity, which also implied a proportional relationship with the membrane thickness after compression in our studies. The relationships of the mean flow pore size between the membrane thickness, fiber diameter and porosity were believed to be independent of the material and orienting pattern of the nanofibers, and could be extended to systems other than PAN.

The electrospun membranes with different fiber diameter or porosity were also used in the particle rejection tests to evaluate their functionality as microfiltration membranes. It was found that at the membrane thickness of ~ 100 μm and membrane porosity of ~ 80%, the membrane with an average fiber diameter of 160 ± 26 nm showed a rejection ratio of > 95% to the particle suspension with a nominal diameter of 0.5 μm. Such membranes should be very suitable to remove bacteria with a diameter of 0.5 μm or above from aqueous solution. It was also found that the particle retention ability was improved as the membranes were compressed in the through-membrane direction. A great increase of 0.2 μm particle rejection ratio from 3.6 % ± 0.3 % to > 90 % was achieved when the porosity of the membrane electrospun from the solution 0.1 H + 7.9 L was compressed from an original value of 82.8 % ± 0.8 % to 60.5 % ± 1.7 %. These studies indicated the pore sizes of electrospun membranes could be well tailored for different applications by tuning the membrane thickness, fiber diameter and porosity.

References

1. Wang, X. F., Chen, X. M., Yoon, K., Fang, D. F., Hsiao, B. S., and Chu, B. (2005) *Environ Sci Technol* **39**, 7684-7691
2. Wang, X. F., Fang, D. F., Yoon, K., Hsiao, B. S., and Chu, B. (2006) *J Membrane Sci* **278**, 261-268
3. Yoon, K., Kim, K., Wang, X. F., Fang, D. F., Hsiao, B. S., and Chu, B. (2006) *Polymer* **47**, 2434-2441
4. Gopal, R., Kaur, S., Feng, C. Y., Chan, C., Ramakrishna, S., Tabe, S., and Matsuura, T. (2007) *J Membrane Sci* **289**, 210-219
5. Tang, Z. H., Wei, J., Yung, L., Ji, B. W., Ma, H. Y., Qiu, C. Q., Yoon, K., Wan, F., Fang, D. F., Hsiao, B. S., and Chu, B. (2009) *J Membrane Sci* **328**, 1-5
6. Yoon, K., Hsiao, B. S., and Chu, B. (2009) *Polymer* **50**, 2893-2899
7. Zong, X. H., Kim, K., Fang, D. F., Ran, S. F., Hsiao, B. S., and Chu, B. (2002) *Polymer* **43**, 4403-4412
8. Hsiao, B. S., Liang, D., and Chu, B. (2007) *Advanced Drug Delivery Reviews* **59**, 1392-1412
9. Mo, X. M., Chen, R., Huang, C., Ke, Q. F., He, C. L., and Wang, H. S. (2010) *Colloids and Surfaces B-Biointerfaces* **79**, 315-325
10. Park, T. G., Yoo, H. S., and Kim, T. G. (2009) *Advanced Drug Delivery Reviews* **61**, 1033-1042
11. Prabhakaran, M. P., Kai, D., Jin, G. R., and Ramakrishna, S. (2011) *Journal of Biomedical Materials Research Part B-Applied Biomaterials* **98B**, 379-386

12. Chang, X. F., Hu, Y., and Xu, Z. L. (2011) *Mater Lett* **65**, 1719-1722

13. Kumar, J., Wang, X. Y., Drew, C., Lee, S. H., Senecal, K. J., and Sarnuelson, L. A. (2002) *Nano Letters* **2**, 1273-1275

14. Forsythe, J. S., Nisbet, D. R., Shen, W., Finkelstein, D. I., and Horne, M. K. (2009) *Journal of Biomaterials Applications* **24**, 7-29

15. Ryu, Y. J., Kim, H. Y., Lee, K. H., Park, H. C., and Lee, D. R. (2003) *Eur Polym J* **39**, 1883-1889

16. Li, D. P., Frey, M. W., and Joo, Y. L. (2006) *J Membrane Sci* **286**, 104-114

17. Ma, H. Y., Burger, C., Hsiao, B. S., and Chu, B. (2011) *J Mater Chem* **21**, 7507-7510

18. Eichhorn, S. J., and Sampson, W. W. (2005) *Journal of the Royal Society Interface* **2**, 309-318

19. Mcguire, K. S., Lawson, K. W., and Lloyd, D. R. (1995) *J Membrane Sci* **99**, 127-137

20. Hernandez, A., Calvo, J. I., Pradanos, P., and Tejerina, F. (1996) *J Membrane Sci* **112**, 1-12

21. http://www.pmiapp.com/publications/docs/Review-Papers/Advances-in-Pore-Structure-Evaluation-by-Porometry.pdf.

22. Jena, A., and Gupta, K. (2005) *Am Ceram Soc Bull* **84**, 28-30

23. ASTM. (2003) Standard test method for pore size characteristics of membrane filters by bubble point and mean flow pore test. F316-03.

24. Lee, J. S., Choi, K. H., Do Ghim, H., Kim, S. S., Chun, D. H., Kim, H. Y., and Lyoo, W. S. (2004) *Journal of Applied Polymer Science* **93**, 1638-1646

25. Seeram Ramakrishna, K. F., Wee-Eong Teo, Teik-Cheng Lim, Zuwei Ma. (2005) *An introduction to Electrospinning and Nanofibers*,

26. Buchko, C. J., Chen, L. C., Shen, Y., and Martin, D. C. (1999) *Polymer* **40**, 7397-7407

27. Lin, K., Chua, K. N., Christopherson, G. T., Lim, S., and Mao, H. Q. (2007) *Polymer* **48**, 6384-6394

28. Megelski, S., Stephens, J. S., Chase, D. B., and Rabolt, J. F. (2002) *Macromolecules* **35**, 8456-8466

29. Shenoy, S. L., Bates, W. D., Frisch, H. L., and Wnek, G. E. (2005) *Polymer* **46**, 3372-3384

30. Shibukaw.T, Sone, M., Uchida, A., and Iwahori, K. (1968) *J Polym Sci A1* **6**, 147-159

31. Wang, R., Liu, Y., Li, B., Hsiao, B. S., and Chu, B. (2012) *J Membrane Sci* **392**, 167-174

32. Mit-uppatham, C., Nithitanakul, M., and Supaphol, P. (2004) *Macromol Chem Physic* **205**, 2327-2338

33. He, J. H., Wan, Y. Q., and Yu, J. Y. (2008) *Fiber Polym* **9**, 140-142

34. Li, D., McCann, J. T., and Xia, Y. N. (2006) *J Am Ceram Soc* **89**, 1861-1869

35. Lee, A., Mcvey, J., Faustino, P., Lute, S., Sweeney, N., Pawar, V., Khan, M., Brorson, K., and Hussong, D. (2010) *Appl Environ Microb* **76**, 695-700

Chapter III Improving Interfacial Bonding Strength between Electrospun Layer and Substrate by Hot Pressing Method

The bonding strength between the electrospun nanofibrous membrane and the non-woven substrate is usually fairly weak. In water filtration, such as ultrafiltraion (UF) and nanofiltration (NF), it is often difficult to hold the structure integrity of the composite membrane in the back flushing process. In this study, a hot-pressing method was applied to improve the bonding strength between the electrospun polyacrylonitrile (PAN) membrane and the polyethylene terephthalate (PET) substrate. Results showed that, by using this method, only limited improvement could be achieved. An interfacial treatment followed by the hot pressing method was later applied. Based on the compression pressure, heating temperatrue and processing time, the bonding strength between the two layers could be reached to be comparable or superior to that of the commerical Koch UF membrane faabricated by the phase inversion method. The microfiltration properties of the electrospun membranes, such as the maximum pore size, the mean flow pore size and the porosity, together with the rejection ratio to the 0.2 μm particle suspension and the pure water flux were fully characterized. The rejection ratio was observed to have increased with the decrease of porosity during compression. The change in the pure water flux after membrane compression was discussed and expalined with the Hagen-Poiseuille model. The electrospun membranes compressed with different pressures were also used

as the scaffold to prepare thin-film nanofibrous composite (TFNC) membranes. Results indicated the electrospun membrane was not the performance-deternining layer. The pure water flux and the rejection ratio of the resulting UF membranes were almost not affected by the structure change of the electrospun membranes within the tested experimental range, implying that an increase in the bonding strength between the supporting layers could be applicable.

3.1 Introduction

With the rapidly growing population, increasing environmental pollutions and uneven distribution of usable water in many parts of the world, obtaining clean drinking water is believed to be one of the new challenges of the 21st century. Among the various methods of water purification, membrane filtration has been proven to be a cost-effective, energy-efficient and environmentally friendly method, and the membrane filtration technology has increased dramatically over the past 30 years [1].

Electrospun nanofibrous membranes, due to their unique structural properties such as high porosity and interconnected pore sizes, have been demonstrated to be effective in the microfiltration applications and shown superior performances than conventional phase inversion membranes with comparable pore sizes. When used as the mid-layer substrate in a UF or NF TFC membranes, they have also improved the permeate flux of the filtration membranes, as discussed in Section 1.2.1.

In membrane filtration process, especially in a long-term operation, one major problem is the membrane inevitably suffers from fouling, which decreases the permeate flux and reduces the membrane efficiency. Although chances of fouling can be

minimized by choosing proper material for the membrane barrier layer, in practical operations, one way to reduce fouling is to use the back flushing technique [2]. During back flushing, the permeate flow is applied through the membrane in the opposite direction of the filtration to remove fouling on the membrane surface [3]. Depending on the type of the filtration membrane, a pressure of several bars (for UF [2,4]) or much higher (for NF, RO) has to be applied to conduct back flushing, which requires the membrane to hold its structure integrity during the process. In the new TFC membrane using electrospun nanofibers membranes, the integration of the top layer and e-spun layer forms a composite layer which can withstand physical back flushing [5]. However, the bonding between the bottom substrate and the middle e-spun layer is relatively weak and highly suspicious for back flushing.

In adhesion theories, adhesion is an attraction between dissimilar surfaces clinging to one another or cohesion between similar molecules. The major mechanisms of adhesion include adsorption theory, mechanical interlocking, diffusion theory and electrostatic interaction. The last two mechanisms are not likely to be involved in the bonding between the electrospun membrane and the PET substrate. Due to the horizontal deposition of the electrospun nanofibers and therefore lack of interpenetration into the void space of PET substrate, mechanical interlocking is also rare. The adsorption theory is most widely applicable to explain the mechanism of adhesion or bonding. In this theory, the adhesion forms between two bodies in intimate contact through interatomic and intermolecular bonds. These bonds could be primary bonds including covalent, ionic or metallic bonds, and secondary interactions such as hydrogen bonding or van der Waals forces [6]. In our research group, the main material for the electrospun layer is poly

(acrylonitrile) (PAN) and massive production of high quality electrospun membranes has been realized. For the interfacial forces between the electrospun PAN membrane with all nanofibers and PET substrate, among the bonds mentioned above, it seems only van der Waals force was involved, and therefore the adhesion was weak.

The objective of this study is to improve the interfacial bonding strength between the PET substrate and the electrospun PAN membrane by an interfacial pretreatment combined with a hot-pressing method. The resulting effects on the filtration properties of the electrospun membrane as well as those of the UF membrane based on the treated electrospun membrane will also be evaluated.

3.2 Experimental

3.2.1 Materials

Poly (acrylonitrile) (PAN) with a weight-average molecular weight (M_w) of 150,000 g/mol was purchased from Scientific Polymer Products. Dimethylformamide (DMF, ACS reagent, ≥ 99.8%) purchased from Sigma-Aldrich Co was used as the solvent. The non-woven polyethylene terephthalate (PET) with the fiber diameter in the range of 10 μm (No. 16-1) was purchased from Sanko Ltd, Japan and used as the substrate of the electrospun PAN membrane. Polycarboxylate microsphere suspension with the nominal bead diameter of 0.2 μm (average diameter 0.189 ± 0.011 μm) was purchased from Polysciences Inc. and used for the particle rejection test. Koch UF membrane (HFK-328) was kindly provided by Koch Membrane Systems, Inc. (Massachusetts, US). Cellulose (Biofloc 96, wood pulp) was supplied by the Tembec Tartas S.A. (Tartas, France). 2,2,6,6-Tetramethylpiperidine-1-oxyl 85 (TEMPO, 98%) was purchased from Acros

Organics. Sodium bromide was purchased from Fisher Scientific. Sodium hypochlorite and dextran with a molecular weight of ~ 2000 kDa were obtained from Sigma-Aldrich.

3.2.2 Preparation and characterization of PAN solutions

The PAN solution with the concentration of 8 wt% was prepared by dissolving the PAN powders in DMF at 60 ℃ and stirring for 1 day to ensure homogeneity.

3.2.3 Electrospinning of PAN nanofibrous membrane

The electrospun PAN membranes were prepared using the multi-jet electrospinning unit developed at Stony Brook University. The process was operated in a closed chamber, with the temperature of 22 ℃ to 25 ℃ and the humidity of 40 % to 50 % controlled with the infrared lamp and the dry air. The electrospinning parameters were as follows. The inner diameter of the spinneret was 1 mm. The spinneret-to-collector distance was 7 cm. The applied voltage was between 20 ~ 22 kV, and the feed rate of the electrospinning solution was 15 μL/min.

3.2.4 Compression of the electrospun membrane

A hydraulic press machine equipped with heating plates (Carver, Inc. U.S.A) was used to compress the membrane. The electrospun membrane with the PET substrate was cut into an area of 10 cm × 10 cm each. Before compression, the membrane was placed between the heating plates without pressure for 15 seconds to be preheated to the desired temperature. The heating temperature and the applied pressure in the hot-press were 80 ℃ to 250 ℃ and 50 ~ 500 psi, respectively. The effect of processing time was evaluated in the range of 5 ~ 60 seconds.

3.2.5 Membrane characterizations of the PAN-PET membranes

The membrane morphology and fiber diameter were characterized by SEM, as described in Section 2.2.3.

The membrane thickness, porosity and pore size characterizations were described in Section 2.2.5.

Bonding strength of PAN nanofibrous membrane to PET substrate was tested by a 90 ° peel test. The PET substrate side of the membrane was fixed to the bench using an adhesive tape (3M, USA). The electrospun membrane side was taped to a Dillon BFG-50N force gauge (Dillon/Quality Plus, Inc.) with an area of 1.0 cm × 0.5 cm. Gradual pulling force was applied at 90 ° manually until the electrospun membrane was separated from the PET substrate. The maximum force was recorded and the bonding strength was calculated as the maximum force divided by the membrane area.

The pure water flux of the membranes was measured by dead-end filtration at the ambient temperature using Milli Q water. The driven pressure of 5 psi was provided with a compressed air unit equipped with a regulator and a pressure gauge. The membrane was tested in a dead-end filtration cell with an effective area of 3.9 cm^2 (Catalogue Number: XX3002500, Millipore, USA). The weight of water through the membrane was measured using an analytical balance. The pure water flux was normalized as weight of water (kg) per unit membrane area (m^2), per unit of time (h) and per unit of pressure (psi).

The particle rejection test was described in Section 2.2.6. 10 mL of 100 ppm particle suspension with an average bead diameter of 0.189 ± 0.011 μm was used as the challenging solution.

3.2.6 Preparation of thin-film nanofibrous composite (TFNC) membranes

The ultrafine cellulose nanofiber aqueous suspension with a concentration of 0.3 wt% was prepared by using the TEMPO-oxidation method, as described by Ma et al [7]. The fabrication procedures of the TFNC membranes are as follows [7,8]. The PAN-PET membranes compressed at 0 psi, 100 psi, 300 psi and 500 psi, respectively, were labeled as M0, M1, M3, M5 for simplicity of discussion. The edges of membranes were tapped onto the glass plate, with the thickness of the tape being ~100 μm. The membranes were later immersed in HCl solution with a pH = 2. After draining the excess solution from the membrane surface, the cellulose aqueous suspension was cast on top of the wet PAN-PET membrane. The TFNC membrane was then dried at 80 ℃ for 10 min. The resulting TFNC membranes with different PAN-PET scaffolds (M0, M1, M3, M5) were labeled as TFNC0, TFNC1, TFNC3, TFNC5. The barrier layer thickness of each TFNC membrane was estimated to be ~ 300 nm based on the concentration of cellulose suspension and the thickness of the tape.

3.2.7 Characterizations of TFNC membranes

The pure water flux of TFNC membranes was tested by using a stirred dead-end ultra-filtration cell (Millipore, cell model 8050, effective area 13.4 cm^2) at room temperature and an applied pressure of 10 psi. The rejection ability of TFNC membranes to the 2 000 kDa dextran solutions was evaluated with 2,000 ppm dextran solution. The applied pressure was fixed at 30 psi. In both tests, the TFNC membranes were first equilibrated with 50 mL pure water at 10 psi before tests [8].

3.3 Results and Discussion

3.3.1 Bonding strength improvement through hot-pressing method and interfacial treatment

The bonding strength of the as-spun PAN membrane with the PET substrate was tested to be 0.07 ± 0.01 bar. Compared to the bonding strength 2.31 ± 0.32 bar of the commercial Koch UF membrane prepared by the phase inversion method, the bonding of the electrospun membrane with its substrate was much weaker. Three reasons were contributed to the low bonding strength. First, the electrospun nanofibers deposited onto the PET substrate in a horizontal way, with only a few angles tilted in the cross-membrane direction. This resulted in almost no penetration into the substrate, and the bonding strength resulted from mechanical interlocking was very little. Second, PAN and PET possessed different chemical natures and lacked strong intermolecular bonds, such as covalent, ionic or hydrogen bonds, and therefore the chemical adhesion was also weak. Third, the surface of the PET substrate was very smooth, which was not in favor of mechanical interlocking as well.

By applying the compression method, it is expected to reduce the distance between molecules forming the adhesive bonds as well as to increase the contact chances of the nanofibers with the substrate, and thereby improve the bonding strength. In order to facilitate the polymer chain movement, heating was applied during pressing. Based on the glass transition temperatures and melting temperatures of the two polymers (PAN: T_g 85 ℃, T_m 317 ℃; PET: T_g 76 ℃, T_m 260 ℃; data from suppliers), a temperature range of 80 ℃ ~ 250 ℃ was tested.

Figure 3.1 showed the bonding strength of the PAN-PET membrane treated at different hot-pressing condition, as compared to that of the original membrane and commercial Koch UF membrane. The bonding strength was improved to different extents by varying the heating temperatures, the pressures at the processing period of 5 seconds. Specifically, at a given heating temperature, the bonding strength was increased with the applied pressure. For example, at 100 ℃ and 50 psi, the bonding strength was 0.09 ± 0.02 bar. An increase in the pressure to 300 psi and 500 psi brought the bonding strength to 0.19 ± 0.04 bar and 0.22 ± 0.04 bar, respectively. The same result was also observed at other heating temperatures.

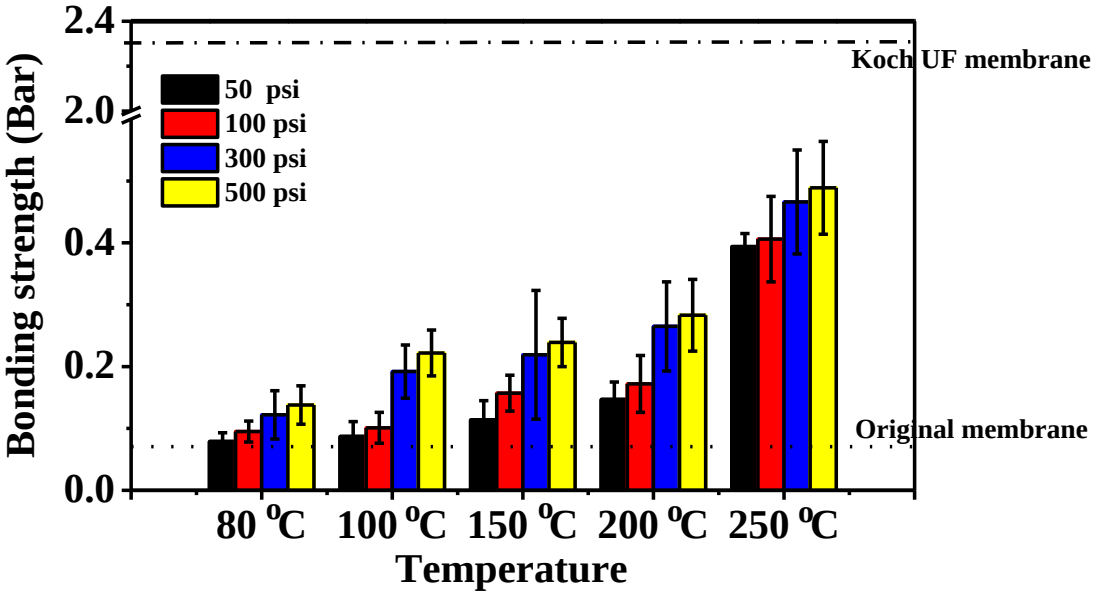

Figure 3.1 Bonding strength of the PAN-PET membrane treated with the hot-pressing method at different conditions for 5 seconds as compared with that of the original membrane and of the Koch UF membrane

To better understand the membrane morphology change in this pressing process, SEM images of the membrane surface were taken and shown in Figure 3.2(a-e). Compared to the original membrane (Figure 3.2(a)), the membranes compressed with pressures below 300 psi showed mere morphology or fiber diameter changes. In this pressure range, the increase in the bonding strength was resulted from closer contacts between the PET surface and the PAN nanofibers, which could lead to a greater van der Waals force. Since the intermolecular force was very weak, the increase in the bonding strength was limited. As the pressure was increased to 300 psi and 500 psi, the fibers were observed to be a little fused together and overlapped, resulting in a slight increase of the fiber diameter in the cross-linked region. To investigate if the nanofibers at the interface underwent the same morphology change as those at the surface, SEM images were taken at the bottom of the PAN membrane after peeling off the PET substrate. It was found from Figure 3.2(f) that the nanofibers in contact with the PET substrate showed almost the same morphology change as those on the surface. The fused fibers were believed to increase the interfacial contact area and contributed to the relatively greater bonding strength increase from 100 to 300 psi when compared to the increase from 50 to 100 psi.

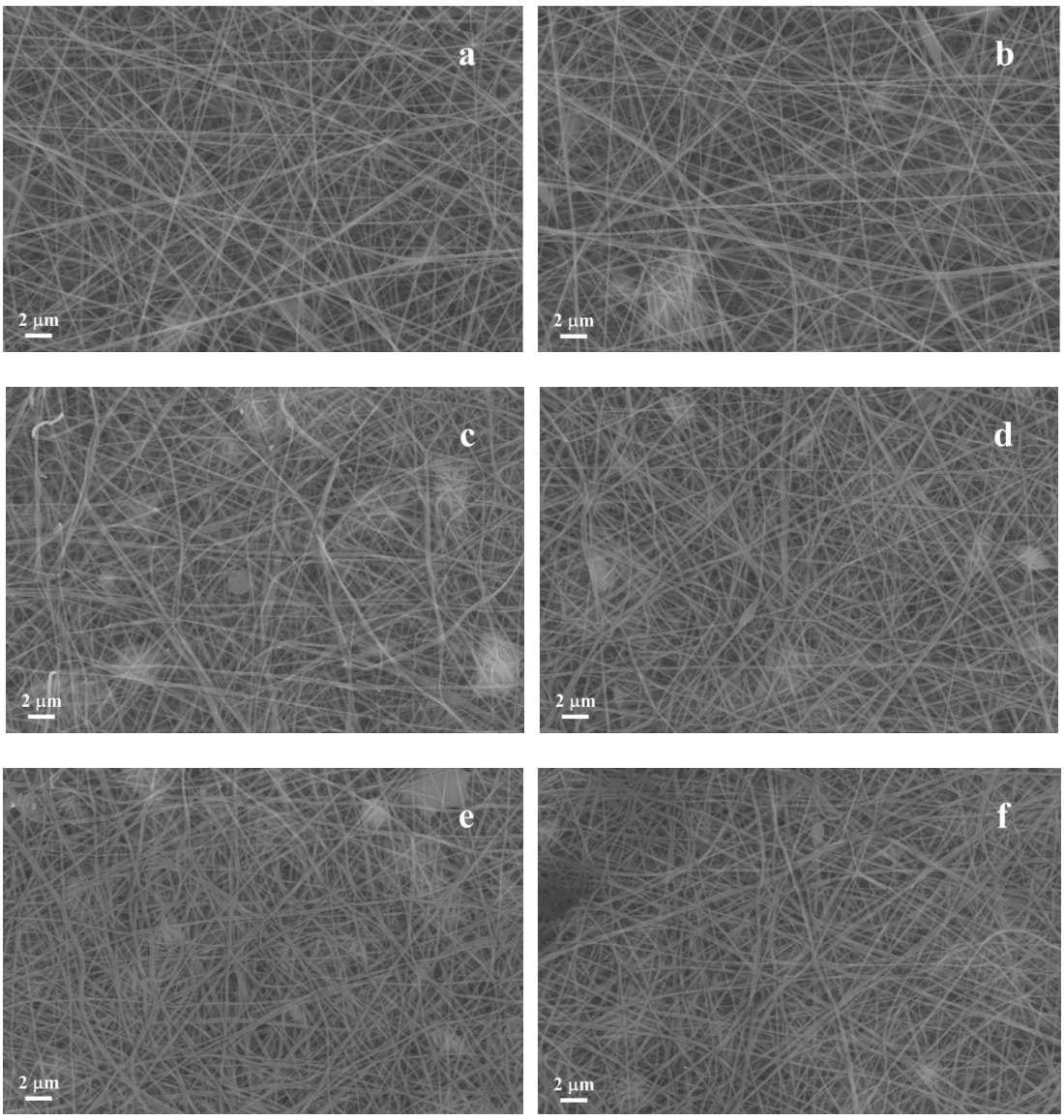

Figure 3.2 SEM images of (a) original PAN electrospun membrane; and the electrospun membranes compressed at the temperature of 100 ℃ and an applied pressure of (b) 50 psi; (c) 100 psi; (d) 300 psi; (e) 500 psi for 5 seconds; (f) bottom morphology of the membrane at the same condition with (e). The average fiber diameter was 172 ± 34 nm, 168 ± 42 nm, 176 ± 40 nm, 181 ± 39 nm, 195 ± 47 nm, 192 ± 48 nm respectively

At a fixed applied pressure, it was seen that the bonding strength was improved with increasing heating temperature. For example, at an applied pressure of 100 psi and a heating temperature of 80 ℃, the bonding strength was 0.095 ± 0.017 bar. As the heating temperature was increased to 100 ℃, 150 ℃, 200 ℃, the bonding strength was slowly increased to 0.10 ± 0.03, 0.18 ± 0.03, 0.17 ± 0.05 bar, respectively. The SEM images of the nanofibers heated at different temperatures (Figure 3.3) revealed no great morphology change had occurred. When the heating temperature reached 250 ℃, which was close to the melting point of PET, the bonding strength showed a relatively sharp increase to 0.41 ± 0.07 bar. However, the SEM image of the PAN-PET interface after the bonding test (Figure 3.4) showed that the PET was partially melted during the hot pressing probably resulted from the partial excessive heat of the heating plate, which greatly increased the bonding strength. Substrate melting caused great membrane deformation and should be avoided in the process. Thus, the hot-pressing process should be carried out below 250 ℃.

By the hot-pressing method in the tested range above, the maximum bonding strength of the PAN-PET membrane reached 0.28 ± 0.06 bar at the treating condition of 200 ℃ and 500 psi for 5 seconds. However, compared to the bonding strength of the Koch UF membrane, it is still much lower. Although a higher pressure above 500 psi could be further applied, it was not likely to greatly improve the bonding strength.

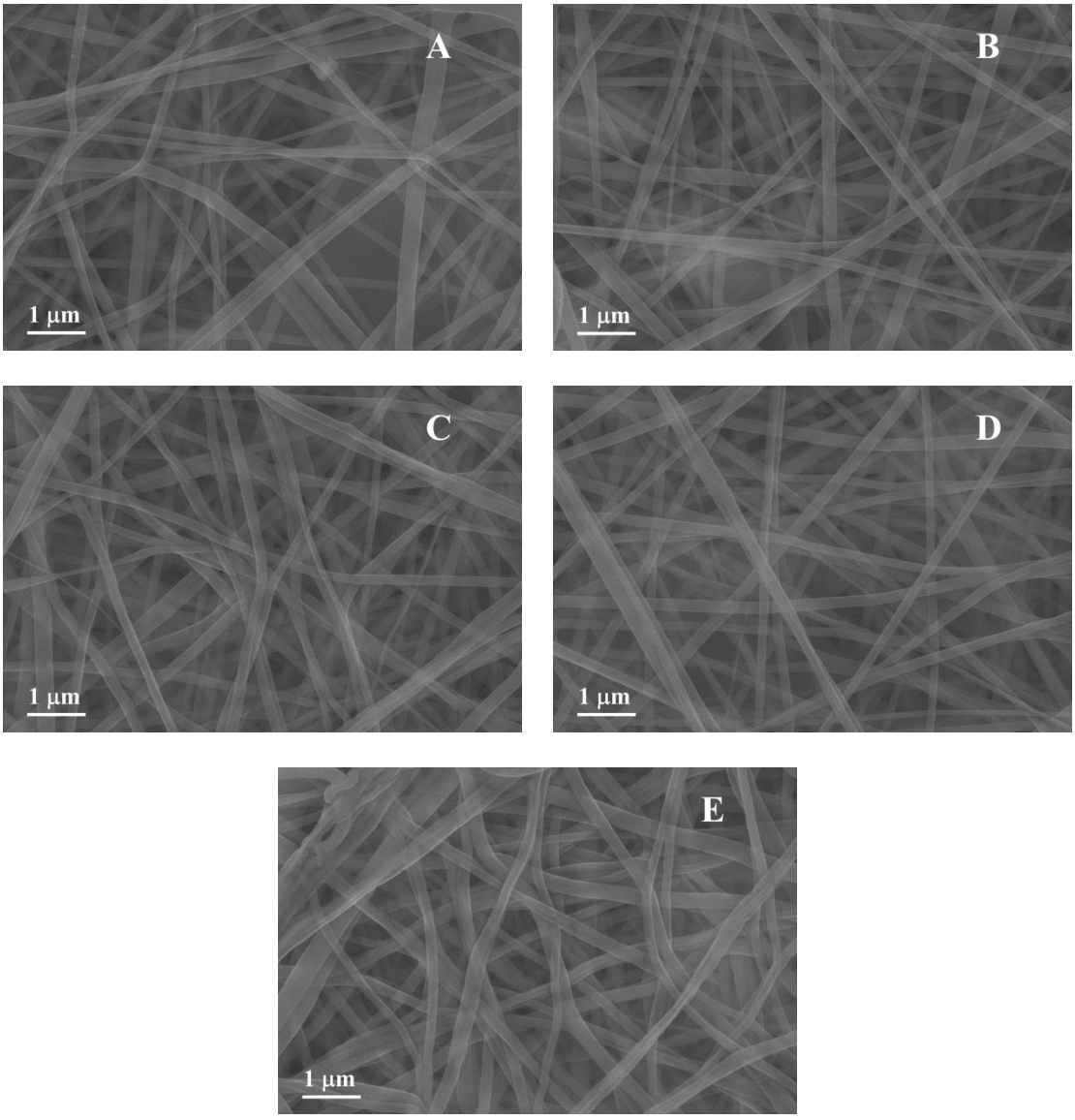

Figure 3.3 SEM images of electrospun PAN membranes compressed at the temperature of (A) 80 ℃; (B) 100 ℃; (C) 150 ℃; (D) 200 ℃; (E) 250 ℃ under the pressure of 100 psi for 5 seconds

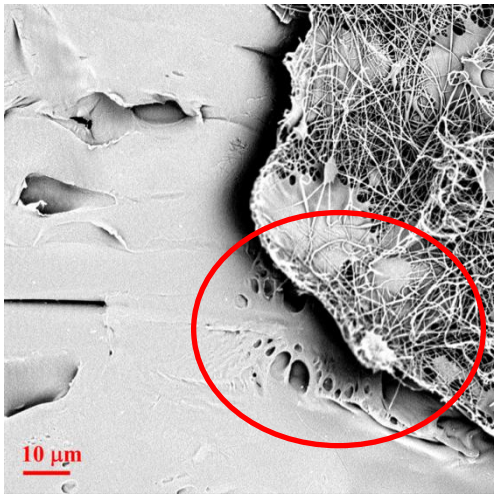

Figure 3.4 SEM image of the PAN-PET membrane interface after the peeling off test. PET substrate was melted in partial areas at the heating temperature of 250 ℃

The effect of processing time was evaluated at the hot-pressing condition of 200 ℃ and 300 psi, as shown in Figure 3.5. The bonding strength was almost not changed for the processing time of 5~30 seconds. With further increase of the time to 60 seconds, the fiber size was increased due to the fusion of fibers (Figure 3.6(D)), which leads to a slight increase of the bonding strength to 0.35 ± 0.06 bar.

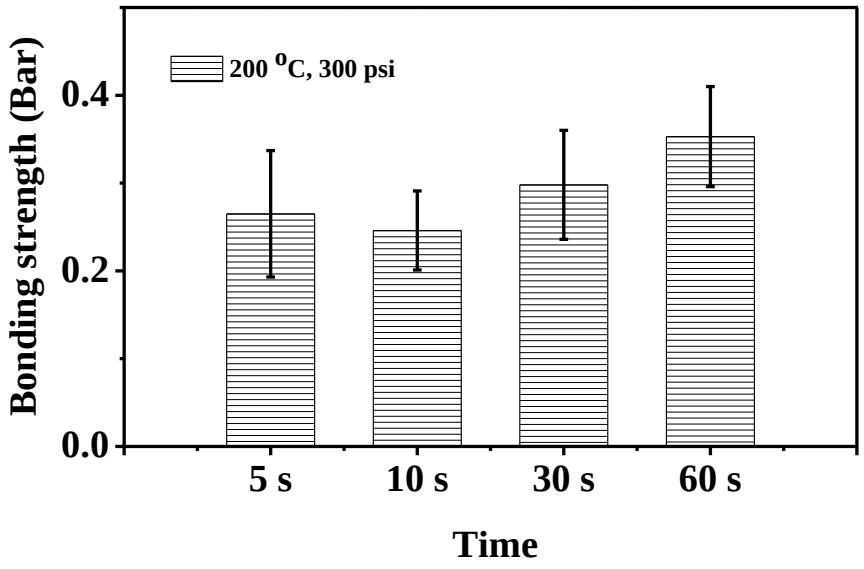

Figure 3.5 Bonding strength of the PET-PAN membrane compressed at 300 psi and 200 ℃ at different process time lengths

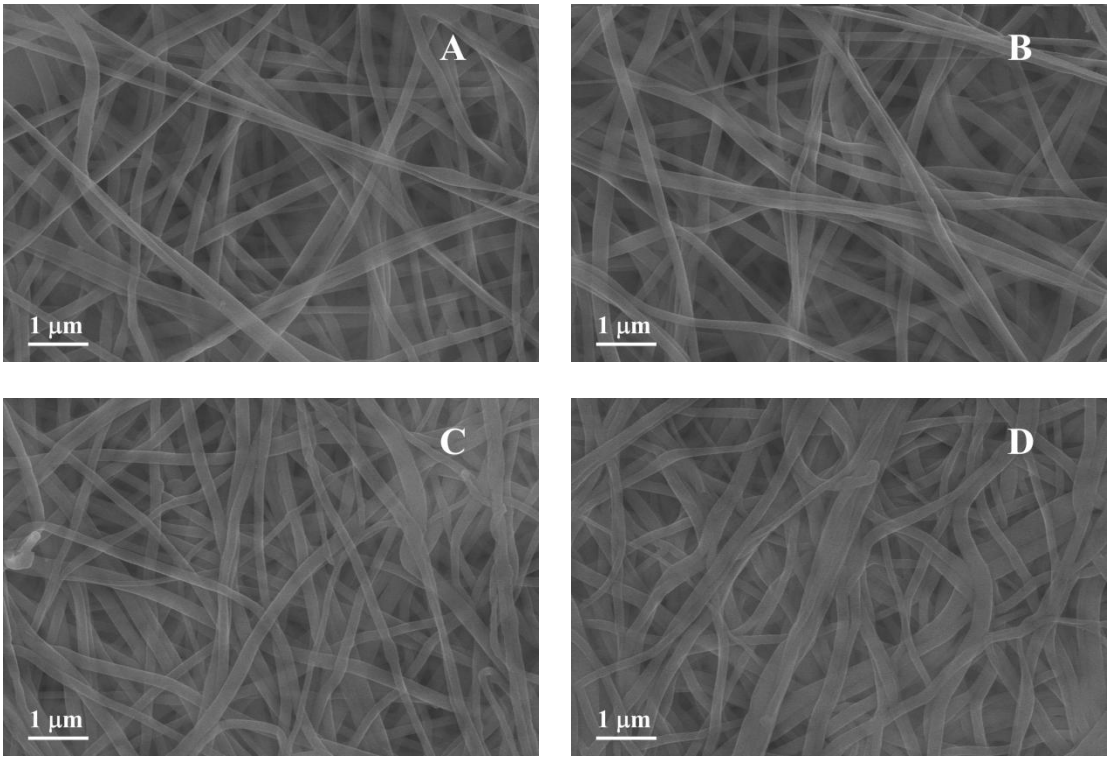

Figure 3.6 SEM images of electrospun PAN after being treated under the condition of 200 ℃ and 300 psi for (A) 5 seconds; (B) 10 seconds; (C) 30 seconds: (D) 60 seconds. The average fiber diameters are 181 ± 47 nm, 184 ± 53 nm, 198 ± 38 nm and 216 ± 62 nm, respectively

Many approaches have been developed to improve the adhesion on a polymeric substrate, either through physical abrasion or chemical modification by increasing surface roughness [9] or increasing the polar components of surface [10-12]. Here we used a simple interfacial treatment between the two layers. Although detailed technical know-hows were not fully explained here, the aim of the treatment was to alter the chemical nature of the PET substrate and to enhance its intermolecular bonding to the electrospun nanofibers.

The effect of interfacial treatment on the bonding improvement was obvious. For example, at the hot-pressing condition of 300 psi and 80 ℃, the bonding strength after the interfacial treatment was 1.48 ± 0.07 bar, over 10 times of that without interfacial treatment. In the meanwhile, increasing the temperature and pressure brought more notable increase in the bonding strength. Figure 3.7 shows the bonding strength of the membrane compressed at 300 psi at different heating temperatures. Because of the polar groups introduced in the interfacial treatment, the chemical bonding between the surface of PET substrate and the PAN nanofibers was greatly enhanced. The bonding strength was 1.48 ± 0.07 bar, 2.25 ± 0.49 bar, 2.49 ± 0.17 bar, 2.78 ± 0.23 bar at 80 ℃, 100 ℃, 150 ℃ and 200 ℃ respectively, corresponding to 20 ~ 39 times increase of the original value. At the condition of 300 psi and 100 ℃, the bonding strength achieved a comparable level to that of Koch UF membrane.

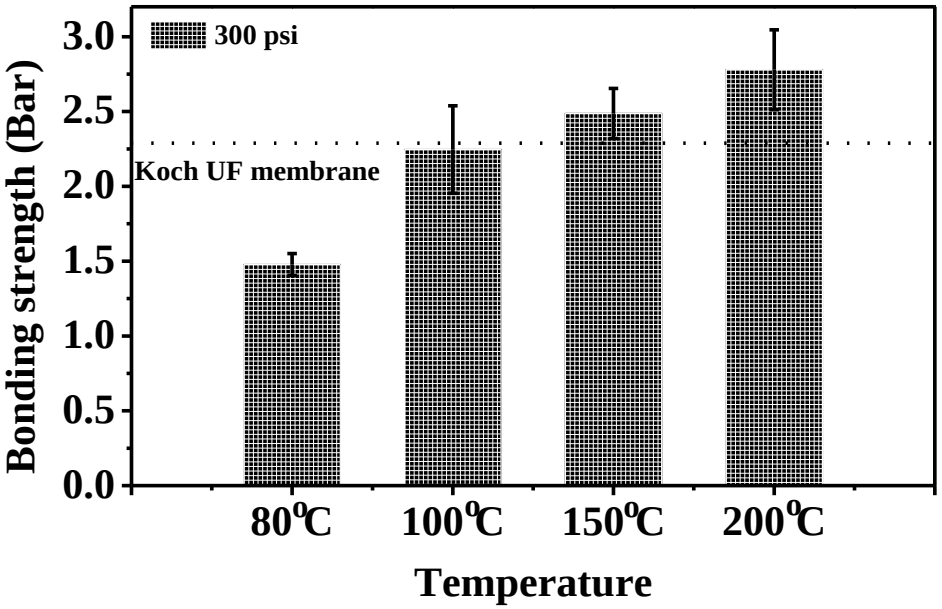

Figure 3.7 Bonding strength of the interfacial-treated PET-PAN membrane compressed at 300 psi and different temperatures for 5 seconds

Figure 3.8 shows the bonding strength change at different applied pressures and 200 ℃ after interfacial treatment. The bonding strengths at pressures of 50 psi, 100 psi, 300 psi and 500 psi were 1.17 ± 0.22, 2.06 ± 0.59, 2.78 ± 0.23 and 3.21 ± 0.38, respectively, corresponding to 16 ~ 44 times of the original membrane bonding strength. It was also shown that the higher pressure was more favorable to achieve better bonding, as the bonding strength was increased by almost 3 folds from the pressure of 50 psi to that of 500 psi. This was probably resulted from the increase of the intermolecular force between nanofibrous membrane and the PET substrate due to the increased contact area and reduced intermolecular distance [13]. At the pressure of 300 and 500 psi, the bonding strength reached a better level than that of the commercial Koch UF membrane, which ensured the PAN-PET membrane capable of withstanding the backflushing.

The effect of processing time was also investigated for the surface treated membrane, as shown in Figure 3.9. Prolonging the hot-pressing process at the condition of 200 ℃ and 300 psi from 5 seconds to 60 seconds increased the bonding strength from 2.78 ± 0.23 bar to 3.37 ± 0.31 bar.

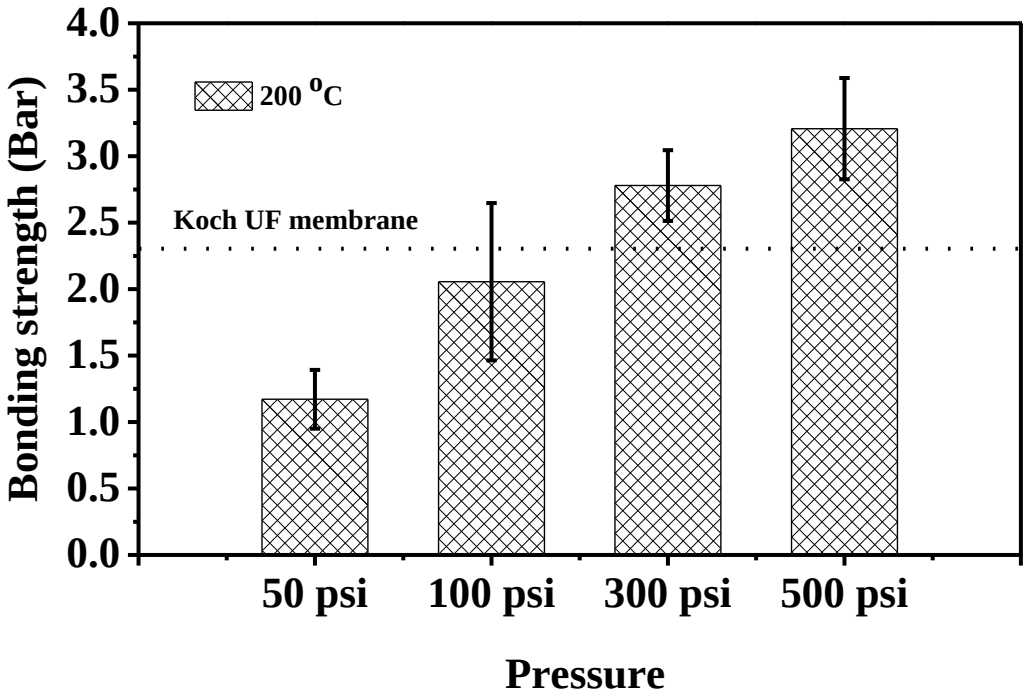

Figure 3.8 Bonding strength of the interfacial-treated PET-PAN membrane compressed at different pressures and 200 ℃ for 5 seconds

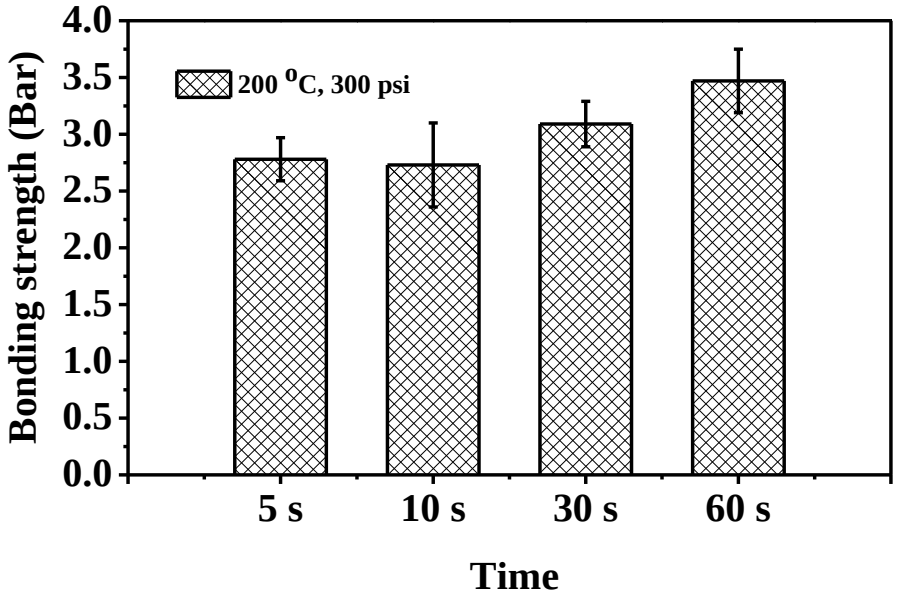

Figure 3.9 Bonding strength of the interfacial-treated PET-PAN membrane compressed at 300 psi and 200 ℃ at different process time lengths

3.3.2 PAN-PET membrane property characterizations after hot-pressing

The PAN membrane had an average fiber diameter of 172 ± 34 nm, a thickness of 90 ± 5 μm (without the PET substrate). The membrane porosity was ~75 %, slightly less than ~80 % due to the drippings as seen in Figure 3.3. Figure 3.10 showed the typical air flow rate measurements at different applied air pressures applied in the porometry test. The mean flow pore size was calculated based on equation (2-2) using the intercepted pressure of the wet curve and the ½ dry curve, and was 0.36 μm in this measurement. Figure 3.11 shows the overall pore size distribution of the membrane, as calculated from the flow rate data. The detectable pore size ranged from 0.093 μm to 0.698 μm, with the most pore size populated in the range between 0.35 μm to 0.40 μm.

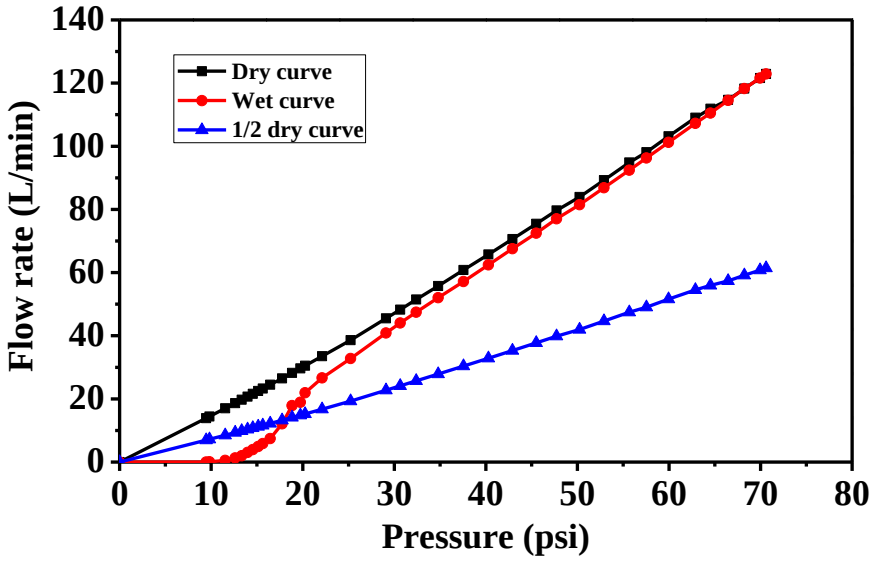

Figure 3.10 Wet and dry curves of original electrospun PAN membrane obtained from the capillary flow porometry

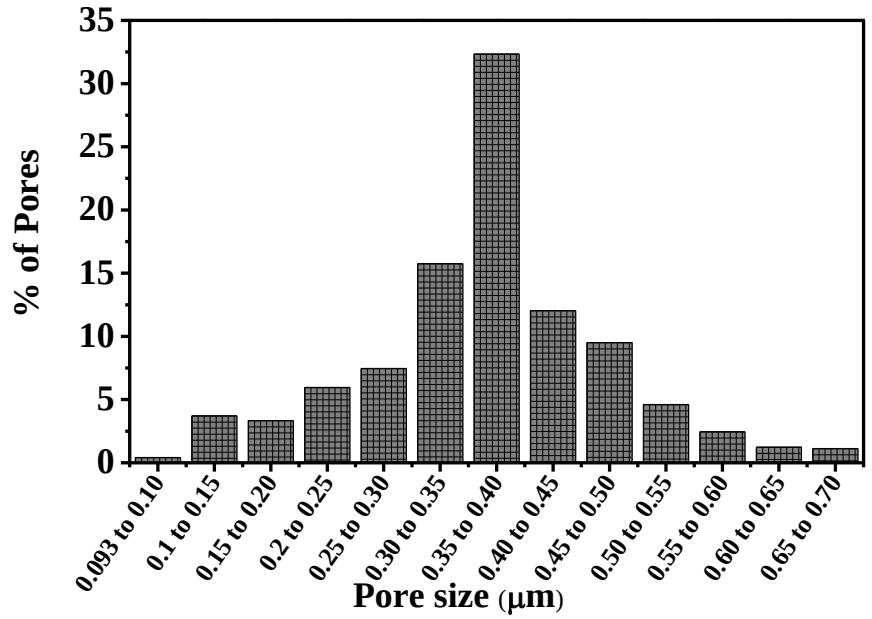

Figure 3.11 Pore size distribution of original electrospun PAN membrane obtained from the capillary flow porometer, with most pore size populated in 0.35 μm to 0.40 μm

The electrospun membrane properties after the hot pressing were fully investigated in terms of pore size, porosity, pure water flux and rejection to particle suspension with the nominal bead diameter of 0.2 μm. The thickness of the original electrospun PAN membrane was 90 ± 5 μm. Compression with pressures of 50 psi, 100 psi, 300 psi, and 500 psi reduced the thickness to 55 ± 3 μm, 43 ± 2 μm, 36 ± 1 μm, 33 ± 1 μm respectively. The membrane porosities were calculated to be 59.4 % ± 2.2 %, 48.1 % ± 2.3%, 38.0 % ± 1.7 %, 32.4 % ± 2.0 % in accordance with the above membrane thicknesses. The small membrane thickness decrease from the pressure of 300 psi to 500 psi indicated the porosity of the membrane had reached a low level and there was limited space in the third dimension (cross-membrane direction) that the nanofibers could be pressed into. The cross section SEM images of the electrospun PAN membranes at different thickness after compression were taken to visualize the structure change (Figure 3.12). It was shown that the void space in the third dimension gradually reduced as more pressure was applied onto the membrane, and the nanofibers became more twisted and pushed into the void space of the neighboring layers (Figure 3.12(D)). At a pressure of 500 psi, the fibers were being more fused together and the void space in the cross sectional dimension almost disappeared.

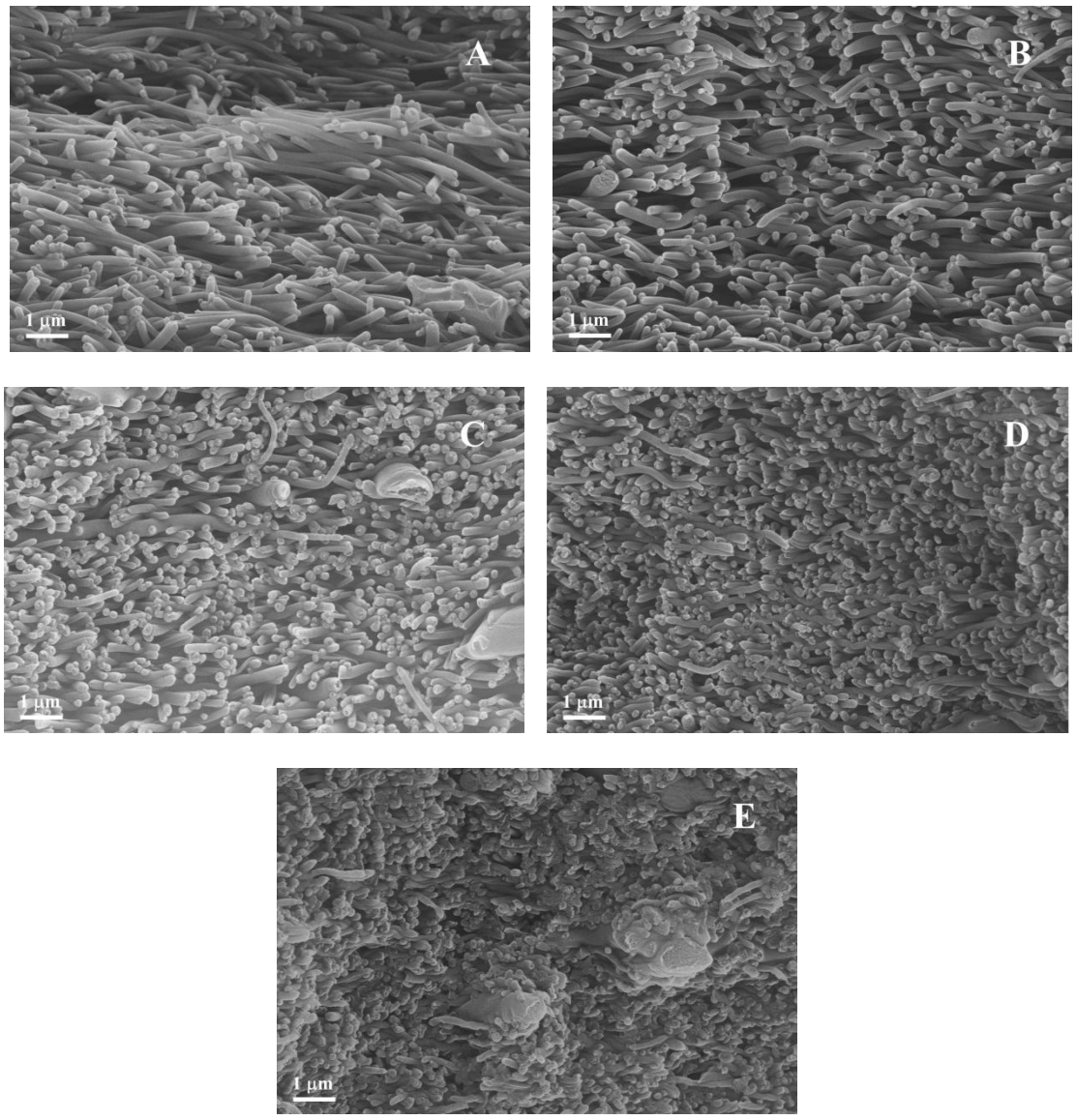

Figure 3.12 Cross-section SEM images of (A) original PAN electrospun membrane; and the electrospun membranes compressed at (B) 50 psi; (C) 100 psi; (D) 300 psi; (E) 500 psi

Along with the thickness change, the maximum pore size and the mean flow pore size were also decreased, as shown in Figure 3.13. The maximum pore size was gradually being reduced from its original value of 0.69 ± 0.01 μm to 0.19 μm as the membrane thickness was decreased to 33 ± 1 μm. The mean flow pore size was found to be 0.36 ± 0.01 μm, 0.21 ± 0.01 μm, 0.18 ± 0.01 μm, 0.14 ± 0.01 μm and 0.13 μm at a membrane thickness of 90 ± 5 μm, 55 ± 3 μm, 43 ± 2 μm, 36 ± 1 μm, 33 ± 1 μm, respectively. It was also noted that the mean flow pore size was being decreased with decreasing membrane thickness in an almost proportional relationship. This finding is in good agreement with the earlier findings in Chapter II, where the mean flow pore size of a compressed membrane was found to be in inverse proportional relationship with one minus the final membrane porosity, or in another word, proportional to the final membrane thickness. The pore size distributions of the membranes also shifted to the small pore size region with the increase of the pressure, as shown in Figure 3.14.

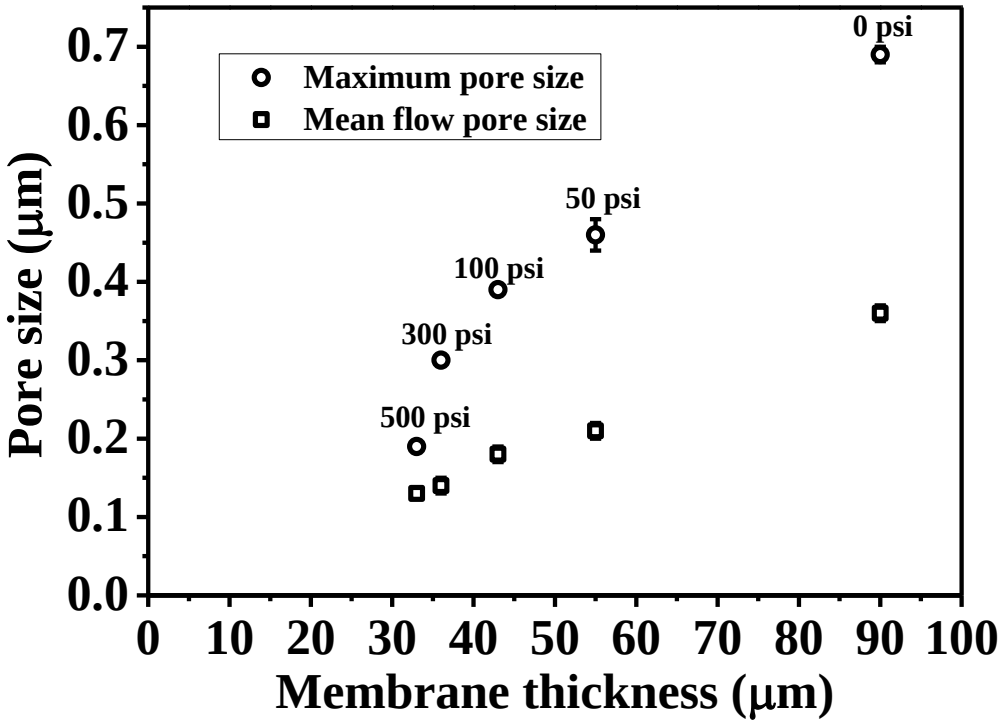

Figure 3.13 Changes of maximum and mean flow pore size with the membrane thickness after compression

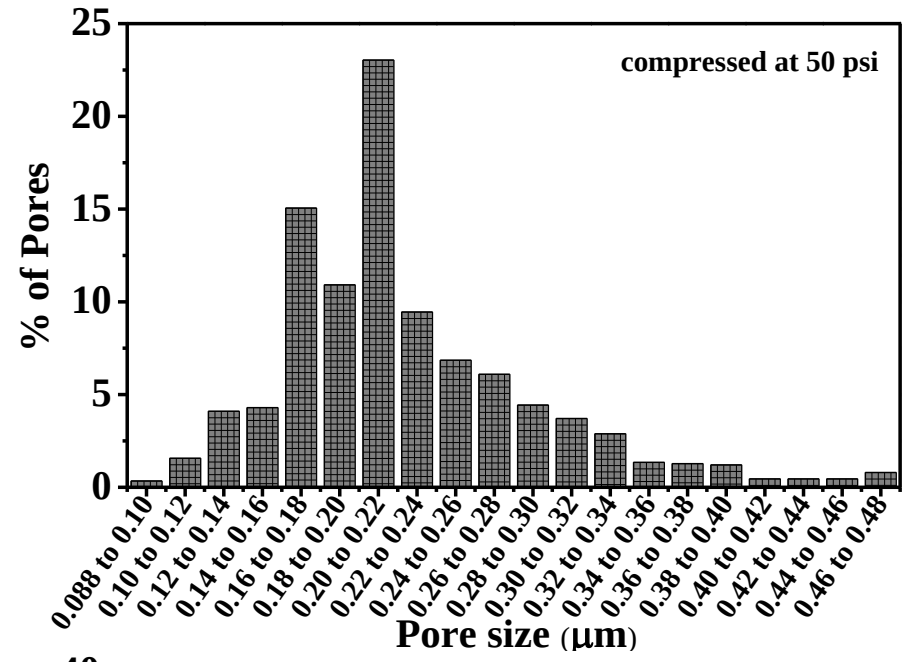
compressed at 50 psi
% of Pores
0
5
10
15
20
25
0.088 to 0.10
0.10 to 0.12
0.12 to 0.14
0.14 to 0.16
0.16 to 0.18
0.18 to 0.20
0.20 to 0.22
0.22 to 0.24
0.24 to 0.26
0.26 to 0.28
0.28 to 0.30
0.30 to 0.32
0.32 to 0.34
0.34 to 0.36
0.36 to 0.38
0.38 to 0.40
0.40 to 0.42
0.42 to 0.44
0.44 to 0.46
0.46 to 0.48
Pore size (μm)

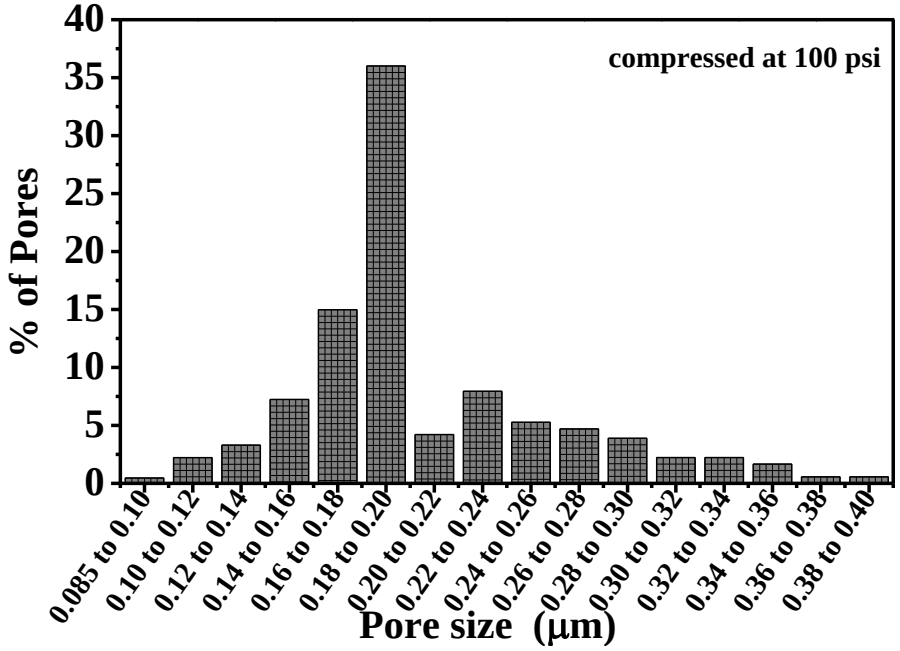
compressed at 100 psi
% of Pores
0
5
10
15
20
25
30
35
40
0.085 to 0.10
0.10 to 0.12
0.12 to 0.14
0.14 to 0.16
0.16 to 0.18
0.18 to 0.20
0.20 to 0.22
0.22 to 0.24
0.24 to 0.26
0.26 to 0.28
0.28 to 0.30
0.30 to 0.32
0.32 to 0.34
0.34 to 0.36
0.36 to 0.38
0.38 to 0.40
Pore size (μm)

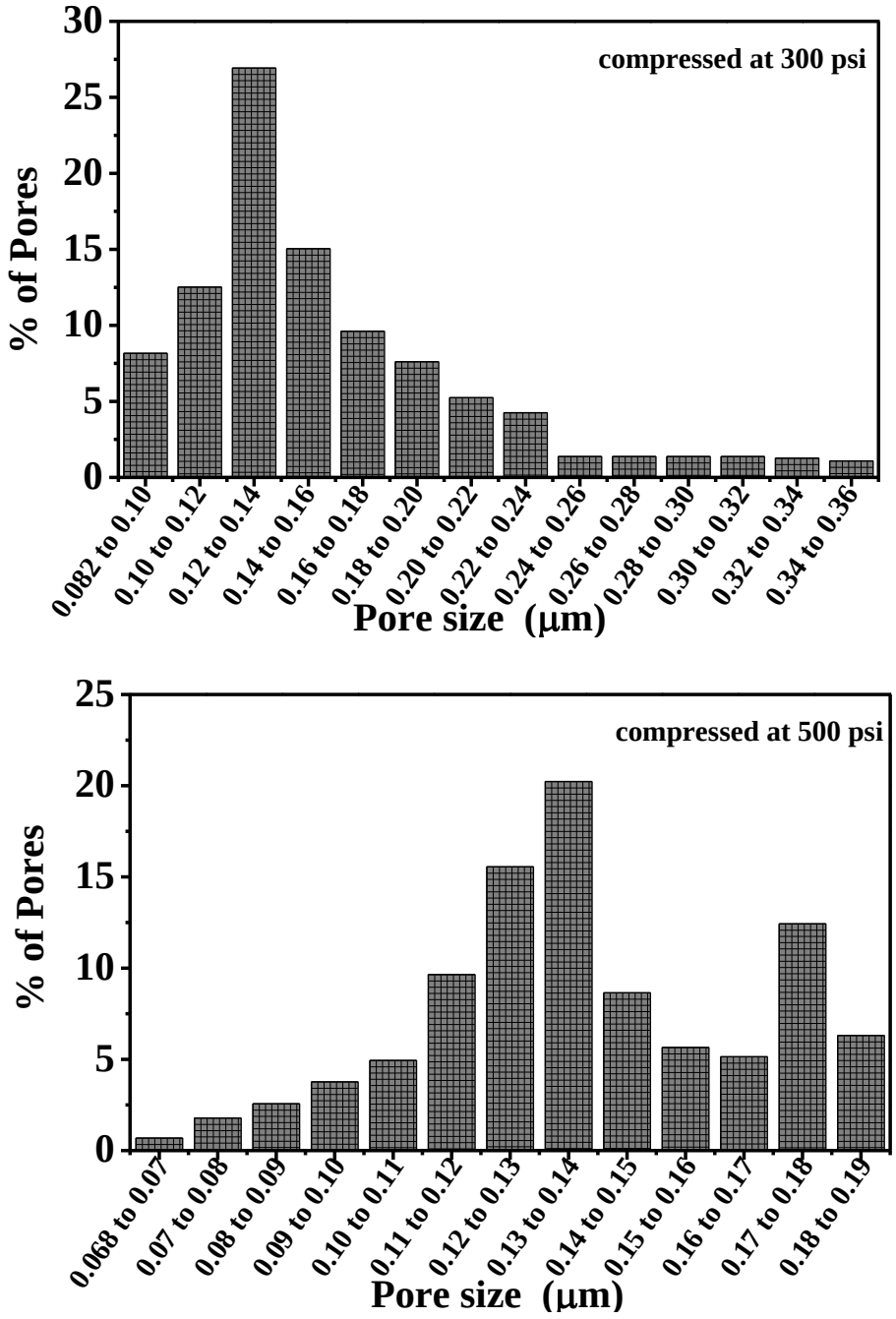

Figure 3.14 Pore size distributions of electrospun PAN membranes with an original thickness of 90 ± 5 μm compressed at different pressures

Because of the large pore size of the original membrane, the rejection ratio to the 0.2 μm particle suspension was very low at 6.8 ± 0.7 %. With the membrane being compressed, the rejection ratio was found to have increased, as shown in Figure 3.15, because the particles had less chance to move sideward in the compressed void space ("pores") in the third dimension. As the void space was compressed smaller, the chance of particle going through the membrane decreased accordingly. Meanwhile, the interpenetration of fibers into neighboring layers at higher pressures (300 psi and 500 psi) cut the pores into smaller sizes in the in-plane direction, which could also contribute to the increase in the rejection ratio. As the membrane thickness was reduced to 33 ± 1 μm, the rejection ratio to the 0.2 μm particles was greatly increased to 85.7 ± 1.5 %.

Pure water flux is an important parameter for a microfiltration membrane as it determines the speed of water permeating through the membrane. The pure water flux change associated with the membrane thickness was shown in Figure 3.15. As the membrane was compressed, it became denser and the pore size became smaller, which resulted in a reduced pure water flux rate through the membrane at a constant driven pressure of 2.5 psi. The flux rate of the original membrane was $4.75 \times 10^3 \pm 408$ L/(m^2h), and gradually decreased to 469 ± 55 L/(m^2h) at the membrane thickness of 33 ± 1 μm, corresponding to a decrease by a factor of 10. It was also found that the pure water flux followed an almost linear relationship with the membrane thickness. The Hagen-Poiseuille model was used to illustrate the results. For electrospun membranes, based on the model the pure water flux can be calculated using the following equation [14,15]

$$J = \frac{\Delta P D^2 \varepsilon}{32 \mu T} \quad (3\text{-}1)$$

where J is water flux (m/s), ΔP is the applied pressure (Pa), D is the mean pore size of the membrane (m), ε is the membrane porosity, μ is the viscosity of water (Pa s), T is the membrane thickness (m).

Based on the finding in Chapter II that the mean flow pore size was almost proportional to the membrane thickness, which was also observed in Figure 3.13 in this study, the pore size D could be expressed as

$$D = Tc_1 \quad (3\text{-}2)$$

where c_1 is a constant.

Recalling that the porosity ε is calculated by equation (2-1) and can be expanded as

$$\varepsilon = 1 - \frac{m/\rho_0}{AT} \quad (3\text{-}3)$$

where m is the membrane weight, ρ_0 is the bulk density of the polymer, A is the membrane area, while these three variables were all kept unchanged during the compression process, equation (3-3) can be further written as

$$\varepsilon = 1 - \frac{c_2}{T} \quad (3\text{-}4)$$

where c_2 is a constant.

Applying equation (3-2) and (3-4) into equation (3-1), the Hagen-Poiseuille equation can be derived into

$$J = \frac{\Delta P c_1^2}{32 \mu} (T - c_2) \quad (3\text{-}5)$$

showing a linear relationship between the water flux J and the membrane thickness T at a fixed applied pressure ΔP. The experimental data, with a R^2 of 0.97 in the linear fitting, as shown in Figure 3.15, were in good agreement with the Hagen-Poiseuille model.

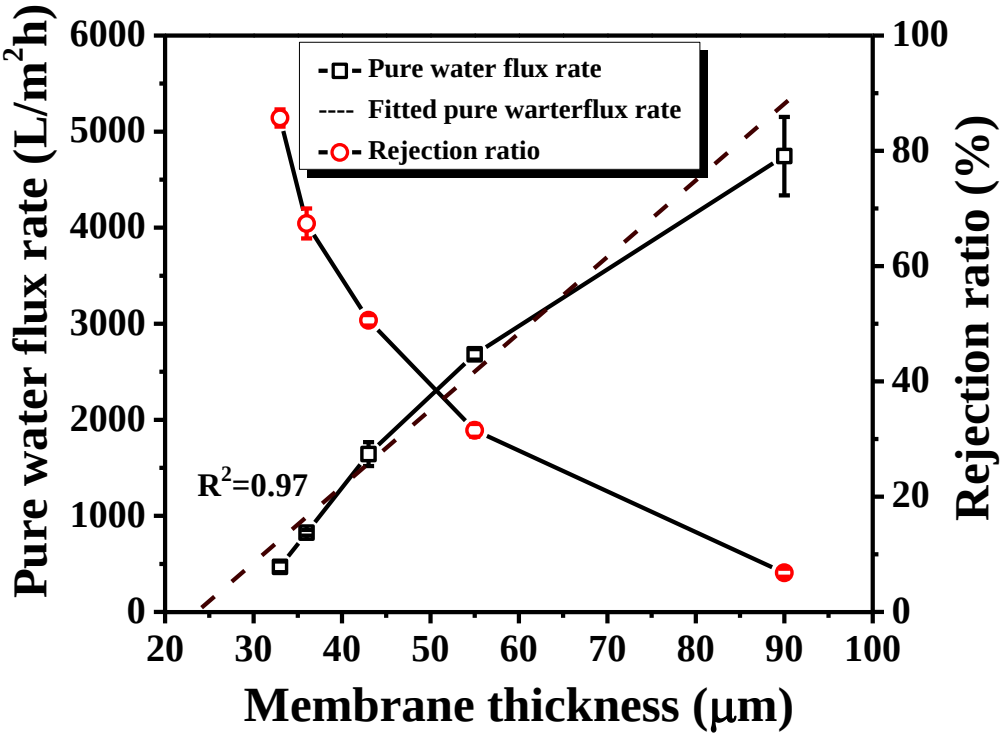

Figure 3.15 Pure water flux rate and 0.2 μm particle rejection ratio of membranes with different thicknesses after compression

3.3.3 Characterizations of TFNC membranes

The TFNC membranes with different PAN-PET scaffolds were tested for pure water flux and rejection ratio by using dextran with molecular weight of 2 000 kDa. The results were summerized in Table 3.1. It was shown that with a cellulose barrier layer thickness of ~300 nm, the pure water flux of TFNC0 (with PAN-PET membrane uncompressed) was 20.3 ± 1.4 $L/m^2 \cdot h \cdot psi$, and the rejection ratio was 88.3 % ± 1.0 %. These data were very close to the results reported by Ma et al.[8], where the TFNC membrane with a cellulose barrier layer thickness of ~300 nm showed a pure water flux of 19.3 $L/m^2 \cdot h \cdot psi$ and a rejection ratio of ~ 90% for the 2 000 kDa dextran solution.

From Table 3.1 with the PAN-PET scaffold compressed, the performance of the resulting UF membranes (TFNC1, TFNC3, TFNC5) was kept almost unchanged. Although the pure water flux of the PAN-PET scaffold (M5) of TFNC5 was decreased to about 1/10 of the initial value (M0) by compression, it was still about 10 times higher than that of the final UF membrane. During the compression, the interconnected open porous structrure of the electrospun scaffold was essentially maintained. Therefore, the fluid passing through the barrier layer suffered littleor no resistance through the PAN-PET scaffold. In this scenario, it appears that the barrier layer played a critical role and became the pure-water-flux-determining layer in the UF membrane. Since all UF membranes had the same thickness and the structure of the barrier layer, the pure water flux and the rejection ratio remained essentially the same by using either compressed or uncompressed substrate supporting layer..

.

Table 3.1 Ultra-filtration performance of TFNC membranes based on different PAN-PET membranes

TFNC membranes	Barrier layer thickness (nm)	Pure water flux ($L/m^2 \cdot h \cdot psi$)	Rejection ratio to 2 000 kDa dextran solution (%)
TFNC0	~ 300	20.3 ± 1.4	88.3 ± 1.0
TFNC1		19.3 ± 1.5	86.0 ± 0.7
TFNC3		19.0 ± 1.0	87.5 ± 1.7
TFNC5		20.2 ± 1.1	87.6 ± 0.9

3.4 Conclusions

For the novel thin film composite (TFC) filtration membrane with an electrospun membrane as the middle layer, the bonding strength between the electrospun PAN membrane and its substrate – a PET non-woven mesh is of importance, especially in the back flushing mode. However, due to the horizontal deposition of nanofibers, the smooth surface and inert chemical nature of the substrate, the bonding strength of the as-spun membrane could often be relatively weak. In this study, a hot-pressing method, together with an interfacial treatment, was applied to improve the bonding strength. Results showed that the hot-pressing method on the as-spun membrane could only improve the adhesion by a limited amount, and the resulting bonding strength was far from sufficient for efficient back flushing. After the interfacial treatment followed by the hot-pressing, the bonding strength could significantly be increased by over 40 times. Higher temperature, greater applied pressure and longer processing time were shown to be in favor of better bonding. Specifically, the bonding strength at a pressing condition of 300 ℃ and 100 psi for 5 seconds reached a comparable level to that of the commercial phase inversion UF membrane, and a superior bonding could be achieved by either applying higher pressure, heating temperature or prolonging the process.

With the electrospun membrane layer being compressed, the maximum pore size, the mean pore size and the porosity were reduced. It was found that the mean flow pore size was almost proportional to the final membrane thickness. This finding was in accordance with the mean flow pore size-porosity relationship obtained in Chapter II, which stated that when an electrospun membrane was compressed, the mean flow pore size was almost in inversely proportional relationship with its final porosity, or equivalently, proportional

to the final thickness within the experimental porosity range of ~ 30% to ~ 80%. With the decrease in the membrane thickness and porosity, the membrane rejection ratio to the 0.2 μm particle suspension was observed to have increased. When the membrane was compressed from an original thickness of 90 ± 5 μm to a final thickness of 33 ± 1 μm, the rejection ratio was significantly increased from 6.8 % ± 0.7 % to 85.7 ± 1.5 %. The pure water flux of the electrospun membrane was also gradually decreased as the membrane was compressed with higher pressure. At the compression pressure of 500 psi, the pure water flux of the electrospun membrane dropped to one tenth of its original value. The pure water flux of the membrane showed an almost linear relationship with the thickness after compression. This finding was well explained by using the Hagen-Poiseuille model with the aid of the pore size-compressed membrane thickness relationship obtained from above and Chapter II.

TFNC membranes were prepared by coating cellulose nanofiber barrier layer of the same thickness onto the PAN-PET membrane compressed at different pressures. UF performance tests showed that the pure water flux and the rejection ratio to 2 000 kDa dextran solution remained almost the same. This finding indicated that the barrier layer played an important role in determining the performance of the UF membrane. The reduction of porosity of the electrospun scaffold was shown to have a negligible effect on the filtration performance of the UF membrane, as long as the scaffold maintained a substantially higher flux than the barrier layer.

Acknowledgements

I wish to thank Dr. Dufei Fang from Stonybrook Technology & Applied Research, Inc. for membrane preparation from the multi-jet electrospinning set-up.

References

1. Moulin, C., Bourbigot, M. M., Tazipain, A., and Bourdon, F. (1991) *Environ Technol* 12, 841-858
2. Salladini, A., Prisciandaro, M., and Barba, D. (2007) *Desalination* 207, 24-34
3. Srijaroonrat, P., Julien, E., and Aurelle, Y. (1999) *J Membrane Sci* 159, 11-20
4. Laitinen, N., Luonsi, A., Levanen, E., and Nystrom, M. (2001) *Sep Purif Technol* 25, 323-331
5. Chu, B., and Hsiao, B. S. (2009) *J Polym Sci Pol Phys* 47, 2431-2435
6. Kinloch, A. J. (1987) *Adhesion and Adhesives: Science and Technology*, 1st ed., Springer
7. Ma, H. Y., Burger, C., Hsiao, B. S., and Chu, B. (2011) *Biomacromolecules* 12, 970-976
8. Ma, H. Y., Yoon, K., Rong, L. X., Mao, Y. M., Mo, Z. R., Fang, D. F., Hollander, Z., Gaiteri, J., Hsiao, B. S., and Chu, B. (2010) *J Mater Chem* 20, 4692-4704
9. Packham, D. E. (2003) *Int J Adhes Adhes* 23, 437-448
10. Brewis, D. M., Mathieson, I., and Wolfensberger, M. (1995) *Int J Adhes Adhes* 15, 87-90
11. Brewis, D. M., Dahm, R. H., and Mathieson, I. (2000) *J Adhesion* 72, 373-386
12. Kharitonov, A. P., and Kharitonova, L. N. (2009) *Pure Appl Chem* 81, 451-471
13. Gady, B., Schleef, D., Reifenberger, R., Rimai, D., and DeMejo, L. P. (1996) *Phys Rev B* 53, 8065-8070

14. Bowen, W. R., Hilal, N., Lovitt, R. W., Sharif, A. O., and Williams, P. M. (1997) *J Membrane Sci* 126, 77-89

15. Yoon, K., Kim, K., Wang, X. F., Fang, D. F., Hsiao, B. S., and Chu, B. (2006) *Polymer* 47, 2434-2441

Chapter IV Improvement of Meltdown Temperature of Polyethylene Lithium-Ion Battery Separator using Electrospun Polyethersulfone Membrane

As an important component in a lithium-ion battery, the separator is required to have the shutdown feature to prevent the thermal runaway within the battery under the condition of overcharge or abuse. When the cell temperature continues to increase above the shutdown temperature, it is essential for the separators to have a high meltdown temperature (MDT) to maintain their integrity and to prevent the direct contact of electrodes. The commercial microporous polyethylene (PE) separators have shutdown temperatures (SDT) between 130 and 140 ℃, and a MDT slightly higher than the SDT. To enhance the MDT and to broaden the safety margin of the PE separator, polyethersulfone (PES), a polymer with great thermal resistance, was electrospun into a nanofibrous membrane and deposited onto the PE film to fabricate a composite separator. Due to the low surface energy and hydrophobic nature of the PE surface, its adhesion to the electrospun PES membrane was very weak. In this work, the PE film was modified with chromic acid. The modified PE film was characterized with AFM and FTIR spectroscopic techniques as well as the water contact angle test. Compared to the original film, the modified PE film showed nearly 10 times increase in the adhesion strength to the electrospun PES membrane. The morphology of the electrospun PES membrane, controlled by different flow rates in the electrospinning process, was also demonstrated to

have a great impact on the adhesion. A 5-fold increase of the adhesion strength was observed when the electrospinning flow rate was increased from 20 μL/min to 60 μL/min. The composite PES/PE/PES separator, structured as a PE film sandwiched in two electrospun PES membranes, maintained the low SDT of 131 ℃ but achieved a significantly higher MDT of 221 ℃. Furthermore, the high porosity of the electrospun membrane ensured that the air permeability of the separator was not sacrificed when compared with the base PE film.

4.1 Introduction

With the widespread use of cell phones, laptop computers and portable electronics nowadays, the battery industry, has shown an enormous growth during the past few years. In the rechargeable battery industry, lithium ion batteries, owing to their advantages, such as better self-discharge performance, longer cycle life, higher energy density and higher operational voltage over the NiCd and NiMH systems [1], have taken up to more than 70% of the market. They have been used in over 90% of cellphones, laptops, camcorders, and many hybrid electric vehicles (HEVs) and electric vehicles (EVs) [2-6].

A lithium-ion battery consists of a metal oxide (e.g. $LiCoO_2$) positive electrode and a graphite negative electrode. A porous film, called the separator, is placed between the two electrodes and is immersed in the ionically conductive electrolyte, normally as $LiPF_6$ dissolved in an organic solvent, such as ethylene carbonate (EC), diethyl carbonate (DEC), ethyl methyl carbonate (EMC) or a mixture of those solvents [7-9]. The separator film plays an important role in the lithium-ion battery. It allows the ionic flow and keeps the positive and negative electrodes apart to prevent short circuits within the battery. The pore size of the film is required to be small enough to prevent dendritic lithium going through, and membranes with the pore sizes in the submicron range ($< 1\ \mu m$) have been shown to be adequate [5,10]. Other requirements for the separator film include chemical and mechanical stability, ease to be wetted by electrolyte, and more importantly, a shutdown feature for good safety.

One of the primary reasons that delay the broad application of lithium ion batteries in the commercial HEV and EV market is the safety issue [2]. Abuse of LIBs, such as high temperature operations and overcharge, can create excessive heat because of exothermic

reactions, which can lead to battery cracking or even explosion. This breakdown requires the battery to have a self-protection function. The microporous polyethylene (PE) separator film, due to its low melting point at around 135 ℃, provides a safety feature to prevent thermal runaway reactions in the battery. When the cell temperature reaches the shutdown temperature, slightly lower than the melting point of PE, the separator works as a thermal fuse by shutting down the pores and thus prevents ionic transport and cell reaction. However, if the temperature is further elevated above the melting point of the separator, the separator is highly likely to undergo a complete melt down and loses its mechanical integrity, which results in the contact of the electrodes and direct chemical reaction, leading to severe damage to the battery [11-13]. An ideal separator should possess a low shutdown temperature and a high meltdown temperature, and therefore could provide a greater safety margin (defined as the difference between MDT and SDT). For the commercially available PE separator films, the MDT is very close to the SDT. To enhance the MDT of the PE separator, many methods have been considered. For example, Celgard, LLC Corp developed the PP/PE bilayers and PP/PE/PP trilayers combing the low melting temperature of PE and the high melting temperature of PP, with the MDT being increased to around 180 ℃ [14]. Chung et al. conducted the PE film coating with various amounts of ethylene glycol dimethacrylate (DEGDMA) by radical polymerization in ethanol solution. The MDT of the coated PE separator was increased to 155 ℃ [15]. They also coated the PE film with nanocomposites composed of DEGDMA polymer and silica nanoparticles, which increased the MDT to 170 ℃. However, this coating approach decreased the porosity of the membrane, and therefore reduced the battery performance [16].

In another respect, electrospinning is a process that produces a continuous string of polymer fibers through the action of an external electric field imposed on a polymer solution. The pore size of the membrane generated by the electrospinning method falls in the range of microns and sub-microns, and the typical porosity is relatively high, up to 70% ~ 80% [17]. One important feature of electrospun mats is that the pore size and the porosity are highly dependent on the fiber diameter, which could be tuned by the electrospinning process [18]. Numerous polymers, such as polyacrylonitrile (PAN) [19], polyethersulfone (PES) [20,21], polyvinyl alcohol (PVA) [22], polyethylene oxide (PEO) [23] have been electrospun and the membranes have been used in different applications including filtration media, biological scaffold, protective fabrics, sensors and so on [24-26]. Notably, the electrospun membrane has also been demonstrated to be capable to use as a LIB separator, but one problem is that the electrospun membrane does not provide the shutdown feature [27,28]. It should be ideal to make a composite membrane which combines the advantages of the PE film (i.e. shutdown feature) and the electrospun membrane.

PES was selected as the material for the electrospun membrane due to its great chemical and mechanical stability, and more importantly, excellent heat resistance (with a T_g ~ 220 ℃ based on different sources) [29,30]. A composite separator film was prepared by depositing the electrospun PES membrane on both sides of a porous PE film, resulting in a sandwiched structure. It was expected that the meltdown temperature would be greatly improved above that of the commercial PP/PE/PP film, while the new sandwiched structure could still keep the low shutdown temperature of the PE film. Also,

due to the high porosity of the electrospun PES membrane, the porosity of the PE film was not likely to be reduced and the performance of the separator would not be sacrificed. To get desirable structure integrity of the PES/PE/PES separator film, a good adhesion between the electrospun PES nanofibrous membrane and the porous PE film is essential. However, the adhesion of PE to other materials is usually poor due to its low surface tension (30-31 dynes/cm), hydrophobic and chemically inert properties [31,32]. Both physical and chemical methods can be used to improve the surface adhesion. Physical method generally involves mechanical abrasion to generate more surface roughness, and therefore enhancing the mechanical interlocking with the adhesive [33,34]. A wide variety of surface chemical modification methods, such as chemical etching [35-39], flame treatment [40], plasma treatment [37], UV exposure [41] have been reported to introduce polar functional groups onto the surface and to increase the surface tension. In this study, a chemical modification method using chromic acid was applied, with the modification degree controlled by the acid treatment time. The electrospun PES membrane was deposited onto the treated PE film directly. The adhesion was also optimized by controlling the morphology of the electrospun PES membranes through the feeding rate of polymer solution during the electrospinning process. The preliminary tests on the separator film properties of the PES/PE/PES composite membrane were carried out at the Exxon Mobil Chemical Corp.

4.2 Experimental

4.2.1 Materials

Poly(ethersulfone) (PES) with a weight-average molecular weight (Mw) of 63,000 g/mol was purchased from Solvay Advanced Polymers. Dimethylformamide (DMF, 99.9%). potassium dichromate and sulfuric acid (95.0 – 98.0 %) were purchased from Sigma Aldrich. The PES was dried at 120 ℃ under vacuum for 6 hours and DMF was dried over molecular sieve (3Å) before use. The polyethylene lithium ion separator film (E25MMS) with an average thickness of 25 μm was provided by the Exxon Mobil Chemical Corp.

4.2.2 Preparation of electrospinning solution

28 wt% of PES was dissolved in the solvent of DMF to make the electrospinning solution [20,21]. The solution was stirred at 90 ℃ for two days to ensure homogeneity.

4.2.3 PE film treatment

The PE film was first immersed in ethanol and washed with DI water several times to remove surface contaminants. For the chromic acid, a ratio of K_2CrO_7:H_2O: H_2SO_4=7:12:150 by weight was selected based on the literature [39]. The PE film was immersed in at room temperature for 0 s, 10 s, 30 s, 60 s, 120 s, 240 s, respectively, then washed in running distilled water overnight, and dried under vacuum before use.

4.2.4 Electrospinning of PES membrane

The experimental set-up used for the electrospinning process is shown in Figure 1.2. Detailed description of the setup could be found in Section 2.2.3. The treated PE film was taped on the alumni foil which was wrapped on a rotating drum (diameter: 10 cm, rotating speed: 300 RPM), and the spinneret-to-collector distance was set at 10.5 cm. A

stepping motor was used to control the oscillatory translational motion of the spinneret to electrospin membrane with uniform thickness. The applied voltage in the electrospinning process was 12 kV. Different flow rates of PES polymer solution (20 μL/min, 40 μL/min, 60 μL/min, 80 μL/min) were tested. The process was operated in a closed chamber, with a temperature of 26 ± 1 ℃ and a relative humidity of 40 ± 2 % measured by a temperature and humidity meter (catalog number: 11-661-19, Fisher Scientific) during the electrospinning process..

4.2.5 Characterizations of the chemically treated PE surface

The surface topology of the PE films was characterized by using an atomic force microscope (AFM) (Dimension 3000, VEECO, Plainview, NY) equipped with version 5.12r5 NanoScope III Software. The chemical change of the surface produced by the chromic acid etching was studied using Fourier transform infrared spectroscopy (FTIR) with attenuated total reflectance (ATR) accessory (Nicolet iS10 spectrophotometer, Thermo Scientific, Inc.). Each sample was scanned 16 times in the 4000-650 cm^{-1} wavenumber range. The surface hydrophobicity was characterized by the water contact angle goniometry (CAM200 Optical Contact Angle Meter, KSV Instruments, LTD). 10 μL of Milli-Q Water was used as the probe liquid. At least three different spots were tested for each sample for consistent results.

4.2.6 Characterizations of electrospun PES membrane and adhesion strength tests

The electrospun PES membrane was deposited on only one side of the treated film in the following tests. The morphology of the electrospun PES membrane was characterized with scanning electron microscopy (SEM, LEO 1550) after gold-sputter coating. The average nanofiber diameter and standard deviation were analyzed from the SEM images

using the LeicaIMGRead software (http://dell.chem.sunysb.edu). The thickness of the PE/PES membrane was measured using a digital micrometer. The thickness of the electrospun membrane layer was calculated by the difference of the PES/PE membrane with that of the PE film. The PES membrane porosity was calculated with equation (2-1), using the PES bulk density of 1.37 g/cm^3 tested by the supplier using the ASTM D792 method.

The adhesion strength was determined by peeling the PES membrane from the PE substrate. To do this, a piece of double-faced adhesive tape was used to stick the PE side of the PE-PES film to the bench, with another tape sticking the PES membrane to a metal piece hooked with a Dillon BFG-50N force gauge. The size of the membrane and the tape used was kept at 10 mm × 5 mm. A pulling force was gradually applied 90 ° upwards until the PES membrane was pulled off the PE film. The maximum force was recorded by the force gauge. The adhesion strength was calculated by the maximum force divided by the membrane area.

4.2.7 Preliminary battery performance tests on the PES/PE/PES membrane

The following separator film properties were tested at the Exxon Mobil Corp. Detailed test procedures, although classified as propriety, followed the standard testing procedures outside ExxonMobil, and were described as follows.

In a **shutdown temperature** measurement, the separator was placed in an impedance measurement cell, and the electrical impedance was measured as a function of temperature. The temperature was recorded as the shutdown temperature where a sharp impedance increase was observed.

Meltdown temperature is a measurement of a separator's ability to hold its mechanical integrity and to provide the safety margin above the shutdown temperature. It is characterized with thermal mechanical analysis (TMA). In the TMA, the separator was held under constant load. The degree of elongation versus temperature was measured. The temperature was recorded as the meltdown temperature where the separator lost its mechanical integrity and the elongation dramatically increased.

The **gurley number** was tested by the method ASTM-D726 (B). It is a measurement of air permeability of the membrane, expressed by the time required for a specific amount of air passing through a specific area of the membrane under a specific pressure. For LIB separator films, separator permeability is usually characterized by air permeability. The gurley number is also a good estimation of the electrical resistance (ER) of the membrane, as it is proportional to the ER for a fixed membrane morphology [5].

Puncture strength is a measurement of the physical strength the separator film can bear in cell assembly and other daily use, as the separator is in direct touch with the rough surfaces of the two electrodes. The puncture strength (PS) is characterized as the weight that has to be applied for a needle to pierce a separator [42].

4.3 Results and Discussions

4.3.1 Characterization of chemically treated PE film

It is known that chemical etching using strong oxidation acid, such as concentrated sulfuric acid, nitric acid and chromic acid, can induce physical and chemical changes to the material surface. These changes of the PE film were characterized with the following methods.

Figure 4.1 shows the 3D surface topography with an area of 10 × 10 μm^2 obtained using AFM for untreated PE surface and the surfaces with different acid treatment time. AFM is a highly sensitive tool that can perform qualitative and quantitative roughness study of the surface morphology and topology in the nano-scale range. The R_{rms} (root mean squared) value of the untreated PE film was 29.9 nm. The Z range, being the maximum height difference between the peaks and valleys, was 201.7 nm. From the 3D representation of the samples, it could be seen that the surface roughness was increased with the acid treatment time. This was also confirmed by the quantitative measurements of the R_{rms} and Z range value. As listed in Table 4.1, both R_{rms} and Z range values were increased with the acid treatment time. Specifically, with the chromic acid treated for 240 s, the R_{rms} of the PE film surface was increased to 56.3 nm, and the Z range was increased to 423.8 nm, representing a remarkable increase in surface roughness.

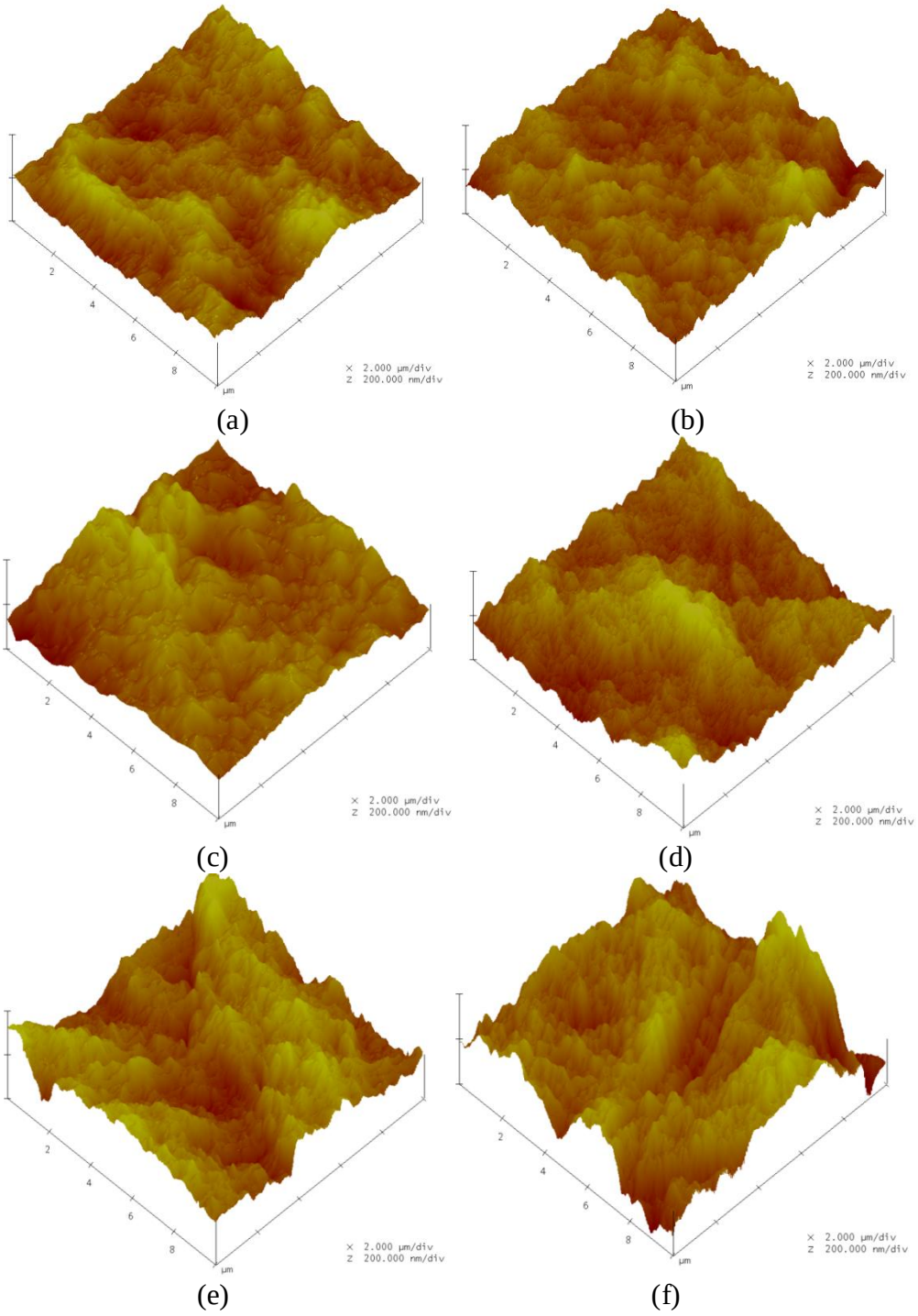

Figure 4.1 AFM images of PE film after treated with chromic acid for (a) 0 s; (b) 10 s; (c) 30 s; (d) 60 s; (d) 120 s; (e) 240 s

Table 4.1 Variation of root mean squared surface roughness R_{rms} and Z range obtained from AFM analysis with respect to different acid treated time.

Acid treated time (s)	R_{rms} (nm)	Z range (nm)
0	29.9	201.7
10	31.0	250.7
30	41.0	293.1
60	45.5	336.4
120	53.3	349.1
240	56.3	423.8

The chemical change of the PE film surface was evaluated by FTIR, as shown in Figure 4.2. The absorption peak at 2360 cm^{-1} for all samples is due to the atmospheric CO_2 [43]. The peaks at 2910, 2846, 1463 and 721 cm^{-1} corresponded to the -CH_2 asymmetric stretching, symmetric stretching, bonding deformation and rocking deformation of polyethylene, respectively [44]. Compared to the untreated surface, the presence of the adsorption peak at 1730 cm^{-1} indicated the existence of C=O functional group, which was introduced by the chromic acid treatment. The strengthening peak signal with treatment time also indicated more polar groups were introduced onto the surface with the acid treatment time. It was also noted that for the PE film treated with chromic acid for 120 and 240 seconds, multiple peaks in the range of 1000 – 1300 cm^{-1} appeared, revealing the generation of C-O groups.

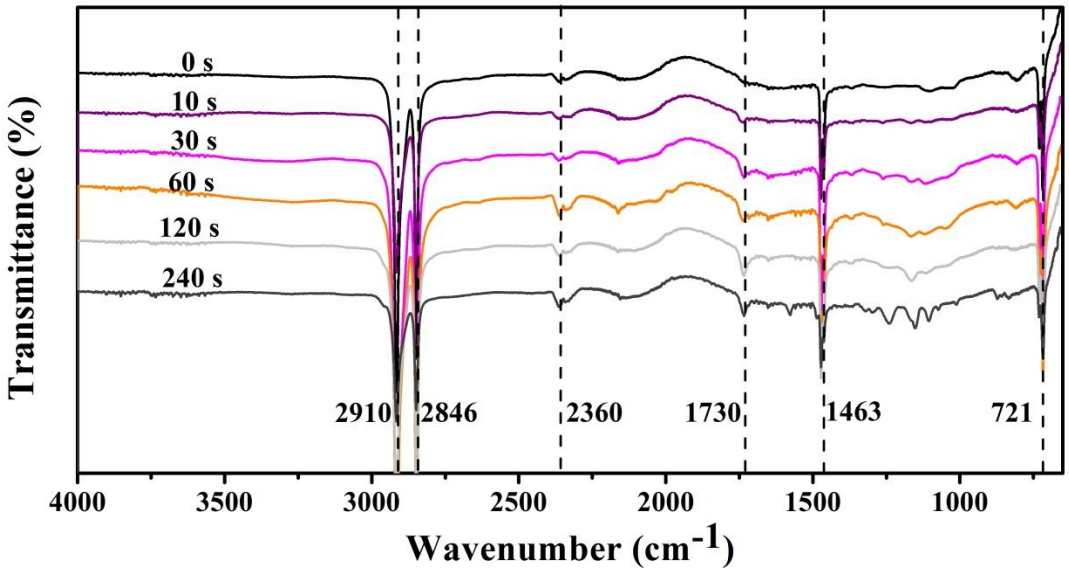

Figure 4.2 FTIR spectra of polyethylene surface with different chromic acid treatment time

The introduction of polar groups was believed to have increased the surface tension, which could also be validated by the water contact angle test. In adhesion science and technology, precise measurements of solid surface energy are generally very difficult. Instead, the water contact angle test can be used to evaluate the surface energy based on Young's equation,

$$\cos\theta = \frac{\gamma_{SG} - \gamma_{SL}}{\gamma_{LG}} \qquad (4\text{-}1)$$

where θ is the water contact angle, γ_{SG}, γ_{LG}, γ_{SL} are the interfacial surface tensions between the solid and the vapor, the liquid and the vapor, and the solid and the liquid, respectively.

The untreated PE film had a water contact angle of $89 \pm 2°$, indicating its hydrophobic nature. With the chromic acid treatment and the prolongation of the treatment time, the water contact angle was gradually decreased to $86 \pm 3°$, $82 \pm 2°$, $79 \pm 1°$, $71 \pm 2°$, $65 \pm 2°$ at 10 s, 30 s, 60 s, 120 s, 240 s, respectively, as shown in Figure 4.3. The decrease in the water contact angle was a result of introduction of more functional groups, resulting in higher surface tension γ_{SG} with longer acid treatment time.

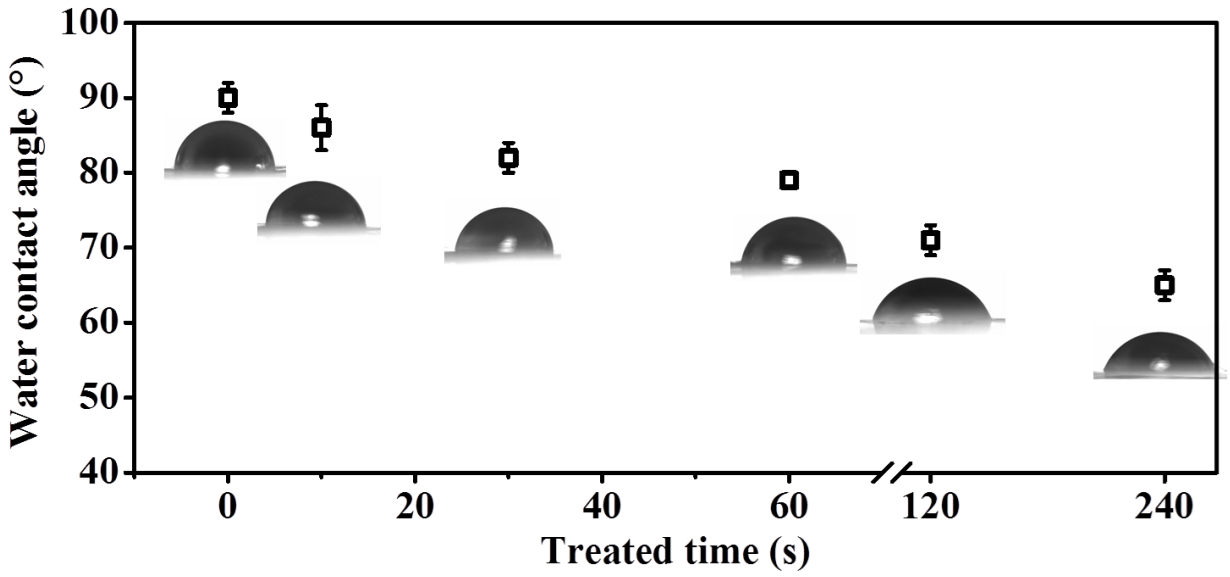

Figure 4.3 Water contact angles of PE separator films treated with chromic acid for different time periods

Another factor, surface roughness, was also considered to contribute to the decrease in the water contact angle. When dealing with the water contact angle on a rough surface, based on the Wenzel model, a roughness factor has to be included and can be adequately expressed by [45]

$$f = \frac{A}{A_0} \tag{4-2}$$

where A is the "real" total surface area, and A_0 is the nominal surface area.

Derived from Young's equation, the Wenzel model can be expressed as,

$$\cos\theta^* = f\cos\theta \tag{4-3}$$

where θ^* is the water contact angle on a rough surface.

As the water contact angles of the PE films fell in the range of 0 ~ 90 °, a longer acid etch time increased the surface roughness factor (as f > 1) to a larger extent, and therefore can result in a smaller water contact angle based on equation (4-3).

4.3.2 Characterizations of electrospun PES membrane and adhesion strength

The effect of chromic acid treatment of the PE film on adhesion is shown in Figure 4.4. With a fixed electrospun membrane morphology at a flow rate of 60 μL/min, the adhesion of the original PE film to the electrospun membrane was 1.06 ± 0.13 N/cm^2. When the PE film was treated with chromic acid, due to the increase in the surface tension and roughness, the adhesion to the electrospun membrane was increased with increasing acid-oxidation time. The PE film treated with chromic acid for 240 s showed an adhesion strength of 10.06 ± 0.76 N/cm^2 to the electrospun PES membrane, indicating a significant improvement of adhesion strength (~10 times) brought by the chromic acid treatment.

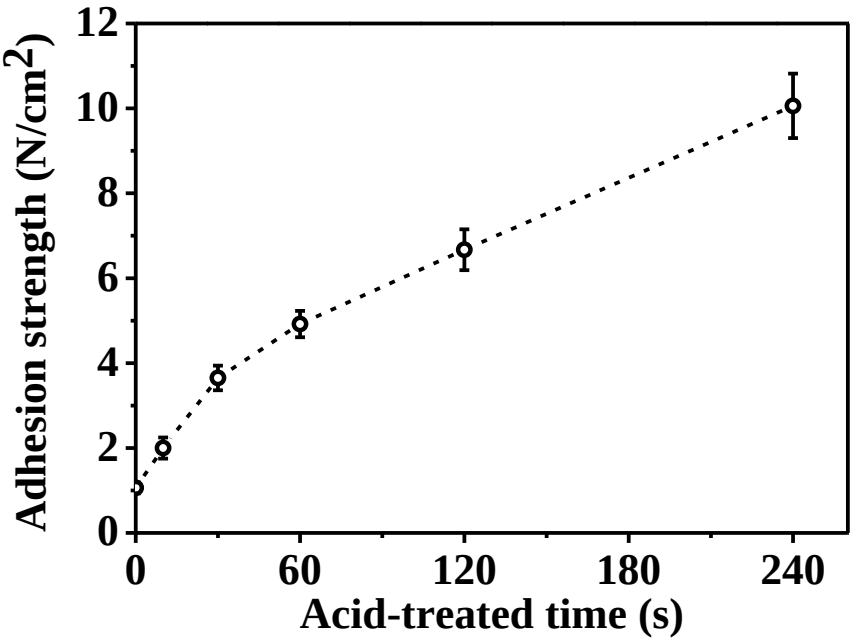

Figure 4.4 Effect of chromic acid treatment time on adhesion of PE film to PES membrane electrospun at a flow rate of 60 μL/min

In another aspect, the morphology of the electrospun PES membrane, such as whether it is nanofiber-dominating or bead-dominating, determines its available contact area to the PE separator film, which could affect the adhesion strength. In addition, the state of the nanofibers, i.e., whether they are dry or wet when deposited onto the PE separator film, also has a great influence on the adhesion [20]. It is known that the morphology of the membrane and the state of fibers can be manipulated by using different electrospinning parameters. Figure 4.5 shows the adhesion strength change with respect to the electrospinning flow rate, with the PE film having been treated with chromic acid for 240 s. At a low flow rate of 20 μL/min, the adhesion strength was 1.87 ± 0.19 N/cm^2. As the flow rate increased to 40 μL/min and 60 μL/min, the adhesion strength increased to 5.09 ± 0.89 N/cm^2 and 10.45 ± 1.05 N/cm^2. A further increase in the flow rate to 80 μL/min resulted in a comparable adhesion strength of 10.40 ± 0.38 N/cm^2 to that at 60 μL/min. By varying the flow rate during electrospinning process, an over 5 times increase in the bonding strength was achieved.

On the other hand, the porosity of the electrospun membrane should also be considered, as a lower porosity than that of the PE film will decrease the performance of the separator. Due to the interconnected pore structure of the electrospun membrane, the porosity reached a high value of 77.9 ± 2.5 % at the flow rate of 20 μL/min. With increasing flow rate, the porosity was gradually decreased to 74.0 ± 1.6 %, 68.4 ± 2.4 % and 66.0 ± 2.8 % at flow rates of 40 μL/min, 60 μL/min and 80 μL/min, respectively. Despite of the decreased porosity of the electrospun PE membrane, it still maintained a higher value than that of the PE film (~ 40% [5]).

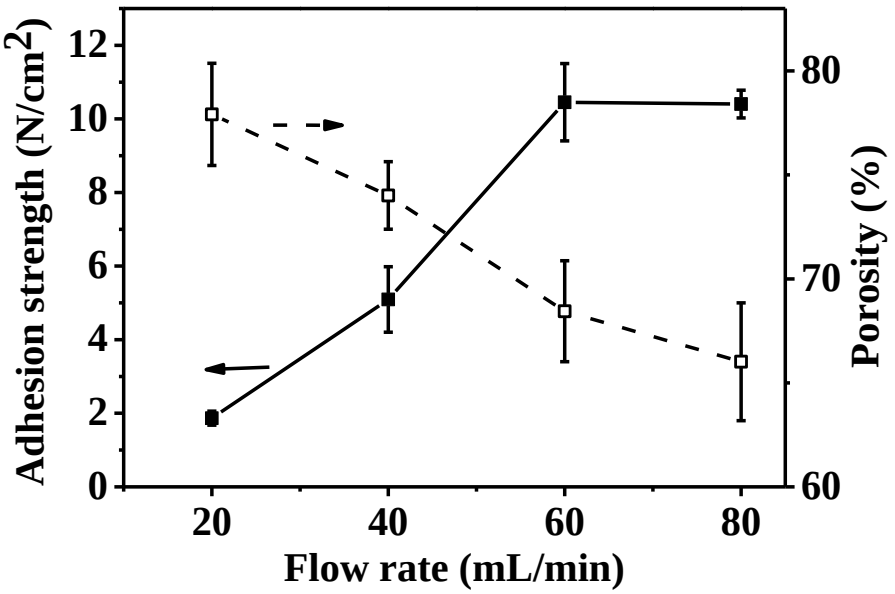

Figure 4.5 Effect of electrospinning flow rate on the adhesion of PE film to the electrospun PES membrane, with the PE film having been treated with chromic acid for 240 s

To assist the understanding of results, SEM images of membranes electrospun at different flow rates are shown in Figure 4.6. The average fiber diameter increased and the fiber diameter distribution became broadened with the increasing the flow rate. The average fiber diameter electrospun at flow rates of 20 μL/min, 40 μL/min, 60 μL/min and 80 μL/min ranged from 396 ± 168 nm, 408 ± 245 nm, 426 ± 225 nm, 550 ± 241 nm, respectively. This change could be due to a greater volume of solution that was drawn away from the needle tip [18]. In terms of fiber morphology, at the low flow rate of 20 μL/min, the membrane structure was dominated with nanofibers. As the flow rate was increased to 40 μL/min, a mixed structure of nanofibers and a greater amount of spindle-shaped fibers was formed. When the flow rate was further increased to 60 μL/min and 80 μL/min, the feeding rate of solution to the spinneret was in excess to the rate of the solution that could be drawn from the spinneret, and the polymer solution dripped onto the membrane. The morphology change of membrane from nanofiber to spindle and solution dripping was believed to have increased the contact area of the electrospun PES membrane to the PE film, which was in favor of higher adhesion. Meanwhile, the residual solvents in the spindle and dripping created a "wet" state of the electrospun membrane on the PE film, and were also desirable for better bonding, so long as the porosity could remain within the acceptable range.

The effect of the morphology change on the electrospun membrane porosity was also obvious. As more beads or dripping resulted in less membrane porosity, which was confirmed by the porosity measurement.

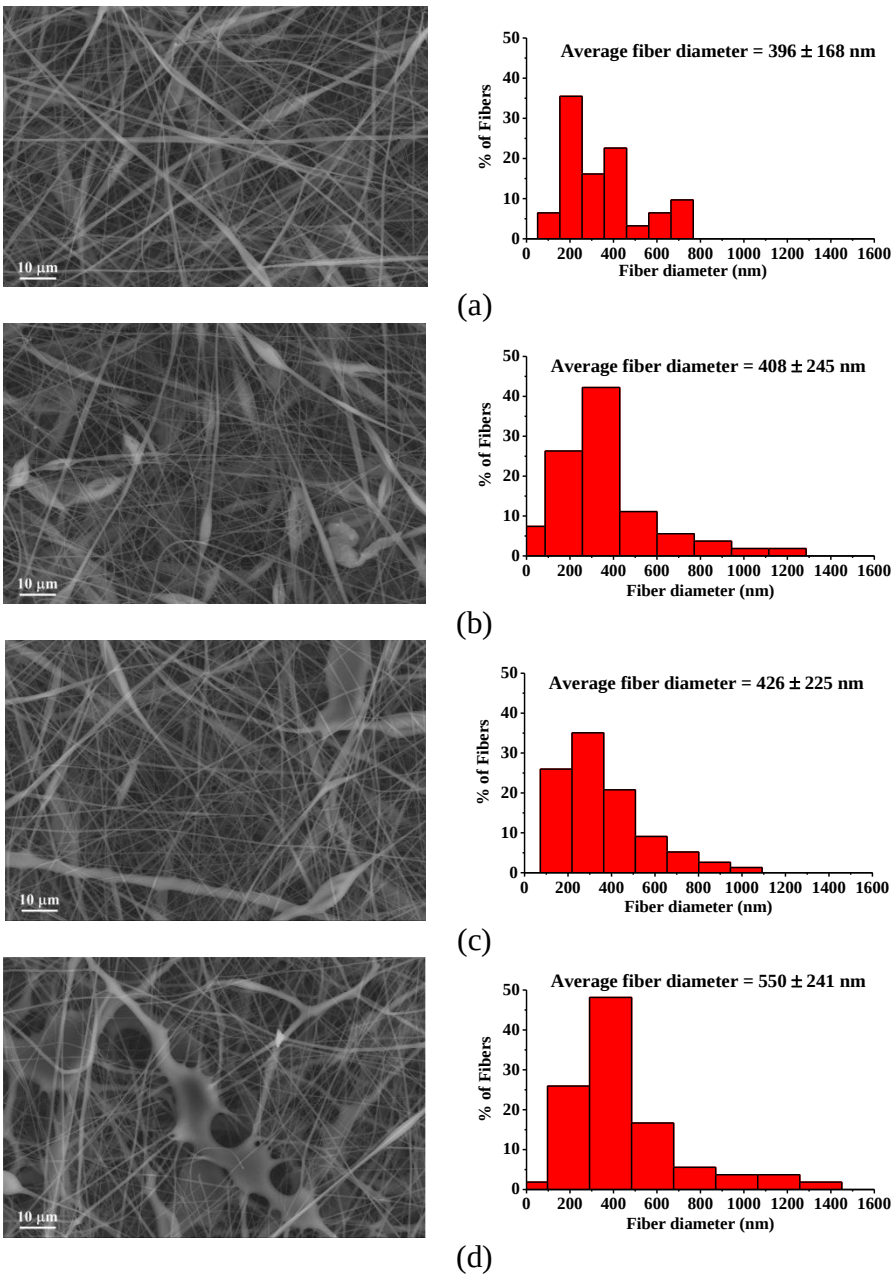

Figure 4.6 SEM images and fiber diameter distribution of electrospun PES membranes at the flow rate of (a) 20 μL/min; (b) 40 μL/min; (c) 60 μL/min; (d) 80 μL/min

4.3.3 Preliminary separator property tests

Some properties of the base PE film, the PES/PE/PES composite film and a Celgard 2320 film was listed in Table 4.2. Compared to the Celgard 2320 film, the base PE film has a higher thickness and a lower porosity, and thus a higher puncture strength and a lower air permeability (i.e., a higher Gurley number). The meltdown temperature was also lower than the commercial Celgard 2320 film due to its single-material component. The PES/PE/PES composite membrane was prepared by electrospinning PES onto both side of the PE film that was treated with chromic acid for 240 seconds membrane was electrospun at a flow rate of 60 μL/min. The thickness of each PES membrane was 9 ± 1 μm, and the resulting thickness of the composite membrane was 43 ± 2 μm. Compared to the base film, the overall porosity of the composite film had a higher porosity due to the introduction of the electrospun PES membrane (porosity ~ 68%). However, the porosity of the air-permeability-determining layer, i.e., the middle PE film layer was not changed, and therefore the gurley number was kept the same. The puncture strength of the composite membrane was slightly lower than the base film, which was probably resulted from the mechanical degradation by the acid etching. The shutdown temperature of the composite film maintained the same as that of the base film. It is not surprising that the meltdown temperature was significantly increased to 221 ℃ by the introduction of PES layer. The safety margin of the separator was greatly broadened. In comparisons to the commercial Celgard 2320 film, the new composite membrane had a lower SD temperature and higher MD temperature, and therefore provided a greater safety margin. The cell performance using the composite membrane has not been tested at the current stage, but it is believed that the result would be very close to that using the base PE film,

as the major properties of the two separators except the thermal property are almost the same.

Table 4.2 Properties of different separator films

	E25MMS (Base film)	Composite membrane	Celgard 2320 (Commercial film)
Composition	PE	PES/PE/PES	PP/PE/PP
Thickness (μm)	25	43 ±2	20
Porosity (%)	36	36 [1] ~ 49 [2]	39
SD temperature (℃)	131	131	139
MD temperature (℃)	153	221	184
Gurley (sec)	640	640	473
Puncture strength (g)	550	544	391

1. Porosity of PE film (air-permeability-determining layer)

2. Porosity of composite membrane calculated from the thickness and porosity of each layer

4.4 Conclusions

The commercial polyethylene LIB separator film has a low meltdown temperature which limits its wide application in HEVs and EVs. To enhance the meltdown temperature, polyethersulfone, a polymer with a higher thermal resistance, was electrospun onto the base PE film on each side to make a composite separator. Due to the chemically inert nature of the PE film and its weak bonding to the electrospun PES membrane, a chemical etching method with chromic acid treatment to the PE film was introduced. The surface topology test with AFM showed that with longer acid treatment time, the surface roughness was increased. FTIR spectroscopy showed that functional polar groups, such as C=O and C-O, were introduced onto the PE film, leading to an increase in the surface tension. The water contact angle on the surface of the PE film could be shown to have decreased with the acid treatment time, due to the increased surface energy and roughness. The PE film treated with chromic acid for 240 seconds showed a 10-fold increase of the adhesion to the electrospun PES membrane when compared with the untreated one. In another aspect, the morphology of the electrospun PES membrane was also demonstrated to have a great impact on the adhesion. "Wet" membranes and those with solution drippings were electrospun at high flow rates, such as 60 μL/min and 80 μL/min, and they could be shown to have better bonding to the PE film. Compared to the nanofiber-dominating electrospun membrane produced at a flow rate of 20 μL/min, they showed ~ 5 times increase in the bonding strength to the acid treated PE film. Although the porosity of the electrospun PES membrane was decreased with increasing flow rate, it still maintained a high enough porosity (~ 68% at 60 μL/min) when compared with that of the base PE film. The separator property tests of the

composite PES/PE/PES membrane showed unchanged air permeability and shutdown temperature due to the existence of the PE film in the middle layer. The meltdown temperature was significantly increased to 221 ℃ compared to the original value of 153 ℃ of the base film, and was higher than the commercial Celgard 2320 film. In comparison with other treatment methods, coating the PE separator film with highly porous electrospun PES membranes could greatly broaden the safety margin of the separator used in lithium-ion batteries, and still keep other separator properties unchanged.

Acknowledgements

The authors acknowledge the contributions of Dr. Andy H. Tsou from ExxonMobil Research and Engineering Company for the separator property tests. The authors also thank graduate student Cheng Pan from Materials Science & Engineering Department at Stony Brook University for kind assistance with the AFM and water contact angle measurements.

Reference

1. Linden, D. (2002) *Handbook of Batteries*, 3rd ed., McGraw-Hill, New York
2. Bandhauer, T. M., Garimella, S., and Fuller, T. F. (2011) *J Electrochem Soc* **158**, R1-R25
3. Lisbona, D., and Snee, T. (2011) *Process Saf Environ* **89**, 434-442
4. Brodd, R. J., Bullock, K. R., Leising, R. A., Middaugh, R. L., Miller, J. R., and Takeuchi, E. (2004) *J Electrochem Soc* **151**, K1-K11
5. Arora, P., and Zhang, Z. M. (2004) *Chem Rev* **104**, 4419-4462
6. Broussely, M., and Archdale, G. (2004) *J Power Sources* **136**, 386-394
7. Broussely, M. (2006) *Electron World* **112**, 16-21
8. Xu, K. (2004) *Chem Rev* **104**, 4303-4417
9. Croce, F., Appetecchi, G. B., Persi, L., and Scrosati, B. (1998) *Nature* **394**, 456-458
10. USABC. (2001) *RFPI*
11. Abraham, K. M. (1993) *Electrochim Acta* **38**, 1233-1248
12. Laman, F. C., Gee, M. A., and Denovan, J. (1993) *J Electrochem Soc* **140**, L51-L53
13. Dahn, J. R., Fuller, E. W., Obrovac, M., and Vonsacken, U. (1994) *Solid State Ionics* **69**, 265-270
14. www.celgard.com/.
15. Chung, Y. S., Yoo, S. H., and Kim, C. K. (2009) *Ind Eng Chem Res* **48**, 4346-4351

16. Yoo, S. H., and Kim, C. K. (2009) *Ind Eng Chem Res* **48**, 9936-9941

17. Huang, Z. M., Zhang, Y. Z., Kotaki, M., and Ramakrishna, S. (2003) *Compos Sci Technol* **63**, 2223-2253

18. Zong, X. H., Kim, K., Fang, D. F., Ran, S. F., Hsiao, B. S., and Chu, B. (2002) *Polymer* **43**, 4403-4412

19. Wang, R., Liu, Y., Li, B., Hsiao, B. S., and Chu, B. (2012) *J Membrane Sci* **392**, 167-174

20. Tang, Z. H., Qiu, C. Q., McCutcheon, J. R., Yoon, K., Ma, H. Y., Fang, D. F., Lee, E., Kopp, C., Hsiao, B. S., and Chu, B. (2009) *J Polym Sci Pol Phys* **47**, 2288-2300

21. Yoon, K., Hsiao, B. S., and Chu, B. (2009) *Polymer* **50**, 2893-2899

22. Greiner, A., Zeng, J., Wendorff, J. H., and Hou, H. Q. (2003) *Abstr Pap Am Chem S* **226**, U405-U405

23. Nagamine, S., Tanaka, Y., and Ohshima, M. (2009) *Chem Lett* **38**, 258-259

24. Greiner, A., and Wendorff, J. H. (2007) *Angew Chem Int Edit* **46**, 5670-5703

25. Li, D., and Xia, Y. N. (2004) *Adv Mater* **16**, 1151-1170

26. Yoon, K., Kim, K., Wang, X. F., Fang, D. F., Hsiao, B. S., and Chu, B. (2006) *Polymer* **47**, 2434-2441

27. Choi, S. S., Lee, Y. S., Joo, C. W., Lee, S. G., Park, J. K., and Han, K. S. (2004) *Electrochim Acta* **50**, 339-343

28. Gopalan, A. I., Santhosh, P., Manesh, K. M., Nho, J. H., Kim, S. H., Hwang, C. G., and Lee, K. P. (2008) *J Membrane Sci* **325**, 683-690

29. http://www.matweb.com.

30. http://www.rtpcompany.com/info/data/1400/RTP1400AG-210.htm.

31. David, E., Lazar, A., and Armeanu, A. (2004) *J Mater Process Tech* **157**, 284-289

32. Ueda, M., Kostov, K. G., Beloto, A. F., Leite, N. F., and Grigorov, K. G. (2004) *Surf Coat Tech* **186**, 295-298

33. Encinas, N., Abenojar, J., and Martinez, M. A. (2012) *Int J Adhes Adhes* **33**, 1-6

34. Henry, C., Minier, J. P., and Lefevre, G. (2012) *Langmuir* **28**, 438-452

35. C. Fonseca, J. M. Perena, J. G. Fatou, and Bello, A. (1985) *Journal of Materials Science* **20**, 3283-3288

36. D. S. Bag, V. P. Kumar, and S. Maiti. (1997) *Die Angewandte Makromolekulare Chemie* **249**, 33-46

37. E. V. Kuvaldina, T. G. Shikova, S. A. Smirnov, and V. V. Rybkin. (2007) *High Energy Chemistry* **41**, 284-287

38. S. L. Favaro, A. F. Rubira, E. C. Muniz, and E. Radovanovic. (2007) *Polymer Degradation and Stability* **92**, 1219-1226

39. Briggs, D. (1976) *Journal of Materials Science* **11**, 1270-1277

40. E. Sheng, I. Sutherland, D. M. Brewis, R. J. Heath, and R. H. Bradley. (1994) *Journal of Materials Chemistry* **4**, 487-490

41. I. Mathieson, and R. H. Bradley. (1995) *INT. J. Adhesion and Adhesives* **16**, 29-31

42. Fjuii, T. M., T. (1998). U.S. Patent 5,759,678

43. Rasko, J. (1998) *Catal Lett* **56**, 11-15

44. Gulmine, J. V., Janissek, P. R., Heise, H. M., and Akcelrud, L. (2002) *Polym Test* **21**, 557-563

45. Lafuma, A., and Quere, D. (2003) *Nat Mater* **2**, 457-460

Chapter V Removal of Cr (VI) from Aqueous Solution using Polyvinylamine Grafted Electrospun Polyacrylonitrile Nanofirous Membrane

A simple and effective way of preparing electrospun nanofibrous microfiltration membrane with positive surface charges for Cr (VI) removal is being reported. Polyacrylonitrile (PAN) was used as the base material and electrospun to form ananofibrous membrane with an average diameter of about 200 nm. Polyvinylamine (PVAm), a polymer with a high positive charge density was grafted and cross-linked onto the nanofibers. The microfiltration characteristics of the modified and original membranes, such as porosity, maximum and mean pore size, pure water flux and mechanical strength were fully investigated. The pH effect and initial Cr(VI) concentration effect on the static adsorption rate were studied in the pH range of 1.0 to 13.0, and the concentration range of 5 mg/L to 100 mg/L, respectively. Both experimental and theoretical results showed the favorable pH range for Cr(VI) adsorption was 3.0 to 5.0. Due to the high surface charge density, the membrane demonstrated a saturation adsorption capacity of 57.1 mg Cr(VI) on a per gram basis of the membrane, or 627.5 mg Cr(VI) per gram of the grafted PVAm based on the calculation using the Langmuir model. The membrane also showed a good Cr(VI) adsorption capacity in the dynamic adsorption test, with a higher adsorption rate obtained at a lower flow rate as a

result of longer contact time between the active sites of the membrane and the Cr (VI) ions. Moreover, this membrane could be easily regenerated from the Cr(VI) adsorption by immersing it into a 0.1M NaOH for 1h. These properties ensured the membrane a very suitable candidate in removing Cr(VI) and other negatively charged species from aqueous solution, and yet without compromising its functionality as a microfiltration membrane.

5.1 Introduction

In both developing and developed countries, the human activities are causing more and more pollutants to water. Among the various contaminants, heavy metals, such as chromium, have highly toxic and non-biodegradable properties and can cause severe problems to both the environment and the living organism. Chromium and its compounds are extensively used in industrial processes such as metal finishing, plating, storage batteries, leather tanning, etc. [1]. It is present in the environment in the oxidation states of Cr (III) and Cr (VI). Cr (III) occurs naturally and stably in the environment and is an essential nutrient, whereas Cr (VI) is high water soluble and toxic [2-4]. Cr (VI) is considered to be carcinogenic and mutagenic in nature according to the International Agency on Cancer (IARC) [5]. Long-time exposure to Cr (VI) has been known to possibly cause dermatitis, damage to liver, kidney circulation, nerve tissue damage and death in large does [6]. Recognizing its toxic effect, the World Health Organization (WHO) has set the maximum allowable level of total chromium in drinking water at 50 μg/L [2]. To avoid the substantial risk to the humans and natural environment, Cr (VI) must be removed from the wastewater before it can be discharged.

Several methods of removing heavy metals from aqueous solution have been reported, including ion exchange [7], chemical precipitation [8,9], electrolysis [10], nanofiltration and reverse osmosis [11-13] and adsorption [14]. Adsorption is either by electrostatic interactions between the different charges of the target ion and the adsorbent, or by chelation (donation of lone-pair electrons to the empty electron orbital of metal ions to form co-ordinate bond). In comparison with other methods, especially from economical and environmental view points, the advantages of adsorption include easy operation,

availability, high efficiency and low cost [15]. A variety of natural and synthetic adsorbents such as biosorbents [16-18], activated carbons [19-23] chitosan [24,25] and ferrihydrite [26,27] have been used in removing heavy metal ions. However, methods using these adsorbents often involve an additional post-treatment procedure, i.e., filtering the adsorbents out from the aqueous solution.

Recently, the electrospun nanofibrous membrane has gained a great deal of attention in various fields such as air filtration[28], tissue engineering [29,30], optical sensor [31], etc. It is also attracting more and more interest in water filtration applications due to its unique structure characteristics, such as up to 80% porosity, symmetric open pore structure formed by entanglement of nanofibers, and controllable pore sizes in the micron and submicron size range [32,33]. For example, electrospun nanofibrous membranes used as microfiltration (MF) membranes showed great advantages over the conventional phase inversion MF membranes on the pure water flux and particle rejection rate [34-36]. Yoon and et al reported novel composite UF and NF membranes using electrospun membranes as the substrate demonstrated great improvements in the water flux when compared with traditional UF/NF membranes [37-40]. Meanwhile, the property of high surface area-to-volume ratio makes the electrospun nanofibrous membrane specifically useful for heavy metal adsorption. Compared to the traditional absorbents, the advantages of the electrospun nanofibrous membrane are that they can function additionally as microfiltration membranes to provide characteristics, such as high permeability, small and regular pore size and ability to withstand relatively higher pressures of up to several hundred psi. The integrated structure as a membrane also ensures that both static and

dynamic adsorption of heavy metal ions from aqueous solution can be performed without additional treatment procedures or specifically constructed devices.

Polyacrylonitrile (PAN) was selected as the material for the electrospun membrane for three reasons. (1) PAN has been widely used in the filtration membranes due to its good solvent resistance [41,42]. (2) It is relatively easy to electrospun PAN into bead-less membrane with thin and uniform nanofibers [36]. (3) The nitrile group of PAN can be modified into different functional groups to meet specific needs. A few researchers have reported heavy metal adsorptions using modified electrospun PAN membrane. For example, Kampalanonwat et al. modified the PAN electrospun membrane with diethylenetriamine (EDTA) via a heterogeneous reaction. The resultant membrane was used for adsorption of Ag(I), Fe(II) and Pb(II) ions [43]. Saeed modified PAN nanofibers with hydroxylamine hydrochloride, and tested it in the Cu(II) and Pb(II) adsorptions [44]. They have also reported a similar work by modifying PAN nanofibers with hydrazine [45]. However, chemical modification of electrospun membranes lacks practical applications, especially in the scale-up and massive production of the membrane. Also, membrane deformation and pore blockage were often observed in the chemical modification.

In the present work, a grafting technique with polycations was applied onto the electrospun PAN nanofibers. Since the primary ionic states of Cr(VI) in solutions are CrO_4^{2-} and $Cr_2O_7^{2-}$, which are both negatively charged, the PAN nanofibers should be grafted with positive charges on the surface. Polyvinylamine (PVAm), a linear hydrocarbon chain with primary amine groups on alternating carbons, was chosen as the grafting polymer. The molar equivalent of primary amine groups for the polymer form of

PVAm is 22.5 meq/g, being the most abundant among the polyamines. The pKa of PVAm is close to that of alkylmonoamines at ~10.6 [46,47], which ensures that the polymer can maintain positive charges over a wide pH range. Although not all the amine groups can be ionized due to the nearest neighbor effect, the free ammonium groups are still able to bind the heavy metal ions by forming chelating complexes [48,49]. As PVAm is water soluble, after being grafted onto the acid-treated PAN nanofibers, it was cross-linked with glutaraldehyde (GA) using a simple immersing method. The microfiltration properties of the membrane before and after grafting were investigated. The effect of pH and the initial metal ion concentration on the static adsorption capacity of the modified membrane towards Cr(VI) were examined. Dynamic adsorption test was performed using a dead-end filtration system. Finally, to test the reusability of the membrane, desorption of the metal ions from the preadsorbed membrane was also studied.

5.2 Experimental

5.2.1 Materials

The PAN powder with the weight-average molecular weight (M_w) of 150,000 g/mol was purchased from Scientific Polymer Products. Dimethylformamide (DMF, 99.9%) purchased from Sigma-Aldrich was used as the electrospinning solvent. The non-woven polyethylene terephthalate (PET No. 16-1) purchased from Sanko Ltd, Japan used as the substrate for the electrospun PAN membrane. The aqueous solution of polyvinylamine (PVAm) (M_w = 340,000 g/mol, hydrolysis degree > 90%) was provided by the BASF Corporation. The following chemicals were purchased from Sigma-Aldrich and used as received. Glutaraldehyde (GA) (50% aqueous solution), hydrochloric acid (36.5%

aqueous solution) and acetone (99.8%) were used for the cross-linking solution. Potassium dichromate (ACS reagent, ≥ 99.0%), diphenylcarbazide (ACS reagent) and sulfuric acid (ACS reagent, 95 - 98%) were used in the Cr(VI) adsorption test.

5.2.2 Electrospinning of PAN nanofibrous membrane

The PAN solution was prepared by dissolving 8 wt% PAN powder into DMF at 60 ℃ and stirred overnight. After being cooled down to room temperature, the solution was fed to the spinneret (diameter 1 mm) tip through a 20 mL BD Luer-Lok ™ syringe (catalog number 309661, BD, USA)at a feeding flow rate of 20 L/min controlled by a programmable syringe pump (Model M061-FD08, Superior Electric Company, USA). The power supply from Glassman High Voltage, Inc was used to supply the applied voltage of 16 kV. A grounded metal drum (diameter: 10 cm) with a rotating speed of 300 rpm was used as the collector and the spinneret-to-collector distance was 9cm. A stepping motor was used to control the oscillatory translational motion perpendicular to the drum rotation direction. The process was operated in a closed chamber, with the temperature of 25 ± 1 ℃ and the relative humidity of 53% ± 3% as monitored using a temperature and humidity sensor, manufactured by Fisher Scientific (catalog number: 11-661-19,). The thickness of final membranes was controlled to 40 ± 3 μm by adjusting the delivered volume of the polymer solution.

5.2.3 Preparation of functional nanofibrous membrane for metal adsorption

To facilitate the grafting of PVAm onto PAN nanofibers, the as-spun nanofibrous membrane was introduced with –COOH group by being immersed in concentrated sulfuric acid at different concentrations (50 wt%, 60 wt%, 70 wt%) for 30 min at room temperature. The membrane was washed with distilled water for several times to remove

the residual sulfuric acid. The hydrolyzed PAN e-spun membrane was then immersed in 3 wt% PVAm aquesou solutions for 15 min. The excessive polymer solution was gently removed from the surface of the membrane with a glass rod. The membrane was dried in the oven at 60 ℃. Cross-linking of the grafted PVAm was applied by immersing the membrane in 80 mM GA aqueous solution for 1 min, followed by drying the membrane in the oven at 60 ℃ [39]. The membrane was then washed in water for several times and dried before tests.

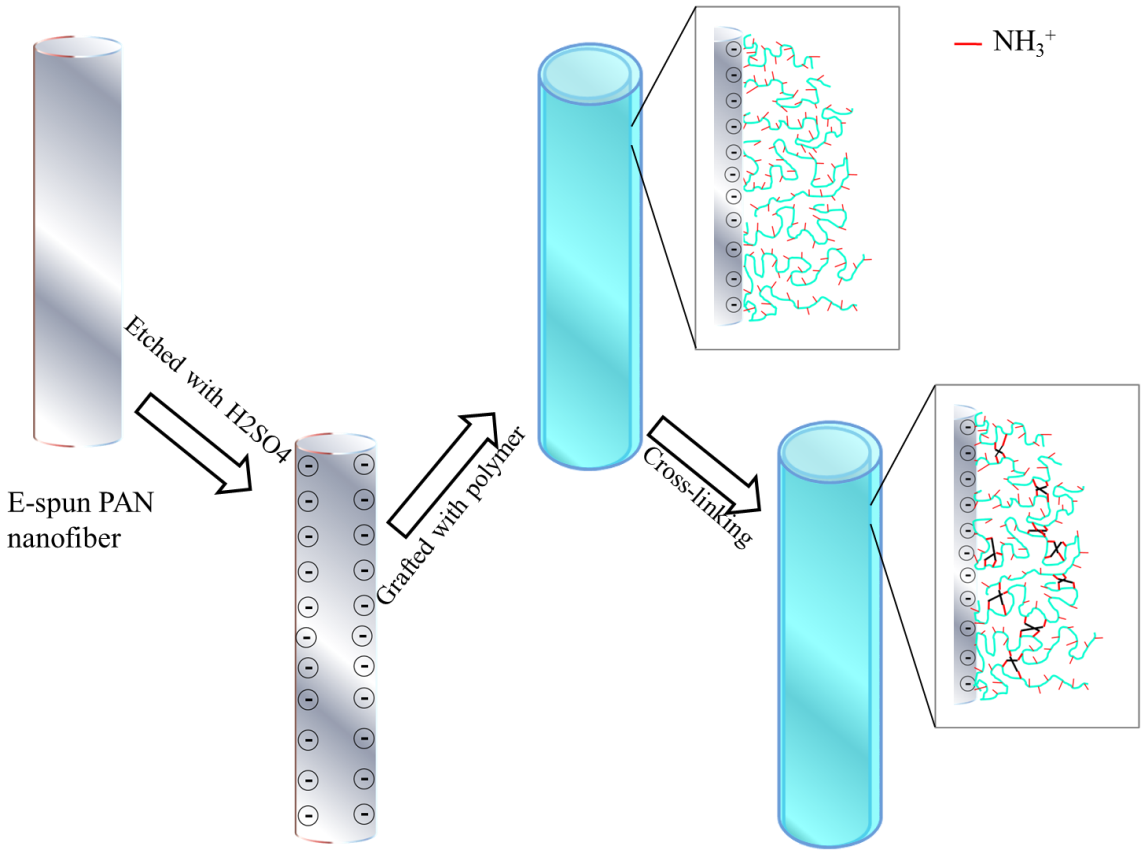

Figure 5.1 Schematic diagram of PVAm grafted electrospun PAN membrane preparation procedure

5.2.4 Characterizations of the original, hydrolyzed and PVAm grafted electrospun PAN membranes

The chemical changes of the PAN membrane after the acid treatment were qualitatively characterized by using Fourier transform infrared spectroscopy (FTIR) with attenuated total reflectance (ATR) accessory (Nicolet iS10 spectrophotometer, Thermo Scientific, Inc.)

The morphology of the membranes was characterized by using a LEO 1550 (LEO, USA) scanning electron microscope (SEM) after gold coating. The fiber diameter was measured from the SEM images using the LeicaIMGRead software (http://dell.chem.sunysb.edu). The fiber diameter was reported as mean ± standard deviation.

The porosity of the membrane was calculated using equation (2-1). For the PVAm grafted membrane, the density of PAN (1.184 g/cm^3 provided by the supplier) was used as the approximate bulk density, since the amount of the PVAm in the final membrane was small (less than 10 wt%) and the density of PVAm (1.08 g/cm^3) is very close to that of PAN. The substrate PET was not included in this calculation.

The mean pore size, the maximum pore size of the nanofibrous membranes were determined by using a capillary flow porometer (Porous Materials Inc, USA). A wetting fluid Galwick^{TM} (Porous Materials Inc, USA) with a surface tension of 15.9 dynes/cm was used to wet the membrane. Air flow rates through the dry and wet membranes were recorded. The maximum pore size and the mean flow pore size were calculated based on the Young-Laplace equation [50].

The pure water flux of the membranes was measured by using the dead-end filtration at room temperature with Milli Q water. A dead-end filtration cell with an effective area of 3.9 cm^2 (Catalogue Number: XX3002500, Millipore, USA) was used. A pressure of 2.5 psi was applied. The water flux was measured using an analytical balance.

The surface areas of the membranes were measured with a Quantachrome NOVA 5-point BET analyzer (Quantachrome Instruments v10.0) using UHP N_2 gas.

The tensile stretching properties of the membranes were tested as follows. After peeling off the PET substrate, all membranes (original, hydrolyzed and PVAm grafted membrane) were cut into a dog bone shape with dimensions of 30 mm × 10 mm × 0.03 mm. They were uniaxially stretched at room temperature using a modified Instron 4442 tensile apparatus under symmetric deformation. The initial length between the clamps was 10 mm, and the stretching rate was 5 mm/min in the test [51].

Surface charge density was measured by acid-base titration [52]. The weighed membrane (~10 mg) was first immersed in 0.05 M NaOH to fully neutralize the amine groups on the surface. After rinsed with DI water, with the surface solution wiped out, the membrane was then placed in 20 mL 0.001M HCl solution for 24 h to protonate the amine groups. The loss of hydrogen ions in the HCl solution, which was in equal amount of the active amine groups, was titrated with standard 0.001 M NaOH. The positive charge density of the membrane was calculated by the reduced amount of H^+ normalized by the membrane weight.

5.2.5 Static metal adsorption evaluations

5.2.5.1 Effect of pH

The adsorption of Cr (VI) was carried out at room temperature (25 ± 1 ℃). To study the effect of solution pH on the adsorption, Cr(VI) solutions with a concentration of 10 mg/L were prepared by dissolving $K_2Cr_2O_7$ in deionized water. The initial pH of the solutions was adjusted between 2.0 and 13.0 using 1N NaOH or HCl aqueous solution. Weighed amount of the modified nanofibrous membranes (5~10 mg) were placed in a flask containing 50.0 mL solutions of Cr(VI). The solutions were stirred at 200 rpm for 24 hours to reach the equilibrated adsorption for the membrane from preliminary tests.

The chromium concentration was measured with UV-Visible Spectroscopy (USB2000, Ocean Optics, Inc.) based on the National Institute for Occupational Safety and Health (NIOSH) manual of analytical methods (NMAM) [53], and described as follows. To get the solution sample for the spectroscopy test, 1 mL of Cr(VI) solution was taken and added to 5~10 mL of 0.5 N sulfuric acid. After adding 0.5 mL Diphenylcarbazide solution into the solution as the indicator, the total solution was adjusted to 25 mL by adding 0.5 N sulfuric acid. The absorbance of the Cr(VI) complex solution was measured at 540 nm. A linear standard curve of the absorbance versus known Cr(VI) concentration (0-100 mg/L) was obtained. The unknown Cr(VI) concentration of the solutions after adsorption was calculated from the standard curve based on the absorbance and the Beer-Lambert law.

The amount of metal ions adsorbed onto the membrane (mg/g) was calculated as follows,

$$q = \frac{(C_0 - C_f)V}{M} \tag{5-1}$$

where q is the amount of metal ions adsorbed (mg/g), C_0 is the initial metal ion concentration, C_f is the final concentration, V is the solution volume (50 mL), and M is the weight of the PVAm-PAN membrane used.

5.2.5.2 Adsorption isotherms

For the sorption isotherms, a series of Cr(VI) solutions with concentrations of 5 mg/L, 10 mg/L, 20 mg/L, 40 mg/L and 100 mg/L, respectively, were prepared. Weighed membranes were placed into flasks containing 50.0 mL of the solutions, with the pH of all solutions being adjusted to the optimized value based on the previous result. The solutions were stirred at 200 rpm for 24 hours and tested according to the methods above.

Saturation adsorption capacity of the membrane was calculated according to the Langmuir model, which is given as follows.

$$\frac{Ce}{Qe} = \frac{Ce}{Qm} + \frac{1}{K_L Q_m} \tag{5-2}$$

Where Q_e is the equilibrium adsorption capacity, C_e is the equilibrium Cr(VI) concentration in solution, Q_m is the saturation adsorption capacity, and K_L is the adsorption equilibrium constant

5.2.6 Dynamic adsorption and desorption evaluations

Dynamic adsorption tests were performed using a dead-end filtration system at a metal ion concentration of 10 mg/L. Before the test, the pH of the metal ion solutions was adjusted to the optimized value for adsorption. The weighed membrane was also pretreated in aqueous solution of the same pH. 50.0 mL metal ion solution was pushed through the membrane at a flow rate controlled with a programmable syringe pump

(Superior Electric Company, USA). Different flow rates were tested to investigate their effect on the adsorption rate.

To determine the reusability of the membrane, a desorption test was performed. After the dynamic adsorption test, the membrane was washed with distilled water several times and dried at room temperature to remove any residual solution on the surface. It was then placed in 50.0 mL aqueous solution with a certain pH value at which the most unfavorable adsorption occurred based on the pH effect test. The solution was stirred at room temperature for 1 h. The metal ion concentration in the desorption solution was measured. The desorption ratio was calculated as one minus the final concentration divided by the initial concentration used in the adsorption test, which was 10 mg/L.

5.3 Results and Discussion

5.3.1 Membrane properties of electrospun PAN membrane (PAN membrane), hydrolyzed electrospun PAN membrane (HPAN membrane) and PVAm grafted electrospun PAN membrane (PVAm-PAN membrane)

To functionalize the membrane with positively charged amine groups, the membrane was first hydrolyzed with strong sulfuric acid to introduce –COOH groups onto the surface, which could enhance the PVAm binding to the nanofibers surface [24,54] due to the electrostatic effect. The chemical changes of the PAN membrane hydrolyzed with different concentration of sulfuric acid were characterized with FTIR, as shown in Figure 5.2. The two bands at ~ 2900 cm^{-1} and the band at ~1450 cm^{-1} are attributed to the $–CH_2$ stretching and bending. The typical sharp peak at ~2250 cm^{-1} is attributed to the C≡N group of the PAN. For the original PAN, a small peak at ~1670 cm^{-1} and multiple peaks

in 1000 ~ 3000 cm^{-1} were observed. These peaks corresponded to C=O and C-O bonds, which might arise from a trace amount of acrylate in the raw polymer. When the membrane was treated with sulfuric acid, a very broad peak at ~3300 cm^{-1} was observed, and was significantly strengthened with increasing concentration of sulfuric acid, indicating more O-H groups were introduced on the membrane surface. Meanwhile, the peak of the C=O bond was shown to have moved slightly left to ~1700 cm^{-1}, which proved the existence of carboxylic acid groups on the surface. The increased intensity of the two peaks of C-O bond at 1000 ~ 3000 cm^{-1} also confirmed that carboxylic acid groups were introduced to the nanofiber surface by the sulfuric acid treatment, and the hydrolization degree was increased with increasing sulfuric acid concentration.

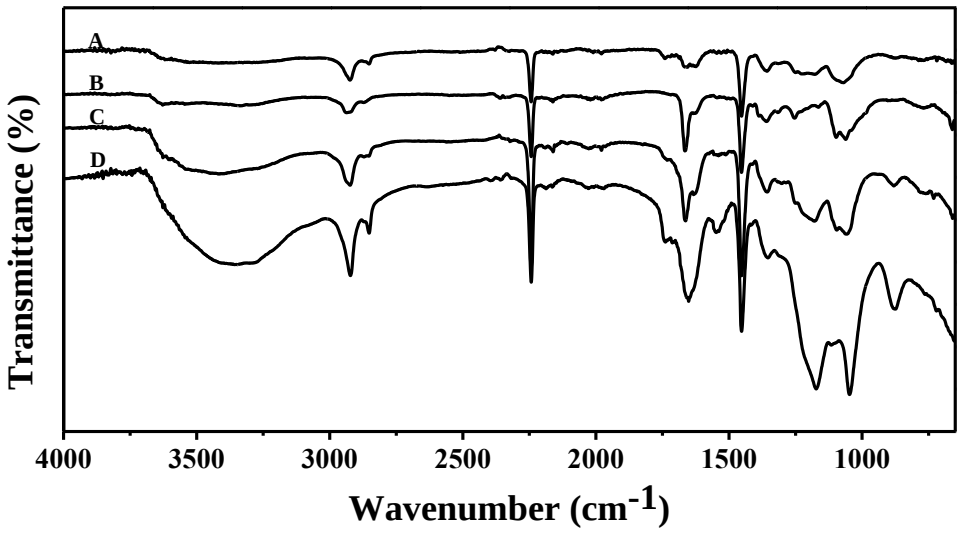

Figure 5.2 FTIR spectrum of (A) orginal electrospun PAN membrane, and electrospun PAN membrane hydrolyzed with (B) 50 wt% H_2SO_4; (C) 60 wt% H_2SO_4; (D) 70 wt% H_2SO_4

The PAN membrane was composed of uniform nanofibers, as shown in Figure 5.3(a), with an average fiber diameter of 214 ± 30 nm. Its porosity was ~ 79%. Compared with the original membrane, the membrane hydrolyzed with 60 wt% H_2SO_4 showed more intertwined nanofibers with very little change in the diameter (219 ± 40 nm), as shown in the SEM image. The overall membrane morphology showed slight shrinkage with less than 3% reduction in size as resulted from the increase in the intertwine of nanofibers. Because of this, the maximum pore size was slightly reduced from 0.91 ± 0.01 μm to 0.90 ± 0.01μm, and the mean pore size was decreased from 0.61 ± 0.01μm to 0.59 ± 0.01 μm. Besides, the formation of acid group on the surface could also enhance the hydrophilicity of the membrane and hence improve the hydrodynamic flow [24]. As a result, despite of the slight decrease in pore size and porosity, the pure water flux was increased from 1762 ± 110 $L/m^2 \cdot h \cdot psi$ to 1957 ± 135 $L/m^2 \cdot h \cdot psi$.

With the grafting treatment, a layer of PVAm was formed on the hydrolyzed PAN nanofibers, followed by cross-linking with GA to be stabilized in aqueous solution. The weight ratio of the PVAm in the whole membrane was 9.1 ± 0.4%, as measured from the membrane weight difference before and after grafting. Adjacent nanofibers conglutinating to each other at junction points was observed in Figure 5.3(c). Moreover, the nanofiber after cross-linking was more compacted from the evidence of the reduced membrane thickness from 40 ± 3 μm to 35 ± 2 μm. The nanofiber diameter was increased to 239 ± 31 nm. As a result, the porosity was decreased to ~71%. In comparisons to the undecorated membrane, the BET surface area was slighted decreased from 24 m^2/g to 22 m^2/g. The maximum pore size was decreased to 0.80 ± 0.03 μm, with the mean pore size

decreased to 0.40 ± 0.01 μm. The pure water flux was lowered down to 645 ± 37 $L/m^{2}{\cdot}h{\cdot}psi$, approximately one third of the original membrane flux.

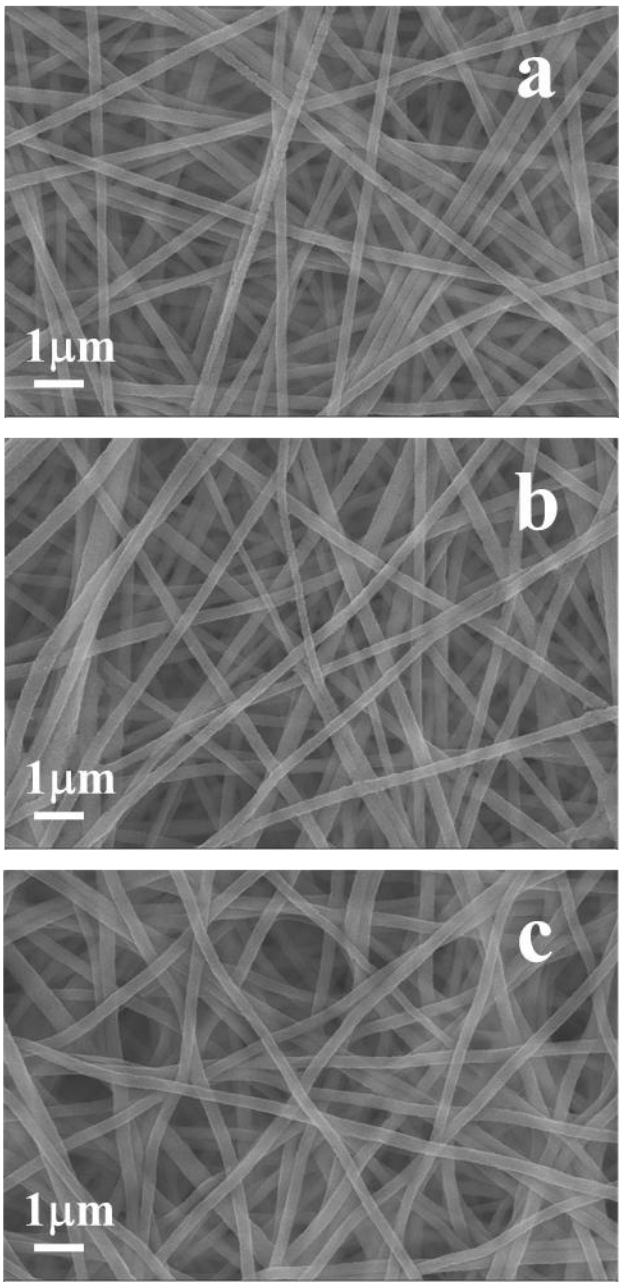

Figure 5.3 SEM image of (a) original electrospun PAN membrane; (b) electrospun PAN membrane hydrolyzed with 60 wt% H_2SO_4; (c) PVAm grafted electrospun PAN membrane

Table 5.1 Properties of the electrospun PAN (PAN) membrane, hydrolyzed electrospun PAN (HPAN) membrane and PVAm grafted PAN (PVAm-PAN) membrane

Membrane	**PAN**	**HPAN**	**PVAm-PAN**
Fiber diameter (nm)	214 ±30	219 ±40	239 ±31
BET surface area (m^2/g)	24	24	22
Porosity	~79%	~78%	~71%
Maximum pore size (μm)	0.91 ±0.01	0.90 ±0.01	0.80 ±0.03
Mean pore size (μm)	0.61 ±0.01	0.59 ±0.01	0.40 ±0.01
Pure water flux (L/m^2·h·psi)	1762 ±110	1957 ±135	645 ±37

In terms of mechanical properties, the hydrolyzed electrospun PAN membrane showed a slight decrease in both Yong's modulus and the elongation-to-break ratio due to the strong acid etching. It is also notable that the PVAm-PAN membrane demonstrated a three times increase in the Young's modulus when compared with the unmodified membrane. The chemical bonding at the joint points of the nanofibers resulted from the cross-linking of PVAm could have contributed to this increase. However, the elongation-to-break ratio was significantly decreased compared to the unmodified membrane. The more fragile structure indicated that the cross-linking degree of the PVAm was relatively high [55] . A lower cross-linking degree could improve the flexibility of the membrane as well as loosen the surface structure, permitting easier accessibility of metal ions to the adsorption sites.

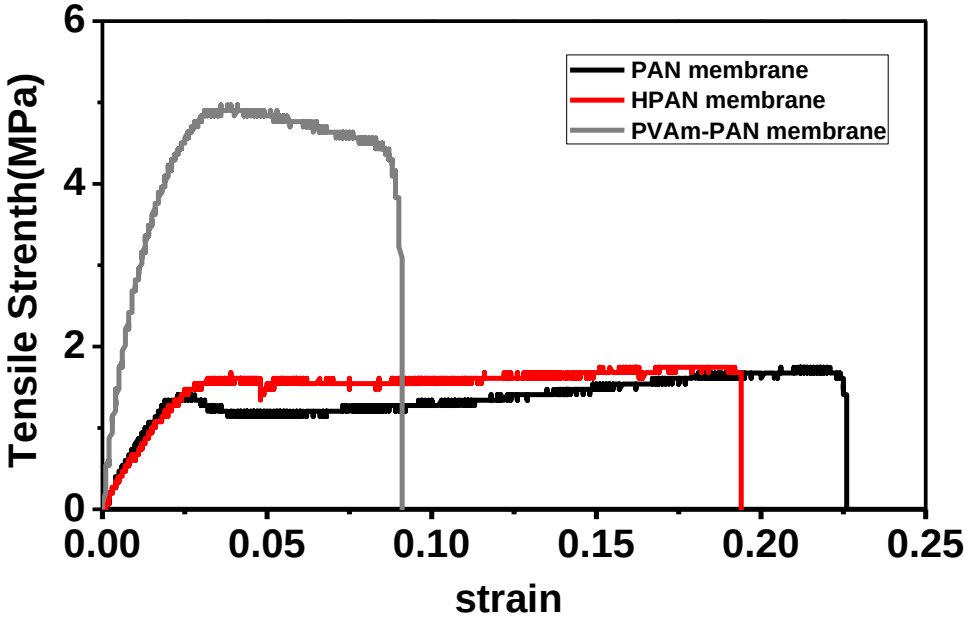

Figure 5.4 Mechanical properties of PAN membrane, HPAN membrane and PVAm-PAN membrane

Table 5.2 Mechanical property of PAN membrane, HPAN membrane and PVAm-PAN membrane

Membrane	PAN	HPAN	PVAm-PAN
Young's modulus (MPa)	66.5	59.1	196.7
Elongation at break	22.6 %	19.4%	9.1%

5.3.2 Static metal adsorption results

5.3.2.1 Effect of pH on static adsorption

In an adsorption process resulted from electrostatic interactions, pH plays an important factor. On the one hand, it affects the pronated degree of amine groups of the PVAm, and thus the active positive site number on the nanofiber surface. On the other hand, Cr(VI) exists in the solution as anions but at different states depending on the pH value. The existing forms include $HCrO_4^-$, $Cr_2O_7^{2-}$, CrO_4^{2-} and more possible sophisticated forms. To evaluate the effect of pH on the metal adsorption, the pH value was varied from 1.0 to 13.0. As shown in Figure 5.5, the equilibrium adsorption rate of Cr(VI) was increased from pH 1.0 to 3.0, where it reached the maximum value of 44.3 ± 1.0 mg/g (milligram Cr(VI) per gram of the membrane) at pH = 3.0. The adsorption rate remained steady above 40.0 mg/g in the pH range of 3.0 to 5.0 with slight decrease as the pH value was increased. At pH = 6.0, the adsorption rate dropped to 35.2 ± 1.5 mg/g, and was quickly decreased to 20.5 ± 1.4 mg/g at pH = 10.0, about half of the maximum adsorption value. At pH = 11.0 and above, the adsorption value was shown to be low at around 4.0 mg/g to 5.0 mg/g, indicating that the adsorption was suppressed under extreme basic conditions.

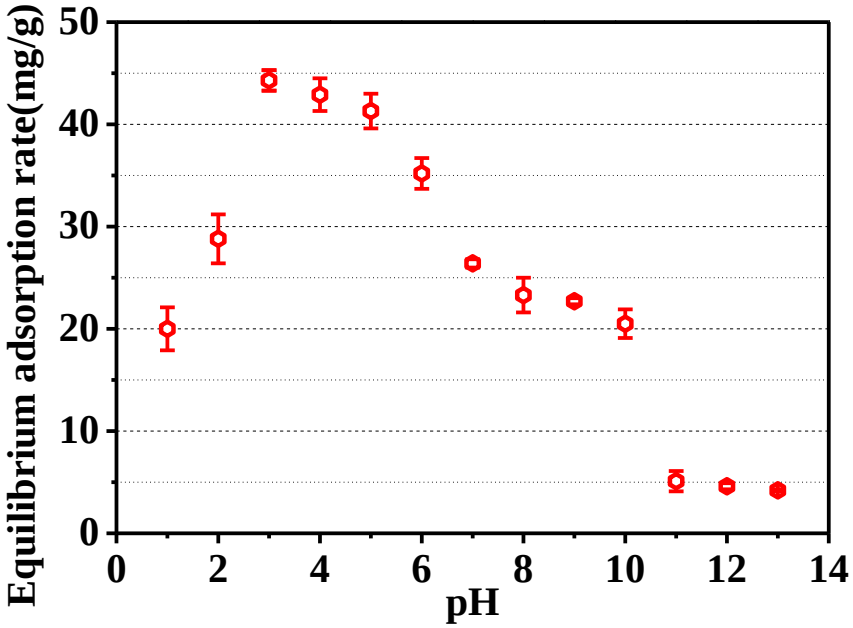

Figure 5.5 Solution pH effect on the static Cr(VI) adsorption. Initial Cr(VI) solution concentration was 10 μg/mL; amount of adsorption is reported as milligrams of Cr(VI) adsorbed per gram of the PVAm-PAN membrane, where PVAm takes up ~ 9% in weight of the membrane

To understand the effect of pH on the Cr (VI) adsorption, a quantitative calculation was performed and discussed as follows. First, the relationship of protonated amine groups ratio versus pH is calculated based on the following equilibrium,

$$[R\text{-}NH_3]^+ <=> [R\text{-}NH_2] + H^+ \qquad pKa = 10.6 \tag{5-3}$$

where $[R\text{-}NH_3]^+$ represents the number of protonated amine groups, and $[R\text{-}NH_2]$ stands for the unprotonated amine groups. If we denote the total amount of active amine groups of the membrane by [N], where

$$[N] = [R\text{-}NH_3]^+ + [R\text{-}NH_2] \tag{5-4}$$

Then, the protonated amine groups ratio $f_{(-NH3+)}$ can be easily derived as

$$f(-NH_3^+) = [R-NH_3^+]/[N] = \frac{1}{10^{pH-10.6}+1} \tag{5-5}$$

Figure 5.6(a) shows the corresponding plot.

In another aspect, Cr(VI) exists in different forms at different pH values, and the following equilibrium conditions apply.

$$H_2CrO_4 <=> [HCrO_4]^- + H^+ \qquad pKa = 0.74 \tag{5-6}$$

$$2[CrO_4]^{2-} + 2H^+ <=> [Cr_2O_7]^{2-} + H_2O \qquad pK = 13.4 \tag{5-7}$$

It is also notable that the following equilibrium also exists,

$$2[HCrO_4]^- <=> [Cr_2O_7]^{2-} + H_2O \tag{5-8}$$

but this equilibrium is independent of pH, so is neglected in the discussion. Considering $Cr_2O_7^{2-}$ has the same charges as CrO_4^{2-}, while it has double the amount of Cr(VI) atom numbers, it can be safely assumed that for a fixed number of positive surface charges, the amount of membrane adsorption will be doubled if the Cr(VI) exists in the form of $Cr_2O_7^{2-}$ than CrO_4^{2-}. Likewise, the adsorption amount to the $HCrO_4^-$ would be the same as

$Cr_2O_7^{2-}$. Since H_2CrO_4 is neutral, no adsorption would occur based on charge interactions. So the adsorption factor due to different forms of Cr(VI) can be defined as

$$f_{(Cr)} = [HCrO_4]^- + [Cr_2O_7]^{2-} + 1/2\ [CrO_4]^{2-} \quad (5\text{-}9)$$

This is a stepwise function calculated from equilibrium (5-6) and (5-7), and its relationship with pH is plotted in Figure 5.6(b).

When both effects are taken into account, the final amount of adsorption change with pH can be expressed as the product of the protonated amine group ratio and the Cr(VI) form factor,

$$F_{(-NH3^+,\ Cr)} = f_{(-NH3^+)} \times f_{(Cr)} \quad (5\text{-}10)$$

As shown in Figure 5.6(c).

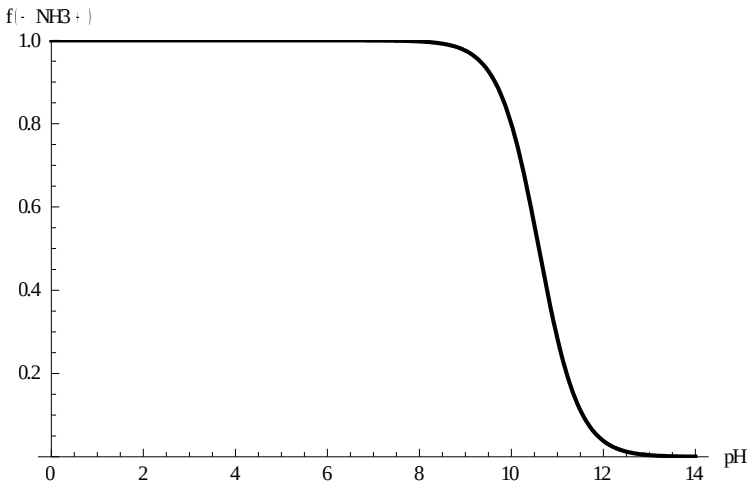
f(NH3)
1.0
0.8
0.6
0.4
0.2
0
2
4
6
8
10
12
14
pH

(a)

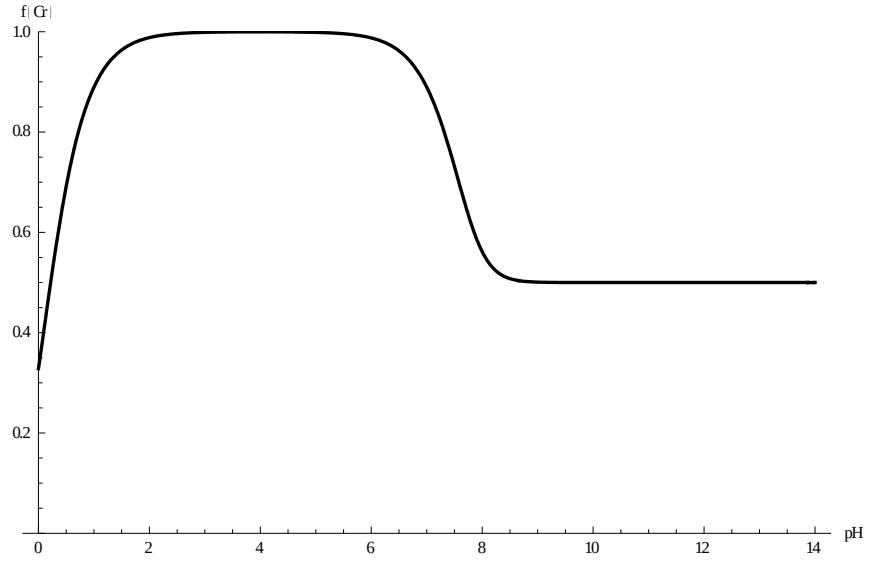
f(Cr)
1.0
0.8
0.6
0.4
0.2
0
2
4
6
8
10
12
14
pH

(b)

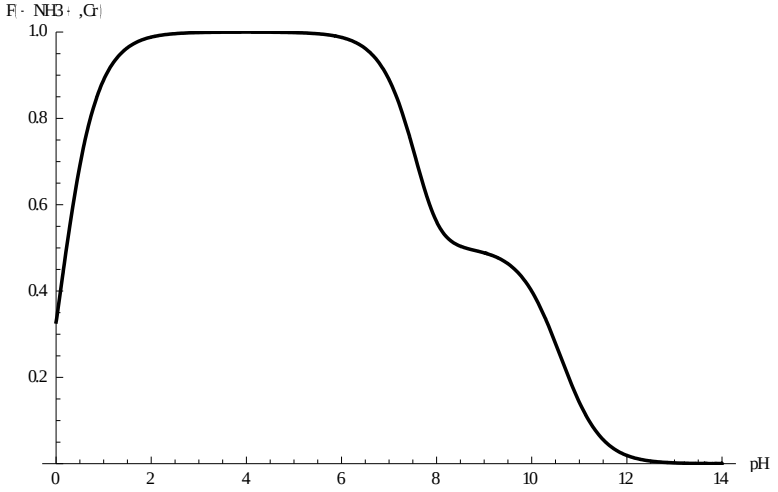

(c)

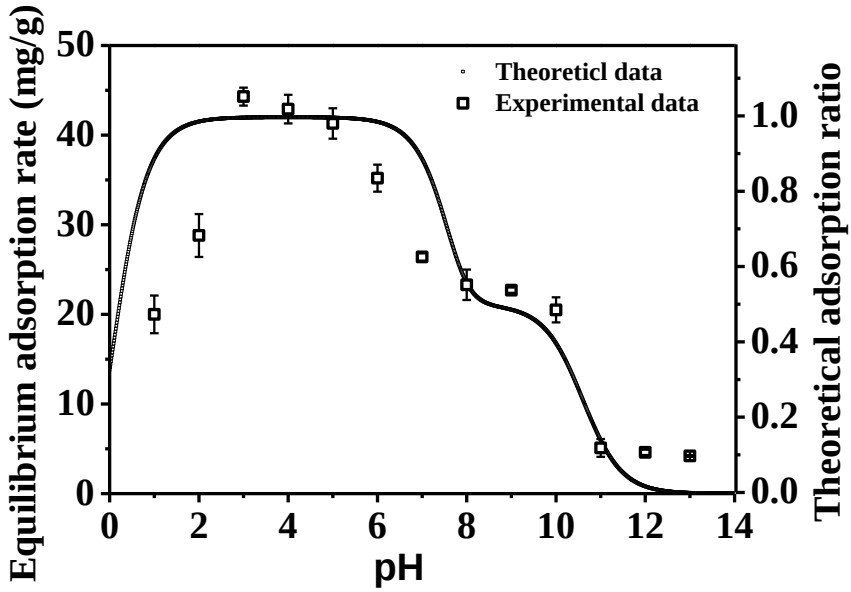

(d)

Figure 5.6 (a) protonated amine group ratio change of the PVAm-PAN membrane with pH; (b) for a fixed amount of positive charges, the Cr(VI) adsorption rate change with pH due to different Cr(VI) existing forms; (c) theoretical amount of adsorption change with pH, by combining the former two factors; (d) agreement between experimental and theoretical adsorption results

As seen in Figure 5.6(c), the theoretical amount of adsorption was increased initially at the extremely acid condition from pH 1.0 to 3.0. In this pH range, H_2CrO_4 was in equilibrium with $HCrO_4^-$ which could interchange with $Cr_2O_7^{2-}$. An increase in the pH value right shifted the equilibrium, which then favored more amounts of negatively charged $Cr_2O_7^{2-}$ and $HCrO_4^-$ ions, resulting in an increase in the amount of adsorption.. At pH = 3.0, the adsorption reached 99.9% of the maximum theoretical value, in good agreement with the experimental data which showed the maximum amount of adsorption occurred at pH = 3.0. At pH values ranging 3.0 to 5.5, almost all (> 99.99%) Cr(VI) exists as $Cr_2O_7^{2-}$, and the theoretical adsorption rate reached and kept its maximum value. With the pH value increase above 5.5, the equilibrium between $Cr_2O_7^{2-}$ and CrO_4^{2-} gradually shifted to the latter one, resulting in a decrease in the amount of adsorption. At pH value of around 8.5, almost all Cr(VI) turned into CrO_4^{2-}, where the amount of adsorption was decreased to half of the maximum theoretical value. The Cr(VI) was kept stable as CrO_4^{2-} in the solution at pH > 8.5, where the effect of protonation degree of amine groups of the absorbent became the determining factor for the adsorption. In the basic condition at pH above 8.5, the protonation ratio of the amine groups started to reduce. For example, compared to the maximum protonation degree in acidic condition where the protonation ratio was 1, the protonation ratio was 99% at pH = 8.5, and decreased to 90% at pH = 9.6, 50% at pH = 10.6. In this region, the amount of adsorption showed a gradual decrease, which was also observed in the experimental data from pH = 8.0 to 10.0. After that, the protonation ratio rapidly reduced to 25% at pH = 11, 4% at pH = 12 and 1% at pH = 12.6, leading to a fast drop on the amount of adsorption.

5.3.2.2 Adsorption isotherm

Sorption isotherm modes, such as the Langmuir model, were widely used to exam the maximum adsorption of an adsorbent. The Langmuir model assumes that the monolayer adsorption of metal ions takes place on a homogenous surface, with no interaction between adsorbed ions. In the isotherm experiments, a series of Cr(VI) solutions at different initial concentrations were used for the metal adsorption test. The solution pH was adjusted to 3.0 to facilitate the metal adsorption based on the previous results. It was seen that when the initial solution concentration was increased from 5.0 mg/L to 10.0 mg/L, the membrane adsorption showed a great increase from 32.8 ± 0.8 mg/g to 44.3 ± 1.0 mg/g. As the solution concentration was further increased to 20.0 mg/L, 40.0 mg/L and 100.0 mg/L, the amount adsorption was gradually increased to 49.0 ± 0.7 mg/g, 52.3 ± 1.7 mg/g and 55.4 ± 2.4 mg/g, respectively. Based on equation (5-2), the relationship of C_e/Q_e versus C_e was plotted in Figure 5.8. A linear relationship with R^2 of 99.93% was obtained, confirming that the adsorption process obeyed the Langmuir model very well.

The theoretical monolayer saturation capacity, calculated as the reciprocal of the slope in Figure 5.8, was 57.1 mg or 1.10 mmol Cr(VI) per gram of the membrane. In the meantime, a titration experiment was carried out to measure the effective amount of protonated amine groups on the surface of the membrane. The charge density determined from the titration experiment was 0.82 mmol/g, which was close to the metal adsorption result. The good agreement indicated the approximate equimolar interaction between the positive charges on the membrane and the negatively charged metal ions [51].

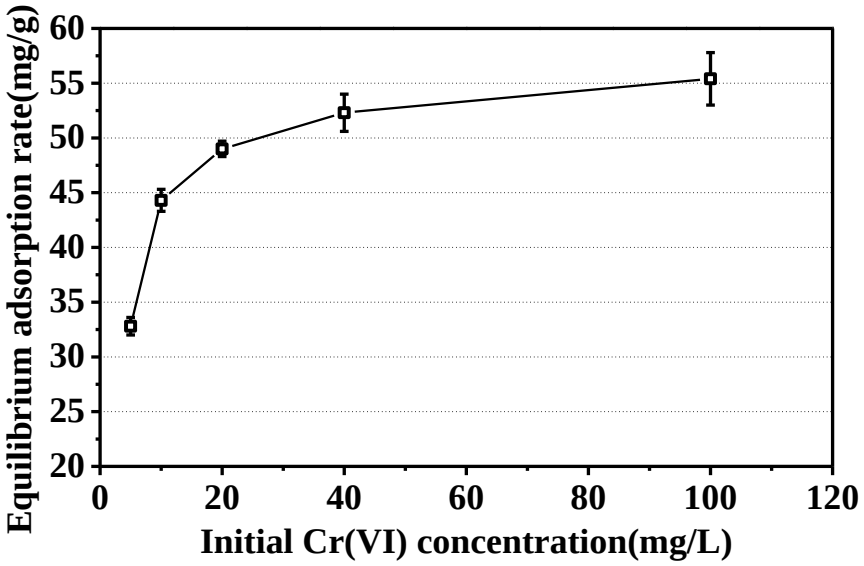

Figure 5.7 Cr(VI) adsorption rates of the PVAm-PAN membrane with different initial Cr(VI) solution concentrations; solution pH = 3.0

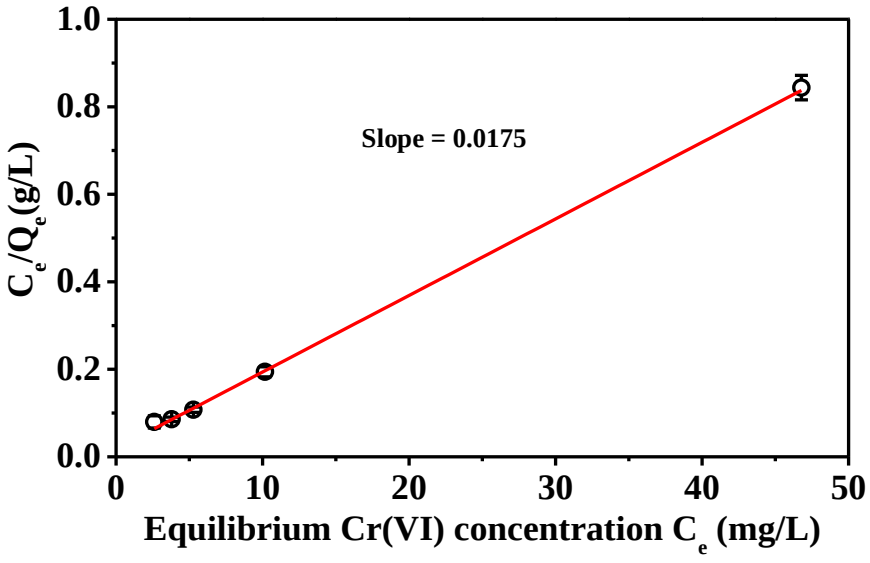

Figure 5.8 Relationship of $C_e/Q_e \sim C_e$ according to the Langmuir model

The adsorption capacity of the PVAm-PAN membrane was compared to that of other adsorbents. Table 5.3 listed the Cr(VI) adsorption capacities of several absorbents, including commercial activated carbons and chitosan. A complete summary of the absorbents for Cr(VI) removal can be found in Mohan's review [56]. Activated carbons were regarded as the most effective adsorbent due to its extremely high surface area (~1000 m^2/g or greater). Reported adsorption capacity ranged from several mg/g to around 200 mg/g. However, the disadvantages on using activated carbons are many. They are relatively expensive – the higher the quality, the greater the cost; they are ineffective to disperse and difficult to recycle and reuse. Using the PVAm-PAN membrane can overcome these limitations. It is an efficient and cost-effective way to remove Cr(VI) ions, and the membrane is very easy to use and to recycle. Although the surface area of the membrane (24 m^2/g) was much lower than that of the activated carbons (around 1/100 ~ 1/50 of the latter one), the adsorption capacity in milligram adsorbed Cr(VI) per gram of the membrane at the optimal adsorption pH (2.0 ~ 4.0 for different adsorbents), was still higher than some of the activated carbons and almost all known biosorbents [57-59], but lower than the commercial activated carbons FS – 100, GA – 3 and SHT. We are also interested in the adsorption capacity of different adsorbent in practical use, namely, their performance in neutral or close-to-neutral solution. The last column showed the adsorption capacity of different adsorbents at pH = 6.0. It was seen that the PVAm-PAN membrane demonstrated a high adsorption capacity of 35.2 mg/g, even higher than (2 ×) the commercial activated carbons.

Since the electrospun PAN membrane was not charged and had no adsorption ability towards Cr(VI), we are especially interested in the adsorption capacity of the functional

polymer PVAm. In the form of thin film with a thickness of 5 μm and a surface area ~0.4 m^2/g, the adsorption capacity of cross-linked PVAm was ~ 0.8 m^2/g. By grafting onto the electrospun nanofibers, the PVAm surface area were greatly increased to 263.7 m^2/g (from the calculation using membrane surface divided by the weight ratio of PVAm in the membrane), and the Cr(VI) adsorption capacity was 627.5 mg Cr(VI) per gram of PVAm. Although the surface area was still lower when compared with that of activated carbons, the adsorption capacity was demonstrated to be more than 6 times higher than some commercial activated carbons, and 4 times higher than the reported chitosan [24,57-59]. In terms of the adsorption rate per surface area, the PVAm-PAN membrane demonstrated over 30 times better performance than the commercial activated carbon FS – 100. The superior adsorption capacity per surface area of both PVAm-PAN membrane and the grafted PVAm also confirmed that the positive charge density of the functional polymer PVAm was very high and should be very suitable for Cr(VI) removal.

Table 5.3 Static Cr(VI) adsorption capacity of different adsorbents

Adsorbent		Surface area (m^2/g)	Initial conc. (mg/L)	Optimal pH	mg Cr(VI) /g at optimal pH	mg Cr(VI) /g at pH = 6.0
Present work	E-spun PAN membrane	26	10	3.0	~ 0	~ 0
	PVAm film (thickness 5 μm)	0.4	10	3.0	0.8	~ 0.6
	PVAm-PAN membrane	24	10	3.0	**57.1**	**35.2**
	surface PVAm	263.7	10	3.0	**627.5**	**386.8**
Synthetic activated carbon from different sources	Coconut shell [57]	1,280	120	3.0-4.0	6.0	2.1
	Wood [58]	1,700	120	2.0	5.1	1.8
	Rubber wood sawdust [58]	1,673	50	2.0	44.1	~ 7
Commercial activated carbons	FS – 100 [59]	937	50	3.0	69.3	~ 16
	GA – 3 [59]	-	50	3.0	101.4	~ 20
	SHT [59]	-	50	3.0	69.1	~ 14
Chitosan	Chitosan coated on oil palm shell [24]	-	20	4.0	154	~ 84

5.3.3 Dynamic adsorption and desorption results

The dynamic metal adsorption test using the PVAm-PAN membrane was easily performed in a dead-end filtration cell. A pure water flux test set-up was directly used without any further modification. The dynamic Cr(VI) adsorption ability of the membrane was evaluated at different solution flow rates through the membrane. At a flow rate of 70 L/m^2h, the adsorption was 36.3 ± 2.6 mg Cr(VI) per gram of the membrane. With the flow rate increased, the dynamic adsorption was decreased. Compared to the amount of membrane adsorption in a static test, the amount of dynamic adsorption ability was reduced with increasing flow rate as contact and interaction time between the metal ions in the solution with the active sites of the functional nanofibrous membrane became shorter. At the flow rate of 200 L/m^2h, the adsorption capacity was reduced to 25.2 ± 2.6 mg/g, approximately half of the static saturation adsorption capacity of the membrane.

Desorption ability helps to recover the metal ions from the membrane and to regenerate the membrane to be reused for metal ion adsorption. It also helps to understand the nature of the adsorption process. The membrane after the dynamic adsorption test was placed in DI water and then in a basic solution with pH = 13.0 for 1 hr. Results showed that no desorption of the metal ions from the membrane into the solution was observed at pH = 7.0, indicating that the metal ion adsorption onto the membrane was an irreversible process and the binding energy between the absorbent and the metal ions was strong. At pH = 13.0, over 98% of the metal ions attracted on the membrane were detected to have been released into the solution, resulting in a well regenerated membrane for repeated use. It is not surprising that a very high desorption

ratio was obtained at such a basic condition. According to the previous calculations, at pH = 13.0 almost all the amine groups of the membrane were fully neutralized, and lost their electrostatic interactions with the negatively charged Cr(VI) ions. This result was also in agreement with the very low static adsorption at pH = 13.0 in the previous tests.

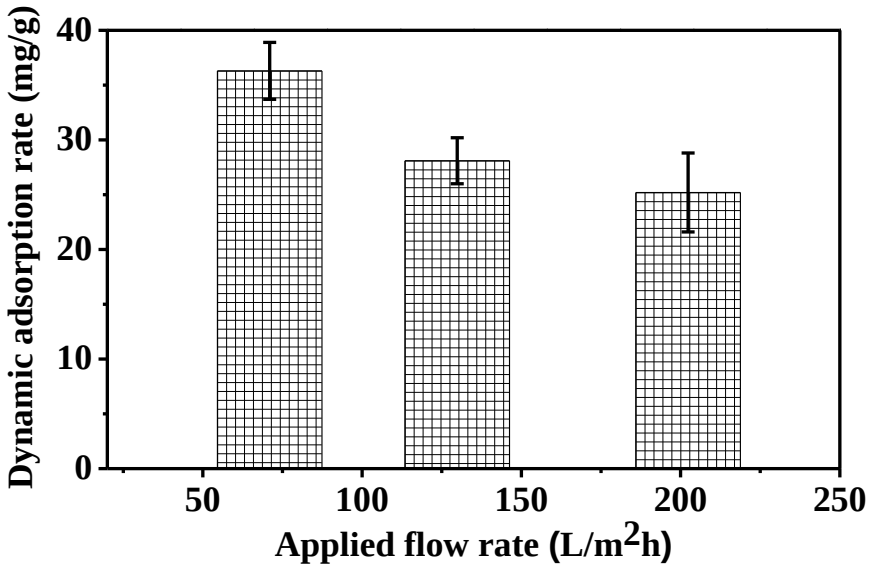

Figure 5.9 Dynamic Cr(VI) adsorption of the PVAm-PAN membrane at different flow rates

5.4 Conclusions

A novel microfiltration membrane with a great Cr(VI) adsorption capacity was prepared. A nanofibrous PAN scaffold with an average fiber diameter of 214 ± 30 nm was prepared with the electrospinning technique and further modified with PVAm using a simple grafting method. PVAm is known for its abundant positively charged amine groups, and should be specifically suitable for adsorbing Cr(VI) from aqueous solution. With PVAm being a water soluble polymer, a cross-linking step using GA was performed after the grafting in order to stabilize it on the nanofibers. The resulting membrane possessed a mean pore size of 0.40 ± 0.01 μm, a porosity of ~71%, a pure water flux of 645 ± 37 $L/m^2 \cdot h \cdot psi$. The modified membrane demonstrated a three times improvement on Young's modulus compared to the original membrane. As an important factor influencing the metal ions adsorption, the pH effect was fully investigated in the range of 1.0 to 13.0. The experimental data agreed well with the theoretical results calculated from the equilibrium constants and equations, with both showing that the maximum adsorption occurred in the pH range of 3.0 to 5.0. The adsorption isotherm data indicated that the adsorption process could be well described with the Langmuir model. Based upon the model the saturated static adsorption capacity was calculated to be 57.1 mg Cr(VI) per gram of the membrane, or 627.5 mg Cr(VI) per gram of the functional material PVAm at pH = 3.0. The bulk membrane adsorption capacity in mg/g was comparable to that of some commercial activated carbons, but the PVAm adsorption capacity in mg/g was more than 6 times higher than that of the commercial activated carbons. Considering the electrospun membrane had only 1/100 ~ 1/50 surface area of activated carbons, and if taking the surface area into account, the membrane demonstrated over 30 times higher

adsorption capacity per surface than activated carbon. The high surface positive charge density of grafted PVAm, which was confirmed from the titration test to be 0.82 mmol/g, was attributed to the high adsorption capacity. The modified membrane was also demonstrated to be suitable for Cr(VI) adsorption in a dynamic filtration process. The adsorption rate was decreased with increasing flow rate through the membrane. With a flow rate of the Cr(VI) solution at 200 L/m^2h, the membrane could still keep an adsorption of 25.2 ± 2.6 mg/g. Finally, the membrane was easily regenerated after the metal ion adsorption by immersing it in the 0.1 M NaOH solution. A desorption ratio of > 98% was obtained. Such a membrane possessed the advantages of small pore sizes, high porosity and high positive charge density, and should be particularly useful in rejecting bacteria and adsorbing negatively charged species from aqueous solution.

References

1. Kobya, M. (2004) *Bioresource Technology* **91**, 317-321
2. Owlad, M., Aroua, M. K., Daud, W. A. W., and Baroutian, S. (2009) *Water Air Soil Poll* **200**, 59-77
3. Yun, Y. S., Park, D., Park, J. M., and Volesky, B. (2001) *Environ Sci Technol* **35**, 4353-4358
4. Sarkar, D., Das, S. K., Mukherjee, P., and Bandyopadhyay, A. (2010) *Clean-Soil Air Water* **38**, 764-770
5. Bandyopadhyay, A., Sarkar, D., Das, S. K., and Mukherjee, P. (2010) *Clean-Soil Air Water* **38**, 764-770
6. Kotas, J., and Stasicka, Z. (2000) *Environ Pollut* **107**, 263-283
7. Sapari, N., Idris, A., and AbHamid, N. H. (1996) *Desalination* **106**, 419-422
8. Kongsricharoern, N., and Polprasert, C. (1995) *Water Sci Technol* **31**, 109-117
9. Nenov, V., Zouboulis, A. I., Dimitrova, N., and Dobrevsky, I. (1994) *Environ Pollut* **83**, 283-289
10. Janssen, L. J. J., and Koene, L. (2002) *Chem Eng J* **85**, 137-146
11. Muthukrishnan, M., and Guha, B. K. (2008) *Desalination* **219**, 171-178
12. Hafiane, A., Lemordant, D., and Dhahbi, M. (2000) *Desalination* **130**, 305-312
13. Abu Qdais, H., and Moussa, H. (2004) *Desalination* **164**, 105-110
14. Gupta, S. K., and Chen, K. Y. (1978) *J Water Pollut Con F* **50**, 493-506
15. Bailey, S. E., Olin, T. J., Bricka, R. M., and Adrian, D. D. (1999) *Water Res* **33**, 2469-2479

16. Pagnanelli, F., Mainelli, S., Veglio, F., and Toro, L. (2003) *Chemical Engineering Science* **58**, 4709-4717

17. Altun, T., and Pehlivan, E. (2008) *Journal of Hazardous Materials* **155**, 378-384

18. Altundogan, H. S., Altundogan, S., Tumen, F., and Bildik, M. (2000) *Waste Manage* **20**, 761-767

19. Meikap, B. C., Acharya, J., Sahu, J. N., Sahoo, B. K., and Mohanty, C. R. (2009) *Chem Eng J* **150**, 25-39

20. Yue, Z. R., Bender, S. E., Wang, J. W., and Economy, J. (2009) *Journal of Hazardous Materials* **166**, 74-78

21. Narayanan, N. V., and Ganesan, M. (2009) *Journal of Hazardous Materials* **161**, 575-580

22. Di Natale, F., Lancia, A., Molino, A., and Musmarra, D. (2007) *Journal of Hazardous Materials* **145**, 381-390

23. Duman, O., and Ayranci, E. (2010) *Journal of Hazardous Materials* **176**, 231-238

24. Nomanbhay, S. M., and Palanisamy, K. (2005) *Electron J Biotechn* **8**, 43-53

25. Sankararamakrishnan, N., Dixit, A., Iyengar, L., and Sanghi, R. (2006) *Bioresource Technology* **97**, 2377-2382

26. Raven, K. P., Jain, A., and Loeppert, R. H. (1998) *Environ Sci Technol* **32**, 344-349

27. Ghimire, K. N., Inoue, K., Yamaguchi, H., Makino, K., and Miyajima, T. (2003) *Water Res* **37**, 4945-4953

28. Podgorski, A., Balazy, A., and Gradon, L. (2006) *Chemical Engineering Science* **61**, 6804-6815

29. Xia, Y. N., Xie, J. W., MacEwan, M. R., and Schwartz, A. G. (2010) *Nanoscale* **2**, 35-44

30. Hsiao, B. S., Liang, D., and Chu, B. (2007) *Advanced Drug Delivery Reviews* **59**, 1392-1412

31. Kumar, J., Wang, X. Y., Drew, C., Lee, S. H., Senecal, K. J., and Sarnuelson, L. A. (2002) *Nano Letters* **2**, 1273-1275

32. Eichhorn, S. J., and Sampson, W. W. (2005) *Journal of the Royal Society Interface* **2**, 309-318

33. Ma, H. Y., Burger, C., Hsiao, B. S., and Chu, B. (2011) *J Mater Chem* **21**, 7507-7510

34. Gopal, R., Kaur, S., Feng, C. Y., Chan, C., Ramakrishna, S., Tabe, S., and Matsuura, T. (2007) *Journal of Membrane Science* **289**, 210-219

35. Gopal, R., Kaur, S., Ma, Z. W., Chan, C., Ramakrishna, S., and Matsuura, T. (2006) *Journal of Membrane Science* **281**, 581-586

36. Wang, R., Liu, Y., Li, B., Hsiao, B. S., and Chu, B. (2012) *Journal of Membrane Science* **392**, 167-174

37. Yoon, K., Hsiao, B. S., and Chu, B. (2009) *Journal of Membrane Science* **326**, 484-492

38. Yoon, K., Kim, K., Wang, X. F., Fang, D. F., Hsiao, B. S., and Chu, B. (2006) *Polymer* **47**, 2434-2441

39. Wang, X. F., Chen, X. M., Yoon, K., Fang, D. F., Hsiao, B. S., and Chu, B. (2005) *Environ Sci Technol* **39**, 7684-7691

40. Ma, H. Y., Yoon, K., Rong, L. X., Mao, Y. M., Mo, Z. R., Fang, D. F., Hollander, Z., Gaiteri, J., Hsiao, B. S., and Chu, B. (2010) *J Mater Chem* **20**, 4692-4704

41. Musale, D. A., Kumari, A., and Pleizier, G. (1999) *Journal of Membrane Science* **154**, 163-173

42. Musale, D. A., and Kumar, A. (2000) *J Appl Polym Sci* **77**, 1782-1793

43. Kampalanonwat, P., and Supaphol, P. (2010) *Acs Appl Mater Inter* **2**, 3619-3627

44. Saeed, K., Haider, S., Oh, T. J., and Park, S. Y. (2008) *Journal of Membrane Science* **322**, 400-405

45. Saeed, K., Park, S. Y., and Oh, T. J. (2011) *J Appl Polym Sci* **121**, 869-873

46. Sumaru, K., Matsuoka, H., and Yamaoka, H. (1996) *J Phys Chem-Us* **100**, 9000-9005

47. Chang, C., Fish, F., Muccio, D. D., and Stpierre, T. (1987) *Macromolecules* **20**, 621-625

48. Pelton, R., and Hong, J. (2002) *Tappi J* **1**, 21-26

49. Kobayashi, S., Suh, K. D., and Shirokura, Y. (1989) *Macromolecules* **22**, 2363-2366

50. Jena, A., and Gupta, K. (2005) *Am Ceram Soc Bull* **84**, 28-30

51. Ma, H. Y., Burger, C., Hsiao, B. S., and Chu, B. (2012) *Biomacromolecules* **13**, 180-186

52. Rudnik, E., Burzynska, L., Dolasinski, L., and Misiak, M. (2010) *Appl Surf Sci* **256**, 7414-7420

53. http://www.cdc.gov/niosh/docs/2003-154/pdfs/7600.pdf.

54. Krentsel, L. B., Kudryavtsev, Y. V., Rebrov, A. I., Litmanovich, A. D., and Plate, N. A. (2001) *Macromolecules* **34**, 5607-5610

55. Liu, J., Cao, D. P., and Zhang, L. Q. (2009) *J Chem Phys* **131**

56. Mohan, D., and Pittman, C. U. (2006) *Journal of Hazardous Materials* **137**, 762-811

57. Selomulya, C., Meeyoo, V., and Amal, R. (1999) *J Chem Technol Biot* **74**, 111-122

58. Karthikeyan, T., Rajgopal, S., and Miranda, L. R. (2005) *Journal of Hazardous Materials* **124**, 192-199

59. Hu, Z. H., Lei, L., Li, Y. J., and Ni, Y. M. (2003) *Sep Purif Technol* **31**, 13-18

Chapter VI Conclusions

Electrospun nanofibers have very high surface area due to the small diameter down to tens of nanometer to sub-micron range, and electrospun nanofibrous membranes can be light-weighted, highly porous with interconnected pores, of have surface-to-weight ratio. They have gained tremendous interest due to their unique structural properties. In this dissertation, attentions have been paid to the fundamental and application-oriented research of electrospun membranes.

In Chapter II, the effects of different parameters such as applied voltage, flow rates and solution properties on the morphology of electrospun nanofibers have been studied. In addition to this, the pore sizes of electrospun membranes have been characterized with the capillary flow porometry. The mean flow pore size relationships with the membrane thickness, fiber diameter and membrane porosity have been fully discussed. Membranes with different pore sizes have also been tested for their functionality as microfiltration membranes for removal of water-borne bacteria, by using spherical particles with different sizes as the simulants.

In Chapter III, the relatively weak bonding between the electrospun PAN membrane with the PET non-woven support, which limits the membrane's application in UF or NF during backflushing, has been greatly improved by an interfacial treatment with the hot-pressing method. The bonding strength can reach a comparable or even better level compared to that of a phase inversion UF membrane. The membranes after compression

have been fully studied in terms of pore size, particle rejection ratio and pure water flux. The UF membranes were prepared by coating cellulose nanofiber barrier layers onto the hot-pressed electrospun membranes. The influences of the compressed electrospun scaffolds on the ultra-filtration performance, such as pure water flux and rejection ratio, to dextran solutions have also been investigated.

In Chapter IV, the application of electrospun nanofibrous membrane in LIB has been demonstrated. A commercial PE separator film has been chemically treated with chromic acid to improve its bonding with other substrates. PES electrospun membranes have been deposited onto the treated PE film to form a composite separator. The properties of PE film after chemical treatment have been characterized by AFM, FTIR and water contact angle. The bonding strength between the PES membrane and the PE film has also been investigated. The thermal properties of the separator film, characterized by SDT, MDT and safety margin, have been greatly improved, and yet the composite separator has not compromised any other properties compared to the original PE film, due to the high porosity of electrospun membrane.

In Chapter V, the electrospun PAN membrane, after surface-functionalized with PVAm by the grafting method, has been used for removal of the heavy metal Cr(VI) from aqueous solution. The microfiltration properties of membranes before and after the modification have been studied. Due to the high positive charge density of PVAm, the saturation adsorption capacity has reached a very high value of 57.1 mg Cr(VI) on a per gram basis of the membrane, or 627.5 mg Cr(VI) per gram of the grafted PVAm. The modified membrane has also been demonstrated to be suitable for Cr(VI) adsorption in a

dynamic filtration process, and it can be regenerated by immersing it in the 0.1 M NaOH solution.

List of References

Abraham, K. M. "Directions in Secondary Lithium Battery Research-and-Development." *Electrochimica Acta* 38, no. 9 (1993): 1233-1248.

Abu Qdais, H., and H. Moussa. "Removal of Heavy Metals from Wastewater by Membrane Processes: A Comparative Study." *Desalination* 164, no. 2 (2004): 105-110.

Ajao, J. A., A. A. Abiona, S. Chigome, A. Y. Fasasi, G. A. Osinkolu, and M. Maaza. "Electric-Magnetic Field-Induced Aligned Electrospun Poly (Ethylene Oxide) (Peo) Nanofibers." *Journal of Materials Science* 45, no. 9 (2010): 2324-2329.

Akthakul, A., W. F. McDonald, and A. M. Mayes. "Noncircular Pores on the Surface of Asymmetric Polymer Membranes: Evidence of Pore Formation Via Spinodal Demixing." *Journal of Membrane Science* 208, no. 1-2 (2002): 147-155.

Alhosseini, S. N., F. Moztarzadeh, M. Mozafari, S. Asgari, M. Dodel, A. Samadikuchaksaraei, S. Kargozar, and N. Jalali. "Synthesis and Characterization of Electrospun Polyvinyl Alcohol Nanofibrous Scaffolds Modified by Blending with Chitosan for Neural Tissue Engineering." *International Journal of Nanomedicine* 7, (2012): 25-34.

Arora, P., and Z. M. Zhang. "Battery Separators." *Chemical Reviews* 104, no. 10 (2004): 4419-4462.

ASTM. "Standard Test Method for Pore Size Characteristics of Membrane Filters by Bubble Point and Mean Flow Pore Test. F316-03.", 2003.

Bag, D.S., V.P. Kumar, and S. Maiti. "Etching of a Low-Density Polyethylene Film by Fuming Nitric Acid." *Die Angewandte Makromolekulare Chemie* 249, (1997): 33-46.

Bandhauer, T. M., S. Garimella, and T. F. Fuller. "A Critical Review of Thermal Issues in Lithium-Ion Batteries." *Journal of the Electrochemical Society* 158, no. 3 (2011): R1-R25.

Barthlott, W., and C. Neinhuis. "Purity of the Sacred Lotus, or Escape from Contamination in Biological Surfaces." *Planta* 202, no. 1 (1997): 1-8.

Baumgart.Pk. "Electrostatic Spinning of Acrylic Microfibers." *Journal of Colloid and Interface Science* 36, no. 1 (1971): 71-79.

Bognitzki, M., W. Czado, T. Frese, A. Schaper, M. Hellwig, M. Steinhart, A. Greiner, and J. H. Wendorff. "Nanostructured Fibers Via Electrospinning." *Advanced Materials* 13, no. 1 (2001): 70-72.

Boussu, K., C. Vandecasteele, and B. Van der Bruggen. "Study of the Characteristics and the Performance of Self-Made Nanoporous Polyethersulfone Membranes." *Polymer* 47, no. 10 (2006): 3464-3476.

Bowen, W. R., N. Hilal, R. W. Lovitt, A. O. Sharif, and P. M. Williams. "Atomic Force Microscope Studies of Membranes: Force Measurement and Imaging in Electrolyte Solutions." *Journal of Membrane Science* 126, no. 1 (1997): 77-89.

Brewis, D. M., R. H. Dahm, and I. Mathieson. "Electrochemical Pretreatment of Polymers with Dilute Nitric Acid Either Alone or in the Presence of Silver Ions." *Journal of Adhesion* 72, no. 3-4 (2000): 373-386.

Brewis, D. M., I. Mathieson, and M. Wolfensberger. "Treatment of Low-Energy Surfaces for Adhesive Bonding." *International Journal of Adhesion and Adhesives* 15, no. 2 (1995): 87-90.

Briggs, D. *Journal of Materials Science* 11, (1976): 1270-1277.

Brodd, R. J., K. R. Bullock, R. A. Leising, R. L. Middaugh, J. R. Miller, and E. Takeuchi. "Batteries, 1977 to 2002." *Journal of the Electrochemical Society* 151, no. 3 (2004): K1-K11.

Broussely, M. "Li-Ion Batteries for High-Tech Applications." *Electronics World* 112, no. 1846 (2006): 16-21.

Broussely, M., and G. Archdale. "Li-Ion Batteries and Portable Power Source Prospects for the Next 5-10 Years." *Journal of Power Sources* 136, no. 2 (2004): 386-394.

Buchko, C. J., L. C. Chen, Y. Shen, and D. C. Martin. "Processing and Microstructural Characterization of Porous Biocompatible Protein Polymer Thin Films." *Polymer* 40, no. 26 (1999): 7397-7407.

Carampin, P., M. T. Conconi, S. Lora, A. M. Menti, S. Baiguera, S. Bellini, C. Grandi, and P. P. Parnigotto. "Electrospun Polyphosphazene Nanofibers for in Vitro Rat Endothelial Cells Proliferation." *Journal of Biomedical Materials Research Part A* 80A, no. 3 (2007): 661-668.

Celebioglu, A., and T. Uyar. "Electrospun Porous Cellulose Acetate Fibers from Volatile Solvent Mixture." *Materials Letters* 65, no. 14 (2011): 2291-2294.

Chang, C., F. Fish, D. D. Muccio, and T. Stpierre. "C-13 and N-15 Nmr Ph Titration of Poly(Vinylamine) - a 2-Stage Process Sensitive to Polymer Tacticity." *Macromolecules* 20, no. 3 (1987): 621-625.

Chang, X. F., Y. Hu, and Z. L. Xu. "Poly(Vinyl Alcohol)-Perfluorinated Sulfonic Acid Nanofiber Mats Prepared Via Electrospinning as Catalyst." *Materials Letters* 65, no. 11 (2011): 1719-1722.

Cho, T. H., M. Tanaka, H. Onishi, Y. Kondo, T. Nakamura, H. Yamazaki, S. Tanase, and T. Sakai. "Battery Performances and Thermal Stability of Polyacrylonitrile Nano-Fiber-Based Nonwoven Separators for Li-Ion Battery." *Journal of Power Sources* 181, no. 1 (2008): 155-160.

Choi, J., K. M. Lee, R. Wycisk, P. N. Pintauro, and P. T. Mather. "Nanofiber Network Ion-Exchange Membranes." *Macromolecules* 41, no. 13 (2008): 4569-4572.

Choi, S. S., Y. S. Lee, C. W. Joo, S. G. Lee, J. K. Park, and K. S. Han. "Electrospun Pvdf Nanofiber Web as Polymer Electrolyte or Separator." *Electrochimica Acta* 50, no. 2-3 (2004): 339-343.

Choi, S. W., S. M. Jo, W. S. Lee, and Y. R. Kim. "An Electrospun Poly(Vinylidene Fluoride) Nanofibrous Membrane and Its Battery Applications." *Advanced Materials* 15, no. 23 (2003): 2027-2032.

Chu, B., and B. S. Hsiao. "The Role of Polymers in Breakthrough Technologies for Water Purification." *Journal of Polymer Science Part B-Polymer Physics* 47, no. 24 (2009): 2431-2435.

Chung, Y. S., S. H. Yoo, and C. K. Kim. "Enhancement of Meltdown Temperature of the Polyethylene Lithium-Ion Battery Separator Via Surface Coating with Polymers Having High Thermal Resistance." *Industrial & Engineering Chemistry Research* 48, no. 9 (2009): 4346-4351.

Cooley, J.F. "Apparatus for Electrically Dispersing Fluids." *US Patent 692,631*, (1902).

Croce, F., G. B. Appetecchi, L. Persi, and B. Scrosati. "Nanocomposite Polymer Electrolytes for Lithium Batteries." *Nature* 394, no. 6692 (1998): 456-458.

Dahn, J. R., E. W. Fuller, M. Obrovac, and U. Vonsacken. "Thermal-Stability of Lixcoo2, Lixnio2 and Lambda-Mno2 and Consequences for the Safety of Li-Ion Cells." *Solid State Ionics* 69, no. 3-4 (1994): 265-270.

David, E., A. Lazar, and A. Armeanu. "Surface Modification of Polytetrafluoroethylene for Adhesive Bonding." *Journal of Materials Processing Technology* 157, (2004): 284-289.

Deitzel, J. M., J. Kleinmeyer, D. Harris, and N. C. B. Tan. "The Effect of Processing Variables on the Morphology of Electrospun Nanofibers and Textiles." *Polymer* 42, no. 1 (2001): 261-272.

Ding, B., C. R. Li, Y. Hotta, J. H. Kim, O. Kuwaki, and S. Shiratori. "Conversion of an Electrospun Nanofibrous Cellulose Acetate Mat from a Super-Hydrophilic to Super-Hydrophobic Surface." *Nanotechnology* 17, no. 17 (2006): 4332-4339.

Doshi, J., and D. H. Reneker. "Electrospinning Process and Applications of Electrospun Fibers." *Journal of Electrostatics* 35, no. 2-3 (1995): 151-160.

Eichhorn, S. J., and W. W. Sampson. "Statistical Geometry of Pores and Statistics of Porous Nanofibrous Assemblies." *Journal of the Royal Society Interface* 2, no. 4 (2005): 309-318.

Encinas, N., J. Abenojar, and M. A. Martinez. "Development of Improved Polypropylene Adhesive Bonding by Abrasion and Atmospheric Plasma Surface Modifications." *International Journal of Adhesion and Adhesives* 33, (2012): 1-6.

Fang, J., H. T. Niu, T. Lin, and X. G. Wang. "Applications of Electrospun Nanofibers." *Chinese Science Bulletin* 53, no. 15 (2008): 2265-2286.

Farahbakhsh, K., C. Svrcek, R. K. Guest, and D. W. Smith. "A Review of the Impact of Chemical Pretreatment on Low-Pressure Water Treatment Membranes." *Journal of Environmental Engineering and Science* 3, no. 4 (2004): 237-253.

Favaro, S. L., A. F. Rubira, E. C. Muniz, and E. Radovanovic. "Surface Modificaiton of Hdpe, Pp and Pet Films with $Kmno_4$/Hcl Solutions." *Polymer Degradation and Stability* 92, (2007): 1219-1226.

Fjuii, T.; Mochizuki, T. "High-Strength Porous Film and Process for Producing the Same" *U.S. Patent 5,759,678*, (1998).

Fong, H., I. Chun, and D. H. Reneker. "Beaded Nanofibers Formed During Electrospinning." *Polymer* 40, no. 16 (1999): 4585-4592.

Fonseca, C., J. M. Perena, J. G. Fatou, and A. Bello. "Sulphuric Acid Etching of Polyethylene Surfaces." *Journal of Materials Science* 20, (1985): 3283-3288.

Formhals, A. "Process and Apparatus for Preparing Artificial Threads." *US Patent 1,975,504*, (1934).

Formo, E., E. Lee, D. Campbell, and Y. N. Xia. "Functionalization of Electrospun Tio2 Nanofibers with Pt Nanoparticles and Nanowires for Catalytic Applications." *Nano Letters* 8, no. 2 (2008): 668-672.

Forsythe, J. S., D. R. Nisbet, W. Shen, D. I. Finkelstein, and M. K. Horne. "Review Paper: A Review of the Cellular Response on Electrospun Nanofibers for Tissue Engineering." *Journal of Biomaterials Applications* 24, no. 1 (2009): 7-29.

Fridrikh, S. V., J. H. Yu, M. P. Brenner, and G. C. Rutledge. "Controlling the Fiber Diameter During Electrospinning." *Physical Review Letters* 90, no. 14 (2003): 144502.

Gady, B., D. Schleef, R. Reifenberger, D. Rimai, and L. P. DeMejo. "Identification of Electrostatic and Van Der Waals Interaction Forces between a Micrometer-Size Sphere and a Flat Substrate." *Physical Review B* 53, no. 12 (1996): 8065-8070.

Gibson, P., H. Schreuder-Gibson, and D. Rivin. "Transport Properties of Porous Membranes Based on Electrospun Nanofibers." *Colloids and Surfaces a-Physicochemical and Engineering Aspects* 187, (2001): 469-481.

Gopal, R., S. Kaur, C. Y. Feng, C. Chan, S. Ramakrishna, S. Tabe, and T. Matsuura. "Electrospun Nanofibrous Polysulfone Membranes as Pre-Filters: Particulate Removal." *Journal of Membrane Science* 289, no. 1-2 (2007): 210-219.

Gopal, R., S. Kaur, Z. W. Ma, C. Chan, S. Ramakrishna, and T. Matsuura. "Electrospun Nanofibrous Filtration Membrane." *Journal of Membrane Science* 281, no. 1-2 (2006): 581-586.

Gopalan, A. I., P. Santhosh, K. M. Manesh, J. H. Nho, S. H. Kim, C. G. Hwang, and K. P. Lee. "Development of Electrospun Pvdf-Pan Membrane-Based Polymer Electrolytes for Lithium Batteries." *Journal of Membrane Science* 325, no. 2 (2008): 683-690.

Grafe, T.H., and K.M. Graham. "Nanofiber Webs from Electrospinning." *Nonwovens in Filtration - Fifth International Conference*, (May, 2003).

Greiner, A., and J. H. Wendorff. "Electrospinning: A Fascinating Method for the Preparation of Ultrathin Fibres." *Angewandte Chemie-International Edition* 46, no. 30 (2007): 5670-5703.

Greiner, A., J. Zeng, J. H. Wendorff, and H. Q. Hou. "Processing Parameters for Electrospun Polyvinylalcohol (Pva) Nanofibers and Uv-Crosslinking of Modified Pva Nanofibers." *Abstracts of Papers of the American Chemical Society* 226, (2003): U405-U405.

Gu, S. Y., J. Ren, and G. J. Vancso. "Process Optimization and Empirical Modeling for Electrospun Polyacrylonitrile (Pan) Nanofiber Precursor of Carbon Nanofibers." *European Polymer Journal* 41, no. 11 (2005): 2559-2568.

Gulmine, J. V., P. R. Janissek, H. M. Heise, and L. Akcelrud. "Polyethylene Characterization by Ftir." *Polymer Testing* 21, no. 5 (2002): 557-563.

Gupta, S. K., and K. Y. Chen. "Arsenic Removal by Adsorption." *Journal Water Pollution Control Federation* 50, no. 3 (1978): 493-506.

Hafiane, A., D. Lemordant, and M. Dhahbi. "Removal of Hexavalent Chromium by Nanofiltration." *Desalination* 130, no. 3 (2000): 305-312.

Haghi, A. K., and G. E. Zaikov. *Electrospinning of Nanofibers from Introduction to Application* Nanotechnology Science and Technology. Hauppauge, N.Y.: Nova Science Publishers, 2011.

He, J. H., Y. Q. Wan, and J. Y. Yu. "Effect of Concentration on Electrospun Polyacrylonitrile (Pan) Nanofibers." *Fibers and Polymers* 9, no. 2 (2008): 140-142.

He, X. L., Y. Zhao, J. P. Li, X. G. Gao, and J. A. Jia. "Porous Cuo Electrospun Fibers and Their Gas Sensing Properties." *Sensor Letters* 9, no. 1 (2011): 294-298.

Henry, C., J. P. Minier, and G. Lefevre. "Numerical Study on the Adhesion and Reentrainment of Nondeformable Particles on Surfaces: The Role of Surface Roughness and Electrostatic Forces." *Langmuir* 28, no. 1 (2012): 438-452.

Hernandez, A., J. I. Calvo, P. Pradanos, and F. Tejerina. "Pore Size Distributions in Microporous Membranes. A Critical Analysis of the Bubble Point Extended Method." *Journal of Membrane Science* 112, no. 1 (1996): 1-12.
Homaeigohar, S. S., K. Buhr, and K. Ebert. "Polyethersulfone Electrospun Nanofibrous Composite Membrane for Liquid Filtration." *Journal of Membrane Science* 365, no. 1-2 (2010): 68-77.

Hsiao, B. S., D. Liang, and B. Chu. "Functional Electrospun Nanofibrous Scaffolds for Biomedical Applications." *Advanced Drug Delivery Reviews* 59, no. 14 (2007): 1392-1412.

http://www.cdc.gov/niosh/docs/2003-154/pdfs/7600.pdf.

http://www.chem.sunysb.edu/WaterFilter/Figures/.

http://www.matweb.com.

http://www.pmiapp.com/publications/docs/Review-Papers/Advances-in-Pore-Structure-Evaluation-by-Porometry.pdf.

http://www.rtpcompany.com/info/data/1400/RTP1400AG-210.htm.

Hu, Z. H., L. Lei, Y. J. Li, and Y. M. Ni. "Chromium Adsorption on High-Performance Activated Carbons from Aqueous Solution." *Separation and Purification Technology* 31, no. 1 (2003): 13-18.

Huang, Z. M., Y. Z. Zhang, M. Kotaki, and S. Ramakrishna. "A Review on Polymer Nanofibers by Electrospinning and Their Applications in Nanocomposites." *Composites Science and Technology* 63, no. 15 (2003): 2223-2253.

Im, J. S., M. Il Kim, and Y. S. Lee. "Preparation of Pan-Based Electrospun Nanofiber Webs Containing Tio2 for Photocatalytic Degradation." *Materials Letters* 62, no. 21-22 (2008): 3652-3655.

Janssen, L. J. J., and L. Koene. "The Role of Electrochemistry and Electrochemical Technology in Environmental Protection." *Chemical Engineering Journal* 85, no. 2-3 (2002): 137-146.

Jena, A., and K. Gupta. "Pore Structure Characterization Techniques." *American Ceramic Society Bulletin* 84, no. 3 (2005): 28-30.

Karthikeyan, T., S. Rajgopal, and L. R. Miranda. "Chromium(Vi) Adsorption from Aqueous Solution by Hevea Brasilinesis Sawdust Activated Carbon." *Journal of Hazardous Materials* 124, no. 1-3 (2005): 192-199.

KastelanKunst, L., V. Dananic, B. Kunst, and K. Kosutic. "Preparation and Porosity of Cellulose Triacetate Reverse Osmosis Membranes." *Journal of Membrane Science* 109, no. 2 (1996): 223-230.

Katti, D. S., K. W. Robinson, F. K. Ko, and C. T. Laurencin. "Bioresorbable Nanofiber-Based Systems for Wound Healing and Drug Delivery: Optimization of Fabrication Parameters." *Journal of Biomedical Materials Research Part B-Applied Biomaterials* 70B, no. 2 (2004): 286-296.

Kharitonov, A. P., and L. N. Kharitonova. "Surface Modification of Polymers by Direct Fluorination: A Convenient Approach to Improve Commercial Properties of Polymeric Articles." *Pure and Applied Chemistry* 81, no. 3 (2009): 451-471.

Kim, I. C., H. G. Yoon, and K. H. Lee. "Formation of Integrally Skinned Asymmetric Polyetherimide Nanofiltration Membranes by Phase Inversion Process." *Journal of Applied Polymer Science* 84, no. 6 (2002): 1300-1307.

Kim, Y., D. Y. Lee, M. H. Lee, N. I. Cho, Y. S. Song, and S. J. Lee. "Characterization of Electrospun Zno Nanofibers." *Journal of the Korean Physical Society* 53, no. 1 (2008): 421-425.

Kinloch, Anthony J. *Adhesion and Adhesives: Science and Technology*. 1st ed.: Springer, 1987.

Kobayashi, S., K. D. Suh, and Y. Shirokura. "Chelating Ability of Poly(Vinylamine) - Effects of Polyamine Structure on Chelation." *Macromolecules* 22, no. 5 (1989): 2363-2366.

Kongsricharoern, N., and C. Polprasert. "Electrochemical Precipitation of Chromium (Cr6+) from an Electroplating Waste-Water." *Water Science and Technology* 31, no. 9 (1995): 109-117.

Krentsel, L. B., Y. V. Kudryavtsev, A. I. Rebrov, A. D. Litmanovich, and N. A. Plate. "Acidic Hydrolysis of Polyacrylonitrile: Effect of Neighboring Groups." *Macromolecules* 34, no. 16 (2001): 5607-5610.

Kumar, J., X. Y. Wang, C. Drew, S. H. Lee, K. J. Senecal, and L. A. Sarnuelson. "Electrospun Nanofibrous Membranes for Highly Sensitive Optical Sensors." *Nano Letters* 2, no. 11 (2002): 1273-1275.

Kuvaldina, E. V. , T. G. Shikova, S. A. Smirnov, and V. V. Rybkin. "Surface Oxidation and Degradation of Polyethylene in a Mixed Argon-Oxygen Plasma." *High Energy Chemistry* 41, no. 4 (2007): 284-287.

Kwon, I. K., S. Kidoaki, and T. Matsuda. "Electrospun Nano- to Microfiber Fabrics Made of Biodegradable Copolyesters: Structural Characteristics, Mechanical Properties and Cell Adhesion Potential." *Biomaterials* 26, no. 18 (2005): 3929-3939.

Lafuma, A., and D. Quere. "Superhydrophobic States." *Nature Materials* 2, no. 7 (2003): 457-460.

Laitinen, N., A. Luonsi, E. Levanen, and M. Nystrom. "Effect of Backflushing Conditions on Ultrafiltration of Board Industry Wastewaters with Ceramic Membranes." *Separation and Purification Technology* 25, no. 1-3 (2001): 323-331.

Laman, F. C., M. A. Gee, and J. Denovan. "Impedance Studies for Separators in Rechargeable Lithium Batteries." *Journal of the Electrochemical Society* 140, no. 4 (1993): L51-L53.

Larrondo, L., and R. S. J. Manley. "Electrostatic Fiber Spinning from Polymer Melts .3. Electrostatic Deformation of a Pendant Drop of Polymer Melt." *Journal of Polymer Science Part B-Polymer Physics* 19, no. 6 (1981): 933-940.

Lee, A., J. Mcvey, P. Faustino, S. Lute, N. Sweeney, V. Pawar, M. Khan, K. Brorson, and D. Hussong. "Use of Hydrogenophaga Pseudoflava Penetration to Quantitatively Assess the Impact of Filtration Parameters for 0.2-Micrometer-Pore-Size Filters." *Applied and Environmental Microbiology* 76, no. 3 (2010): 695-700.

Lee, C. H., H. J. Shin, I. H. Cho, Y. M. Kang, I. A. Kim, K. D. Park, and J. W. Shin. "Nanofiber Alignment and Direction of Mechanical Strain Affect the Ecm Production of Human Acl Fibroblast." *Biomaterials* 26, no. 11 (2005): 1261-1270.

Lee, J. S., K. H. Choi, H. Do Ghim, S. S. Kim, D. H. Chun, H. Y. Kim, and W. S. Lyoo. "Role of Molecular Weight of Atactic Poly(Vinyl Alcohol) (Pva) in the Structure and Properties of Pva Nanofabric Prepared by Electrospinning." *Journal of Applied Polymer Science* 93, no. 4 (2004): 1638-1646.

Li, D., J. T. McCann, and Y. N. Xia. "Electrospinning: A Simple and Versatile Technique for Producing Ceramic Nanofibers and Nanotubes." *Journal of the American Ceramic Society* 89, no. 6 (2006): 1861-1869.

Li, D. P., M. W. Frey, and Y. L. Joo. "Characterization of Nanofibrous Membranes with Capillary Flow Porometry." *Journal of Membrane Science* 286, no. 1-2 (2006): 104-114.

Li, D., and Y. N. Xia. "Electrospinning of Nanofibers: Reinventing the Wheel?" *Advanced Materials* 16, no. 14 (2004): 1151-1170.

Li, W. J., R. Tuli, X. X. Huang, P. Laquerriere, and R. S. Tuan. "Multilineage Differentiation of Human Mesenchymal Stem Cells in a Three-Dimensional Nanofibrous Scaffold." *Biomaterials* 26, no. 25 (2005): 5158-5166.

Li, Z. J., S. Q. Zhou, and J. H. Qiu. "Combined Treatment of Landfill Leachate by Biological and Membrane Filtration Technology." *Environmental Engineering Science* 24, no. 9 (2007): 1245-1256.

Lin, D. J., C. L. Chang, T. C. Chen, and L. P. Cheng. "Microporous Pvdf Membrane Formation by Immersion Precipitation from Water/Tep/Pvdf System." *Desalination* 145, no. 1-3 (2002): 25-29.

Lin, K., K. N. Chua, G. T. Christopherson, S. Lim, and H. Q. Mao. "Reducing Electrospun Nanofiber Diameter and Variability Using Cationic Amphiphiles." *Polymer* 48, no. 21 (2007): 6384-6394.

Lin, T., H. X. Wang, H. M. Wang, and X. G. Wang. "The Charge Effect of Cationic Surfactants on the Elimination of Fibre Beads in the Electrospinning of Polystyrene." *Nanotechnology* 15, no. 9 (2004): 1375-1381.

Linden, D. *Handbook of Batteries*. 3rd ed. New York: McGraw-Hill, 2002.

Lindner, J. P., C. Roben, A. Studer, M. Stasiak, R. Ronge, A. Greiner, and H. J. Wendorff. "Reusable Catalysts Based on Dendrimers Trapped in Poly(P-Xylylene) Nanotubes." *Angewandte Chemie-International Edition* 48, no. 47 (2009): 8874-8877.

Lisbona, D., and T. Snee. "A Review of Hazards Associated with Primary Lithium and Lithium-Ion Batteries." *Process Safety and Environmental Protection* 89, no. 6 (2011): 434-442.

Liu, H. F., X. M. Li, G. Zhou, H. B. Fan, and Y. B. Fan. "Electrospun Sulfated Silk Fibroin Nanofibrous Scaffolds for Vascular Tissue Engineering." *Biomaterials* 32, no. 15 (2011): 3784-3793.

Liu, J., D. P. Cao, and L. Q. Zhang. "Static and Dynamic Properties of Model Elastomer with Various Cross-Linking Densities: A Molecular Dynamics Study." *Journal of Chemical Physics* 131, no. 3 (2009).

Ma, H. Y., C. Burger, B. S. Hsiao, and B. Chu. "Ultra-Fine Cellulose Nanofibers: New Nano-Scale Materials for Water Purification." *Journal of Materials Chemistry* 21, no. 21 (2011): 7507-7510.

Ma, H. Y., C. Burger, B. S. Hsiao, and B. Chu. "Ultrafine Polysaccharide Nanofibrous Membranes for Water Purification." *Biomacromolecules* 12, no. 4 (2011): 970-976.

Ma, H. Y., C. Burger, B. S. Hsiao, and B. Chu. "Nanofibrous Microfiltration Membrane Based on Cellulose Nanowhiskers." *Biomacromolecules* 13, no. 1 (2012): 180-186.

Ma, H. Y., K. Yoon, L. X. Rong, M. Shokralla, A. Kopot, X. Wang, D. F. Fang, B. S. Hsiao, and B. Chu. "Thin-Film Nanofibrous Composite Ultrafiltration Membranes Based on Polyvinyl Alcohol Barrier Layer Containing Directional Water Channels." *Industrial & Engineering Chemistry Research* 49, no. 23 (2010): 11978-11984.

Ma, Z. W., Z. W. Lan, T. Matsuura, and S. Ramakrishna. "Electrospun Polyethersulfone Affinity Membrane: Membrane Preparation and Performance Evaluation." *Journal of Chromatography B-Analytical Technologies in the Biomedical and Life Sciences* 877, no. 29 (2009): 3686-3694.

Marshall, A. D., P. A. Munro, and G. Tragardh. "The Effect of Protein Fouling in Microfiltration and Ultrafiltration on Permeate Flux, Protein Retention and Selectivity - a Literature-Review." *Desalination* 91, no. 1 (1993): 65-108.

Martin, C. R. "Membrane-Based Synthesis of Nanomaterials." *Chemistry of Materials* 8, no. 8 (1996): 1739-1746.

Mathieson, I., and R. H. Bradley. "Improved Adhesion to Polymers by Uv/Ozone Surface Oxidation." *INT. J. Adhesion and Adhesives* 16, no. 1 (1995): 29-31.

Mcguire, K. S., K. W. Lawson, and D. R. Lloyd. "Pore-Size Distribution Determination from Liquid Permeation through Microporous Membranes." *Journal of Membrane Science* 99, no. 2 (1995): 127-137.

Mchugh, A. J., and D. C. Miller. "The Dynamics of Diffusion and Gel Growth During Nonsolvent-Induced Phase Inversion of Polyethersulfone." *Journal of Membrane Science* 105, no. 1-2 (1995): 121-136.

Megelski, S., J. S. Stephens, D. B. Chase, and J. F. Rabolt. "Micro- and Nanostructured Surface Morphology on Electrospun Polymer Fibers." *Macromolecules* 35, no. 22 (2002): 8456-8466.

Mit-uppatham, C., M. Nithitanakul, and P. Supaphol. "Ultratine Electrospun Polyamide-6 Fibers: Effect of Solution Conditions on Morphology and Average Fiber Diameter." *Macromolecular Chemistry and Physics* 205, no. 17 (2004): 2327-2338.

Mo, X. M., R. Chen, C. Huang, Q. F. Ke, C. L. He, and H. S. Wang. "Preparation and Characterization of Coaxial Electrospun Thermoplastic Polyurethane/Collagen Compound Nanofibers for Tissue Engineering Applications." *Colloids and Surfaces B-Biointerfaces* 79, no. 2 (2010): 315-325.

Mohan, D., and C. U. Pittman. "Activated Carbons and Low Cost Adsorbents for Remediation of Tri- and Hexavalent Chromium from Water." *Journal of Hazardous Materials* 137, no. 2 (2006): 762-811.

Morton, W.J. "Method of Dispersing Fluids." *US Patent 705,691*, (1902).

Moulin, C., M. M. Bourbigot, A. Tazipain, and F. Bourdon. "Design and Performance of Membrane Filtration Installations - Capacity and Product Quality for Drinking-Water Applications." *Environmental Technology* 12, no. 10 (1991): 841-858.

Muthukrishnan, M., and B. K. Guha. "Effect of Ph on Rejection of Hexavalent Chromium by Nanofiltration." *Desalination* 219, no. 1-3 (2008): 171-178.

Nagamine, S., Y. Tanaka, and M. Ohshima. "Fabrication of Hollow Tio2 Fibers Templated by Electrospun Aqueous Poly(Ethylene Oxide) (Peo) Solution." *Chemistry Letters* 38, no. 3 (2009): 258-259.

Nagamine, S., Y. Tanaka, and M. Ohshima. "Fabrication of Hollow Tio(2) Fibers Templated by Electrospun Aqueous Poly(Ethylene Oxide) (Peo) Solution." *Chemistry Letters* 38, no. 3 (2009): 258-259.

Nakao, S. "Determination of Pore-Size and Pore-Size Distribution .39 Filtration Membranes." *Journal of Membrane Science* 96, no. 1-2 (1994): 131-165.

Nenov, V., A. I. Zouboulis, N. Dimitrova, and I. Dobrevsky. "As(Iii) Removal from Aqueous-Solutions Using Nonstoichiometric Coprecipitation with Iron(Iii) Sulfate and Filtration or Flotation." *Environmental Pollution* 83, no. 3 (1994): 283-289.

Nomanbhay, S. M., and K. Palanisamy. "Removal of Heavy Metal from Industrial Wastewater Using Chitosan Coated Oil Palm Shell Charcoal." *Electronic Journal of Biotechnology* 8, no. 1 (2005): 43-53.

Packham, D. E. "Surface Energy, Surface Topography and Adhesion." *International Journal of Adhesion and Adhesives* 23, no. 6 (2003): 437-448.

Park, T. G., H. S. Yoo, and T. G. Kim. "Surface-Functionalized Electrospun Nanofibers for Tissue Engineering and Drug Delivery." *Advanced Drug Delivery Reviews* 61, no. 12 (2009): 1033-1042.

Pathak, A. N. "Membrane Technology with Special Reference to Filtration and Reverse Osmosis." *Journal of Scientific & Industrial Research* 56, no. 6 (1997): 335-345.

Pelton, R., and J. Hong. "Some Properties of Newsprint Impregnated with Polyvinylamine." *Tappi Journal* 1, no. 10 (2002): 21-26.

Prabhakaran, M. P., D. Kai, G. R. Jin, and S. Ramakrishna. "Guided Orientation of Cardiomyocytes on Electrospun Aligned Nanofibers for Cardiac Tissue Engineering." *Journal of Biomedical Materials Research Part B-Applied Biomaterials* 98B, no. 2 (2011): 379-386.

Ramakrishna, S., K. Fujihara, W. E. Teo, T. Yong, Z. W. Ma, and R. Ramaseshan. "Electrospun Nanofibers: Solving Global Issues." *Materials Today* 9, no. 3 (2006): 40-50.

Rasko, J. "Ftir Study of the Photoinduced Dissociation of Co2 on Titania-Supported Noble Metals." *Catalysis Letters* 56, no. 1 (1998): 11-15.

Rudnik, E., L. Burzynska, L. Dolasinski, and M. Misiak. "Electrodeposition of Nickel/Sic Composites in the Presence of Cetyltrimethylammonium Bromide." *Applied Surface Science* 256, no. 24 (2010): 7414-7420.

Ryu, Y. J., H. Y. Kim, K. H. Lee, H. C. Park, and D. R. Lee. "Transport Properties of Electrospun Nylon 6 Nonwoven Mats." *European Polymer Journal* 39, no. 9 (2003): 1883-1889.

Saeed, K., S. Y. Park, and T. J. Oh. "Preparation of Hydrazine-Modified Polyacrylonitrile Nanofibers for the Extraction of Metal Ions from Aqueous Media." *Journal of Applied Polymer Science* 121, no. 2 (2011): 869-873.

Salladini, A., M. Prisciandaro, and D. Barba. "Ultrafiltration of Biologically Treated Wastewater by Using Backflushing." *Desalination* 207, no. 1-3 (2007): 24-34.

Sapari, N., A. Idris, and N. H. AbHamid. "Total Removal of Heavy Metal from Mixed Plating Rinse Wastewater." *Desalination* 106, no. 1-3 (1996): 419-422.

Seeram Ramakrishna, Kazutoshi Fujihara, Wee-Eong Teo, Teik-Cheng Lim, Zuwei Ma. *An Introduction to Electrospinning and Nanofibers*, 2005.

Selomulya, C., V. Meeyoo, and R. Amal. "Mechanisms of Cr(Vi) Removal from Water by Various Types of Activated Carbons." *Journal of Chemical Technology and Biotechnology* 74, no. 2 (1999): 111-122.

Sheng, E., I. Sutherland, D. M. Brewis, R. J. Heath, and R. H. Bradley. *Journal of Materials Chemistry* 4, (1994): 487-490.

Shenoy, S. L., W. D. Bates, H. L. Frisch, and G. E. Wnek. "Role of Chain Entanglements on Fiber Formation During Electrospinning of Polymer Solutions: Good Solvent, Non-Specific Polymer-Polymer Interaction Limit." *Polymer* 46, no. 10 (2005): 3372-3384.

Shibukaw.T, M. Sone, A. Uchida, and K. Iwahori. "Light-Scattering Study of Polyacrylonitrile Solution." *Journal of Polymer Science Part a-1-Polymer Chemistry* 6, no. 1pa1 (1968): 147- 159.

Simons, HL. "Process and Apparatus for Producing Patterned Non-Woven Fabrics " *US Patent 3,280,229*, (1966).

Srijaroonrat, P., E. Julien, and Y. Aurelle. "Unstable Secondary Oil Water Emulsion Treatment Using Ultrafiltration: Fouling Control by Backflushing." *Journal of Membrane Science* 159, no. 1-2 (1999): 11-20.

Stasiak, M., A. Studer, A. Greiner, and J. H. Wendorff. "Polymer Fibers as Carriers for Homogeneous Catalysts." *Chemistry-a European Journal* 13, no. 21 (2007): 6150-6156.

Sumaru, K., H. Matsuoka, and H. Yamaoka. "Exact Evaluation of Characteristic Protonation of Poly(Vinylamine) in Aqueous Solution." *Journal of Physical Chemistry* 100, no. 21 (1996): 9000-9005.

Supaphol, P., C. Mit-uppatham, and M. Nithitanakul. "Ultrafine Electrospun Polyamide-6 Fibers: Effects of Solvent System and Emitting Electrode Polarity on Morphology and Average Fiber Diameter." *Macromolecular Materials and Engineering* 290, no. 9 (2005): 933-942.

Tamura, T., and H. Kawakami. "Aligned Electrospun Nanofiber Composite Membranes for Fuel Cell Electrolytes." *Nano Letters* 10, no. 4 (2010): 1324-1328.

Tang, Z. H., C. Q. Qiu, J. R. McCutcheon, K. Yoon, H. Y. Ma, D. F. Fang, E. Lee, C. Kopp, B. S. Hsiao, and B. Chu. "Design and Fabrication of Electrospun Polyethersulfone Nanofibrous Scaffold for High-Flux Nanofiltration Membranes." *Journal of Polymer Science Part B-Polymer Physics* 47, no. 22 (2009): 2288-2300.

Tang, Z. H., J. Wei, L. Yung, B. W. Ji, H. Y. Ma, C. Q. Qiu, K. Yoon, F. Wan, D. F. Fang, B. S. Hsiao, and B. Chu. "Uv-Cured Poly(Vinyl Alcohol) Ultrafiltration Nanofibrous Membrane Based on Electrospun Nanofiber Scaffolds." *Journal of Membrane Science* 328, no. 1-2 (2009): 1-5.

Taylor, G. "Disintegration of Water Drops in Electric Field." *Proceedings of the Royal Society of London Series a-Mathematical and Physical Sciences* 280, no. 1380 (1964): 383-397.

Thompson, C. J., G. G. Chase, A. L. Yarin, and D. H. Reneker. "Effects of Parameters on Nanofiber Diameter Determined from Electrospinning Model." *Polymer* 48, no. 23 (2007): 6913-6922.

Tomadakis, M. M., and S. V. Sotirchos. "Effective Knudsen Diffusivities in Structures of Randomly Overlapping Fibers." *Aiche Journal* 37, no. 1 (1991): 74-86.

Tomadakis, M. M., and S. V. Sotirchos. "Knudsen Diffusivities and Properties of Structures of Unidirectional Fibers." *Aiche Journal* 37, no. 8 (1991): 1175-1186.

Toncheva, A., M. Spasova, D. Paneva, N. Manolova, and I. Rashkov. "Drug-Loaded Electrospun Polylactide Bundles." *Journal of Bioactive and Compatible Polymers* 26, no. 2 (2011): 161-172.

Tripatanasuwan, S., Z. X. Zhong, and D. H. Reneker. "Effect of Evaporation and Solidification of the Charged Jet in Electrospinning of Poly(Ethylene Oxide) Aqueous Solution." *Polymer* 48, no. 19 (2007): 5742-5746.

Tungprapa, S., T. Puangparn, M. Weerasombut, I. Jangchud, P. Fakum, S. Semongkhol, C. Meechaisue, and P. Supaphol. "Electrospun Cellulose Acetate Fibers: Effect of Solvent System on Morphology and Fiber Diameter." *Cellulose* 14, no. 6 (2007): 563-575.

Ueda, M., K. G. Kostov, A. F. Beloto, N. F. Leite, and K. G. Grigorov. "Surface Modification of Polyethylene Terephthalate by Plasma Immersion Ion Implantation." *Surface & Coatings Technology* 186, no. 1-2 (2004): 295-298.

USABC. "Development of Low Cost Separators for Lithium-Ion Batteries." *RFPI*, (2001).

Uyar, T., J. Hacaloglu, and F. Besenbacher. "Electrospun Polyethylene Oxide (Peo) Nanofibers Containing Cyclodextrin Inclusion Complex." *Journal of Nanoscience and Nanotechnology* 11, no. 5 (2011): 3949-3958.

Vijayakumar, G. N. S., S. Devashankar, M. Rathnakumari, and P. Sureshkumar. "Synthesis of Electrospun Zno/Cuo Nanocomposite Fibers and Their Dielectric and Non-Linear Optic Studies." *Journal of Alloys and Compounds* 507, no. 1 (2010): 225-229.

Wang, H. Y., Y. K. Feng, H. Y. Zhao, R. F. Xiao, J. Lu, L. Zhang, and J. T. Guo. "Electrospun Hemocompatible Pu/Gelatin-Heparin Nanofibrous Bilayer Scaffolds as Potential Artificial Blood Vessels." *Macromolecular Research* 20, no. 4 (2012): 347-350.

Wang, R., Y. Liu, B. Li, B. S. Hsiao, and B. Chu. "Electrospun Nanofibrous Membranes for High Flux Microfiltration." *Journal of Membrane Science* 392, (2012): 167-174.

Wang, S. D., Y. Z. Zhang, H. W. Wang, G. B. Yin, and Z. H. Dong. "Fabrication and Properties of the Electrospun Polylactide/Silk Fibroin-Gelatin Composite Tubular Scaffold." *Biomacromolecules* 10, no. 8 (2009): 2240-2244.

Wang, X. F., X. M. Chen, K. Yoon, D. F. Fang, B. S. Hsiao, and B. Chu. "High Flux Filtration Medium Based on Nanofibrous Substrate with Hydrophilic Nanocomposite Coating." *Environmental Science & Technology* 39, no. 19 (2005): 7684-7691.

Wang, X. F., D. F. Fang, K. Yoon, B. S. Hsiao, and B. Chu. "High Performance Ultrafiltration Composite Membranes Based on Poly(Vinyl Alcohol) Hydrogel Coating on Crosslinked Nanofibrous Poly(Vinyl Alcohol) Scaffold." *Journal of Membrane Science* 278, no. 1-2 (2006): 261-268.

Wang, Y. Y., F. Hammes, M. Duggelin, and T. Egli. "Influence of Size, Shape, and Flexibility on Bacterial Passage through Micropore Membrane Filters." *Environmental Science & Technology* 42, no. 17 (2008): 6749-6754.

Wu, S. J., Q. D. Tai, and F. Yan. "Hybrid Photovoltaic Devices Based on Poly (3-Hexylthiophene) and Ordered Electrospun Zno Nanofibers." *Journal of Physical Chemistry C* 114, no. 13 (2010): 6197-6200.

www.celgard.com/.

Xu, K. "Nonaqueous Liquid Electrolytes for Lithium-Based Rechargeable Batteries." *Chemical Reviews* 104, no. 10 (2004): 4303-4417.

Yoo, S. H., and C. K. Kim. "Enhancement of the Meltdown Temperature of a Lithium Ion Battery Separator Via a Nanocomposite Coating." *Industrial & Engineering Chemistry Research* 48, no. 22 (2009): 9936-9941.

Yoon, K., B. S. Hsiao, and B. Chu. "Formation of Functional Polyethersulfone Electrospun Membrane for Water Purification by Mixed Solvent and Oxidation Processes." *Polymer* 50, no. 13 (2009): 2893-2899.

Yoon, K., K. Kim, X. F. Wang, D. F. Fang, B. S. Hsiao, and B. Chu. "High Flux Ultrafiltration Membranes Based on Electrospun Nanofibrous Pan Scaffolds and Chitosan Coating." *Polymer* 47, no. 7 (2006): 2434-2441.

You, Y., B. M. Min, S. J. Lee, T. S. Lee, and W. H. Park. "In Vitro Degradation Behavior of Electrospun Polyglycolide, Polylactide, and Poly(Lactide-Co-Glycolide)." *Journal of Applied Polymer Science* 95, no. 2 (2005): 193-200.

Yung, L., H. Y. Ma, X. Wang, K. Yoon, R. Wang, B. S. Hsiao, and B. Chu. "Fabrication of Thin-Film Nanofibrous Composite Membranes by Interfacial Polymerization Using Ionic Liquids as Additives." *Journal of Membrane Science* 365, no. 1-2 (2010): 52-58.

Zhang, S. H., X. G. Jian, and Y. Dai. "Preparation of Sulfonated Poly(Phthalazinone Ether Sulfone Ketone) Composite Nanofiltration Membrane." *Journal of Membrane Science* 246, no. 2 (2005): 121-126.

Zhao, Y. H., Y. L. Qian, B. K. Zhu, and Y. Y. Xu. "Modification of Porous Poly(Vinylidene Fluoride) Membrane Using Amphiphilic Polymers with Different Structures in Phase Inversion Process." *Journal of Membrane Science* 310, no. 1-2 (2008): 567-576.

Zong, X. H., H. Bien, C. Y. Chung, L. H. Yin, D. F. Fang, B. S. Hsiao, B. Chu, and E. Entcheva. "Electrospun Fine-Textured Scaffolds for Heart Tissue Constructs." *Biomaterials* 26, no. 26 (2005): 5330-5338.

Zong, X. H., K. Kim, D. F. Fang, S. F. Ran, B. S. Hsiao, and B. Chu. "Structure and Process Relationship of Electrospun Bioabsorbable Nanofiber Membranes." *Polymer* 43, no. 16 (2002): 4403-4412.